REPORT DOCUMENTATION PAGE

Form Approved OMB No. 0704-0188

1. AGENCY USE ONLY (Leave blank)	2. REPORT DATE	3. REPORT TYPE AND DATES COVERED
	23-August 2000	Final Report, Aug 99 – Aug 00

4. TITLE AND SUBTITLE

In-situ Eutectic High-temperature Ti-based Composites

5. FUNDING NUMBERS

F61775-99-WE031

6. AUTHOR(S)

Deputy Director Sergiy A Firstov

7. PERFORMING ORGANIZATION NAME(S) AND ADDRESS(ES)

Francevych Institute for Problems of Materials Science
3, Krzhyzhanovskoho Street
Kiev-142 03142
Ukraine

8. PERFORMING ORGANIZATION REPORT NUMBER

N/A

9. SPONSORING/MONITORING AGENCY NAME(S) AND ADDRESS(ES)

EOARD
PSC 802 BOX 14
FPO 09499-0200

10. SPONSORING/MONITORING AGENCY REPORT NUMBER

SPC 99-4031

11. SUPPLEMENTARY NOTES

12a. DISTRIBUTION/AVAILABILITY STATEMENT

Approved for public release; distribution is unlimited.

12b. DISTRIBUTION CODE

A

13. ABSTRACT (Maximum 200 words)

This report results from a contract tasking Francevych Institute for Problems of Materials Science as follows: The contractor shall investigate cast Ti-Si-X and Ti-B-X eutectic alloys. Emphasis shall be placed on investigating the structure and physico-mechanical properties (strength, fracture toughness, long term high temperature hardness etc) in a range from room temperature up to 1000oC. Composites will be varied in composition and volume content of reinforcing phases and matrix to find the best combination of heat resistance and fracture toughness, with a final selection and optimizion of compositions which are most promising for high-temperature applications.
The contractor shall emphasize a low-cost approach for producing materials throughout the research with arc- or electron-beam melting, focusing on existing experimental alloys which can be improved by optimizing the structural parameters of the composites and phase and chemical compositions of the constituent phases.

14. SUBJECT TERMS

EOARD, Structural Materials, Metals & alloys, Aeroengines, space materials, Titanium in-situ composites

15. NUMBER OF PAGES

79

16. PRICE CODE

N/A

17. SECURITY CLASSIFICATION OF REPORT	18. SECURITY CLASSIFICATION OF THIS PAGE	19. SECURITY CLASSIFICATION OF ABSTRACT	20. LIMITATION OF ABSTRACT
UNCLASSIFIED	UNCLASSIFIED	UNCLASSIFIED	UL

IN-SITU EUTECTIC HIGH-TEMPERATURE TI-BASED COMPOSITES

The final report

submitted by Institute for Metal-Ceramic Research of Ukraine under Prof. Sergiy O. Firstov

European Office of Aerospace Research and Development Contract F61775-99-WE031

August 2000

CONTENT

INTRODUCTION

Working temperatures of conventional titanium heat-resistant alloys are in the range between 350°C (VT3-1) and 600°C (VT18U). Under higher temperatures, intergranular fracture takes place that results in a drastic decrease of mechanical properties [1]. This temperature range is an area of nickel heat-resistant alloys. But developers of Ti alloys do not leave attempts to improve their heat resistance to the level of higher, "nickel," temperatures. An actuality of this problem is more than obvious; especially taking into account that titanium is lighter practically in two times than nickel. Please compare their specific weights, (γ_{Ti} = 4,5 g/cm^3 and γ_{Ni} = 8,9 g/cm^3).

Analysis of composition and properties of the well-known heat-resistant alloys (VT18U, Timetal 1100, IMI834 etc.) shows that possibility of their solid solution hardening is practically exhausted. It would be expedient to use traditional way of precipitation hardening with different phases like oxides, nitrides, borides, or carbides. But our and literature data [2] show that hardening with oxides and nitrides are non-effective (or even harmful) due to high solubility of oxygen and nitrogen in titanium resulting in brittleness of alloys [3].

Carbon and boron have low solubility in titanium. They form thermodynamically stable carbides TiC and borides TiB_2 [4]. This opens possibility to strengthen titanium alloys with these interstitial phases. But up to present, only a few examples of successful application of boron hardening are known exceptionally in powder materials like XD TiAI [5, 6]. This is due to good compatibility of TiB particles with titanium [7]. The satisfactory compatibility with titanium has TiC also [7], but samples of successful application of carbide hardening for Ti alloys are not known yet. Nevertheless, carbide strengthening as well as boride one is undoubtedly perspective to improve high temperature properties of Ti alloys.

As modern more perspective and sampled way of improving high temperature properties of titanium alloys is the intermetallic strengthening. To develop novel titanium heat resistant materials aluminides Ti_3Al, TiAl, as well as silicides Ti_5Si_3 are the most preferable [8-10]. In already patented and studied alloys of system Ti-AI-Si [10,11] the aluminides play as a matrix and the silicides Ti_5Si_3 play as strengthening refractory phase. The composites were obtained with the only granule powder metallurgy using, in some cases, self-combustion high temperature synthesis [10].

Thus, as follow from the above, the composites of Ti-Si-X and Ti-B-X are as the most perspective titanium high temperature materials. In this connection, the objective of the Project under consideration was the study of influence of chemical composition, structure and methods of production on mechanical and physical properties of alloys of Ti- Si-X and Ti-B-X systems pursuing the development of new high temperature titanium alloys for industry.

The data obtained devoted to the Ti-Si-X and Ti-B-X systems are given below in two the separate chapters. It must be noted too that Chapter I contains the special section concerning the role of gallium.

CHAPTER I. STRUCTURE AND PROPERTIES OF THE TI-SI-X – ALLOYS.

The data as to Ti-Al-Si phase diagrams may be found in [12]. The feature of this Ti-Al-Si diagram (Fig.1) is presence of long row of eutectic alloys between the Ti_5Si_3 silicides and β(α)-Ti, α_2-Ti_3Al aluminides (at 30 at% Al) and γ-TiAl (~50 at % Al) along isoconcentrate of ~10 at % Si (7.5 wt.%).

At the point l_1, solidus temperature is maximal and is equal 1545°C. Compositions of solid and liquid phases are equal and, hence, the system given can be considered as a quasibinary-like one. Along both side, liquidus temperatures decreases and conodes between silicides and corresponding aluminides turn in direction of decreasing temperatures. Polytermical section of system is shown in Fig.2. It is possible to see that in dependence on aluminium content β←→α-transformation takes place at different temperatures determining different heat resistance of alloys.

The presence of eutectic alloys area in the Ti-Al-Si-system is the most interest for the Project given. As to the up-to-date conception, the cast eutectic alloys possess enhanced heat resistance in comparison with other compositions because in a course of eutectic crystallization the particles (colony) of refractory (melting temperature is 2120°C) and thermodynamically stable (ΔF is – 147 kcal/mol) silicides Ti_5Si_3 pierce titanium matrix producing natural (in situ) composite. Composite effect may be significant in such compositions, it is determined by size and morphology of silicide phase. It would be interested to note here that solubility of aluminum in Ti_5Si_3 reaches ~10%. According to X-rays data aluminium substitutes silicon. Hence, the silicide formula in system given is $Ti_5(Si,Al)_3$. Contrary, the solubility of silicon in α-Ti, aluminides α_2-Ti_3Al and γ-TiAl is very small and does not exceed ~1 at.% [12].

In such a way, phase equilibria analysis as well as building Ti-Al-Si-diagram allow to find the area which is the most perspective to find and develop new high temperature alloys. This area is the area of a-Ti + $Ti_5(Si,Al)_3$ eutectic alloys. In order to determine a composition of new material, it is necessary to conduct, first of all, optimization of composition on basic elements those are Al and Si, and, at the second, to check possibility of additional alloying with different elements to obtain the best ratio of mechanical properties. Besides that, checking influence of solidification conditions (size ingot effect) on structure and properties of small and big ingots was planned.

1.1. MATERIALS, TECHNOLOGIES OF PRODUCTION OF ALLOYS, METHODS OF TESTING AND RESEARCH

Materials under study were melted with the electron-beam smelter EPLU-4 based on the modernized vacuum induction heater ISB-0,04. As the base of the charges was VT5 Ti alloy's scrap and silicon, grade KP1. Ingots of 55-mm diameter and up to 700-mm length were used. Small ingots of 35-40 g weight were used for laboratory research. Method of melting was vacuum-arc melting equipped with permanent unspent tungsten electrode. To study an influence of additional alloying a number of alloys were smelted too. All the alloys are listed in Tables 1– 4.

Table 1. Alloys and their compositions. Weight of ingots are 10 kg.

№ of alloy alloyings, wt.%	1*	2	3	4**	5	6	7	8	9	10
Si	4.2	4.82	5.3	5.2	7.07	9.5	2	2.55	3.5	3.5
Al	4.5	2.97	5	4.2	2.51	3.5	5.4	6.4	5.9	4.3
Zr	-	-	-	-	-	-	5.3	12.4	9.6	6.2

№ of alloy alloyings, wt.%	11	12	13**	14	15	16	17	18	19
Si	4.05	4.7	4.95	5.5	5.79	6.02	6.2	6.6	9
Al	2.6	4.4	4.75	5.1	4.1	4.57	5.4	5.65	5
Zr	3.9	9.4	3.9	7.2	5.1	4.0	6	5.4	6

* Additional alloying 2.5Cr +2.35 Mo
** Admixtured with 0.75 Mn

Table 2. Alloys and their compositions. Weight of small ingots are ~35 g.

№ of alloy alloyings, wt.%	1a	2a	3a (iodide)	4a (sponge)
Si	4.0	6.0	4.0	4.0
Al	0	3.0	3.0	3.0
Zr	5.0	7.0	5.0	5.0

Table 3. Alloys and their compositions. Weight of big ingots are ~ 40 kg.

№ of alloy alloyings, wt.%	1b	2b	3b	4b	5b
Si	0	4.7	2.5	3.5	11
Al	2.6	2.2	5.5	5.8	9.5
Zr	2.8	6.6	5.5	5.7	6.5

Table 4. Compositions of additionally alloyed Ti-Al-S alloys. Weight of small ingots are ~35 g.

Compo, wt.%→ N of alloys ↓	Al	Si	Zr	Additional alloying					
				V	Cr	Ge	Sn	Y	Ga
1c	3	4	5	2…4					
2c	3	4	5		3				
3c	3	4	5			3			
4c	3	4	5				5		
5c	3	4	5					0.4	
6c	4.8	5.5	5.3						5
7c	5	10	-						5

Structure and phase composition were tested with light (Jenophot-200) and electron (JEM-100CXII) microscopes and X-rays difractomer (DRON-3).

Mechanical properties were measured under bending and tension tests in temperature range 20-1000^{0}C. Size of samples was of 2.5 x 5 x 35 mm (for bending), and 3 mm diameter and length 37 mm (for tension). Fracture toughness K_{1c} was measured under the FSU standard GOST 25.506-85 at bending of 2.5 x 5 x 35 mm samples with initiating electro-spark notch of 0.08 mm radius and 2.5 mm length.

To obtain the composition-heat resistance diagram one of the express methods namely method of long term hardness (hardness after loading with 1 kg for 1 hour, 3600 s, HV1-3600 as well as short-term hardness with 1 kg for 1 min, 60 s, HV1-60 [13]) was applied. The tests were done at 504, 698 and 892°C that is 0.4, 0.5, and 0.6 of melting temperature of titanium T_{mlt}. To eliminate thermal stresses and homogenize solid solution samples were heat treated at 850°C for 1 hour before the tests.

The tests on long-term strength were done under tension in accordance with the FSU standard GOST 10.145.581. Diameter of samples was 5 mm. The dependence of stress – time to failure were derived.

1.2. OPTIMIZING COMPOSITIONS OF THE CAST TI-AL-SI ALLOYS

Some early works devoted studies of structure and properties of Ti-Al-Si alloys note the positive influence of zirconium on their high temperature properties [14, 15]. Choosing the series of concrete alloys a possible way of influence of Zr on properties of the Ti-Al-Si alloys under study was analyzed additionally, and subsequently the whole raw of compositions including zirconium was involved in series of alloys for the study (Table 1).

Prescribing specific concentrations of basic components of alloys namely silicon and aluminium, as well as zirconium we preceded from the considerations as the next:

3.1. The role of silicon

Silicon is the main alloying element.

Owing to the eutectic reaction / transformation

$$L \rightarrow \alpha + Ti_5Si_3,$$

that takes place at temperature 1330°C, strengthening phase is formed from refractory silicide particles having melting temperature T_{mlt} of Ti_5Si_3 around 2320°C. Varying concentration of silicon in comparatively wide interval, variation of volume content of silicide phase, its size and morphology takes place resulting in a complex of mechanical properties of alloys.

3% of Si is a critical concentration. With concentrations of Si above 3%, normal eutectic alloys take place, when concentrations of Si is lower 3%, silicide phase precipitates from solid β-phase in accordance with the reaction of decomposition

$$\beta \rightarrow \alpha + Ti_5Si_3.$$

Such the silicides are named as secondary ones those differ from primary eutectic silicides precipitating directly from a liquid melt [3]. The alloys strengthened with secondary silicides are named as eutectoid ones.

Thus, to get eutectic compositions in the Ti-Si-system, silicon in amount more than 3% is needed. At concentrations of silicon less than 3%, eutectoid alloys are formed. These alloys may considered as perspective too because when decomposing, the supersaturated solid solution forms very fine solid phase, as a rule. This influences always positively on mechanical properties of materials.

3.2. The role of aluminum

It is known that aluminum increases heat resistance of α-Ti, therefore it is added in practically all Ti alloys. Average aluminum content in alloys is 4 – 6%. Above these figures, some isolation of α_2-phase begins to take place that leads to embrittlement of alloys. However, embrittlement of titanium can take place when aluminum content is less than 2 wt.% [14]. That is why, there are practically no alloys with content of aluminum less than 3%. But optimizing concentration of aluminum in Ti-Al-Si alloys it is necessary to keep in mind that alloying with aluminum increases solubility of silicon in α-titanium that influences negatively on plasticity of alloys [16].

3.3. The role of zirconium

Zirconium in amount of <6 mass % increases strength of the Ti-6Al alloys with no practical decrease of their plasticity [14]. As it was found in this work, zirconium increases the high temperature properties of Ti-Al-Si alloys. Being soluted in silicide, zirconium makes it smaller that improves mechanical properties of material as a whole. The chemical formula of silicide with participation of zirconium is $Ti_4Zr_6Si_3$, and taking into account the solubility of aluminum up to ~10 at%, it is $Ti_4Zr_6Al_xSi_3$. But alloying Ti with >6 mass % Zr leads to the sharp decrease of fracture toughness and corrosion resistance [14].

In accordance with analysis of influence of different elements on mechanical properties of titanium and Ti-Si alloys the series of experimental alloys of 19 compositions listed in Table 1 was smelted with electron beam ELLU-4 equipment. Among them there are eutectoid alloys (alloys 7, 8), hypereutectic alloys (alloys 5, 19) and the most numerous group of hypoeutectic alloys with silicon content 3-8%. All the alloys were additionally alloyed with 2.5 – 6.4% Al, and its the largest part – with 2.9 – 12.4% Zr.

Concentration of silicon as a main alloying element of alloys determines their structure (Fig. 3), morphology and volume of strengthening silicide phase that results finally in properties of material as a whole.

As the decisive mechanical property in order to select optimal composition of Ti-Si-Al-alloys the heat resistance were chosen. In the work given, long-term (for 1 hour) hardness was chosen as an indicator of this property.

Figures 4 and 5 show curves of long-term hardness of alloys listed in Table 1 in dependence on content of Si and Zr in them. The tendencies are visible clearly for all three temperatures as follows.

The first, as for silicon, we can note that heat resistance maximum is shifted a little from the pure eutectic composition to hypoeutectic ones. This maximum corresponds to 4-6 wt.% of Si. At temperatures above 700°C, the dependence of long-term hardness on silicon content is weakened, but even at 900°C this maximum may be recognized. The weakening is connected with that circumstance that under these temperatures the processes of diffusion weakening and recrystallization are beginning actively. Besides that, it was found that at temperatures 700°C and above dissolving and coagulating silicide Ti_5Si_3 phases take place [16].

The second, at content of zirconium more than 6 wt.% heat resistance significantly increases (Fig. 5). In Fig. 4, data for each temperature is contoured with upper and lower curves. Points near lower curves correspond to compositions with no Zr or with its small content lower than 4 wt.%. Optimal content of zirconium may be determined via simple reconsideration of obtained data in coordinates HV1-3600 – Zr, mas.% (Fig. 5). It is seen that alloys with zirconium content of 6-9 mas.% have the highest heat resistance.

1.3. STUDY OF STRUCTURE, MECHANICAL PROPERTIES, AND FRACTURE MECHANISMS OF THE CAST TI-AL-SI ALLOYS

1.3.1. Structure

As it was mentioned above, among the Ti-Al-Si alloys studied, two groups of compositions have the practical interest namely: eutectoid and hypoeutectic alloys. Please see their compositions in Table 2.

In the first group of alloys, where silicon content is less than 3 %, at the real rates of ingots cooling, strengthening silicide phases are formed as result of eutectoid decomposition in accordance with

$$\beta\text{-Ti} \leftrightarrow \alpha\text{-Ti} + Ti_5Si_3. \quad (1)$$

As a result of this decomposition the fine silicide phase (Fig. 6a) ensuring rather high strength at satisfactory, that is very important, plasticity is formed. But such alloys have low heat resistance, their structures are thermally unstable. In these alloys being heated to 900°C for 1 hour, silicide phase dissolves fully in matrix making it supersaturated with silicon (Fig. 6d). Plasticity of such alloys drops drastically.

In the second group of alloys silicon content is in the interval 3≤Si≤8 %. In these alloys, strengthening silicide phase is formed immediately from liquid smelt as a result of reaction

$$L \rightarrow \beta\text{-Ti} + L \leftrightarrow \alpha\text{-Ti} + E, \quad (2)$$

where L is liquid smelt, E is eutectic $\beta(\alpha) + Ti_5Si_3$, at real rates of cooling. Here, as the basic structural element is eutectic colonies consisting of α-Ti and rather large plate-like silicide particles (Fig. 6b). Namely these colonies realize basic strengthening effect of theses structures. Plates of the secondary silicides Ti_5Si_{3sec} may precipitate along boundaries of initial β-Ti grains. Such the structures ensure the enhanced heat resistance of eutectic compositions in comparison with eutectoid ones due to additional composite strengthening effect. But due to rough morphology of eutectic colonies their plasticity is low, as a rule. In comparison with eutectoid alloys the eutectic (hypoeutectic) ones show enhanced thermal stability. Quenching them from 1000°C and long-term annealing at 800°C for 10 hours lead the only to some enlargement silicide particles (Fig. 6e).

Alloys with silicon content more than 8 mas. % are hypereutectic ones. We did not consider them in details because due to their rough structural morphology (Fig. 6c) they have no serious practical interest.

1.3.2. Mechanical properties

Typical mechanical properties of selected alloys are shown in Table 5.

Table 5. Mechanical properties of the cast Ti-Si-Al-Zr alloys.

Property	*Unit of measure*	Temperature °C	Alloy 7 (eutectoid)	Alloy 17 (near-eutectic)	Alloy 19 (hypereutectic)
Density	g/cm^3	20	4.6	4.7	4.52
Hardness, H	*MPa*	20	4500	5540	5770
Young's modulus, E	*MPa*	20	141	146	-
Yield stress	*MPa*	20	-	-	-
		600	310	708	-
		800	270	193	317
Tensile strength	*MPa*	20	627	740	580
		300	754	786	545
		600	484	735	390
		800	337	350	375
Elongation	%	20	0	0	0
		300	0	0	0
		600	8.21	0.3	0
		800	6.50	6.1	1.2
Fracture toughness, K_{1c}	$MPa \cdot m^{1/2}$	20	20	17	-
		600	25	19	-
		800	17	15	-
Compressive strength	*MPa*	20	1510	1660	-
		600	797	925	-
		800	280	305	-
		1000	-	52	-

Samples were made of large ingots of 10 kg weight. The tests were conduct at temperatures 20 – 800°C in air. The tests at 1000°C were conducted in vacuum.

As it is seen from the data shown, the change of mechanical properties with temperature meets fully the consideration mentioned above.

Eutectoid alloy (alloy 7) is not so strong but more plastic than eutectic ones. It has also better fracture toughness. Near-eutectic alloy (alloy 17) is stronger and harder, it has less plasticity and fracture toughness up to high temperature. The highest brittleness has hypereutectic alloy (alloy 19). The presence of eutectic frame made of refractory silicide phase in the structure of eutectic alloys ensures high strength under compression and high tribological properties as well (preliminary data).

1.3.3. Fracture mechanisms

Fracture mechanisms were studied with scanning electron microscopy of samples tested on fracture toughness. As the first feature of brittle fracture of the cast Ti-Si alloys is an independence of a place of its origin on a notch. The cracks start from both the notch and its opposite side of sample. Fractographical analysis shows (Figure 7) that this effect is promoted by not only structural defects of casting but large particles of α-Ti-phase precracked in a course of loading (Fig. 7a). By the second one is the important thing that even large enough silicide particles being microcracked do not delaminate themselves from α-Ti-matrix (Fig. 7a-c). This points out the high adhesive strength of particles with matrix that realizes in good high temperature strength of the Ti-Si alloys. Fracture mechanism in all the temperature interval studied is cleavage with some portion of ductile pores (voids) coalescence (Fig. 7c).

Data obtained show also that fracture toughness of the Ti-Si-Al alloys is determined basically by silicon concentration in them: the lower silicon, the better fracture toughness. As the second factor influencing on fracture toughness is size and morphology of hard particles of the second phase. It is known that in dependence on toughness of matrix, in a course of pre-deformation, particles may be as both the sources of crack origin or obstacles for cleavage crack spreading. As follows from fractographical analysis data, the rough silicide particles of eutectic colonies fail by cleavage at all temperatures that may explain the low figures of fracture toughness. In alloys where matrix has some plasticity and contains fine particles some features like small separate dimples may be found in fracture surface (Fig. 7c) that evidences on failure with pores coalescence. At temperatures above 500°C, ductile features occupy the large part of surface that results in higher fracture toughness.

In such a way, the study of structure, mechanical properties and fracture mechanisms in a wide temperature range of the cast Ti-Si-alloys show that eutectoid and hypoeutectic alloys of this system with 2-6 wt.% silicon content alloyed additionally with Al and Zr are highly strong and heat resistant materials those could be as a perspective base to develop novel heat resistant compositions.

1.4. STUDY OF STRUCTURE AND MECHANICAL PROPERTIES OF THE SELECTED ALLOYS OF TI-SI-AL-ZR SYSTEM OF SMALL (UP TO 100 G) AND LARGE (UP TO 40 KG) INGOTS.

It is a widely recognized that the structure of eutectic conglomerates is so numerous not only among alloys of different systems but even among one system. In dependence on solidification conditions the same eutectic may show different morphology [13,15]. By the main factors determining structure of the concrete eutectic are conditions of cooling and volume ratio phases in the eutectic mixture resulted from composition of a given alloy, i.e. position of eutectic point in the system. In practice, the rate of eutectic solidification (supercooling extent) is determined mainly by a size (weight) of an ingot. Hence, the ingot weight is important and must be taken into account analyzing mechanical properties of Ti-Si-Al-Zr alloys under study. There is another important factor influencing strongly on mechanical properties of alloys namely purity of initial components. In the first turn, it concerns titanium itself. Its properties depend strongly on amount of such additives as oxygen, nitrogen, and carbon [14].

The influence of both the factors (weight of ingots and purity of initial titanium) is seen well analyzing mechanical properties of Ti-Si-Al-Zr alloys given in Tables 6 and 7. There are shown the data of mechanical tests on tension of alloys of different compositions made of iodide titanium in small ingots of weight P ~ 35 g and made of remelted with electron beam in the ELLU-4 facility in big ingots of weight P = 40 kg prepared with VT5 alloy scrap.

Table 6. Mechanical properties of the cast Ti-Al-Si-Zr alloys of small ingots at different temperatures.

		alloy 1a	*alloy 2a*	*alloy 3a*	*alloy 4a*
Yield stress, MPa	25	386	968	1010	-
	600	300	705	593	524
	800	-	309	285	227
Strength, MPa	25	579	1009	1055	640
	600	343	705	633	647
	800	-	393	303	262
Elongation, %, 10^{-3} s^{-1}	25	2.5	0.3	0.3	0
	600	9.5	0.2	22	2.4
	800	-	11.4	14	18

Table 7. Mechanical properties of the cast Ti-Al-Si-Zr alloys of big ingots at different temperatures.

		alloy 1b	*alloy 2b*	*alloy 3b*	*alloy 4b*	*alloy 5b*
Yield stress, MPa	25	495	-	-	-	-
	300	256	-	-	-	-
	600	219	345	103	708	-
	800	-	316	270	193	393
Strength, MPa	25	510	450	621	770	689
	300	265	475	754	786	519
	600	244	358	484	735	368
	800	-	218	337	350	412
Elongation, %, 10^{-3} s^{-1}	25	7.5	0	0	0	0
	300	7.1	0	0	0	0
	600	6.2	0.3	8.21	0.3	0
	800	-	0.8	6.5	6.1	0.8

Compositions of alloys listed in Table 6 are given in Table 2. Compositions of alloys listed in Table 7 are given in Table 3.

As follows from Tables 6 and 7, properties of small ingots are higher than of big ones. It is seen that the properties of alloys melted from iodide titanium (total content of O, N, C is <0.5%) are higher for 20-40% than alloys using titanium sponge as well as VT5 scrap. It would be noted specially that alloy 1a (Table 6) containing no Al shows plasticity 2.5%. Transition to hypereutectic alloys (alloy 5b, Table 7) leads to rough silicide morphology resulting in decreasing both strength and plasticity of alloys even at high temperatures.

1.5. INVESTIGATION OF INFLUENCE OF SILICIDE PHASE VOLUME AND ADDITIONAL ALLOYING ON MECHANICAL PROPERTIES OF THE CAST TI-AL-SI ALLOYS

1.5.1. Influence of silicide phase volume content on properties of the Ti-Al-Si alloys

Among factors determining mechanical properties of investigated Ti-Si two phase alloys, as the most significant are volume content and morphology of strengthening silicide phase.

As to the morphology, it is determined by the physical nature of alloying elements. It means that an influence on it is very complicated task. As to the amount of silicide phase particles Ti_5Si_3, it is able to be fully controlled. It is determined with silicon content in alloy. The value of it may be obtained with calculation shown in [17] as cited below

$$f \cong \frac{[Si] \cdot \rho_{\alpha ss}}{q_{Si} \cdot \rho_{Ti_5Si_3}} [vol.\%], \quad (3)$$

where [Si] is concentration of silicon in alloy, mas.%, q_{si} is weight portion of silicon in Ti_5Si_3 silicide (~0.26) [3]; $\rho_{\alpha ss}$ and $\rho_{Ti_5Si_3}$ are densities of α-solid solution and silicide respectively. As to our estimation, in Ti-Al-Si-Zr alloy studied $\rho_{\alpha ss} = 4.63$ g/cm^3 and $\rho_{Ti_5Si_3} = 3.56$ g/cm^3 according to [18]. Calculating with (3) we can obtain

$$f \cong 5[Si], \text{wt.\%}. \quad (4)$$

Thus, taking into account the formula (4) we can analyze mechanical properties of alloys in dependence on volume content of strengthening silicide phase using just silicon content in alloys as their main alloying element.

Data of mechanical tests under bending of few alloys differing with silicon are shown in Fig. 8, where clear dependence of strength and plasticity on silicon is seen: the higher silicide phase volume part, the higher strength and the lower plasticity.

Short-term (HV1-60) hardness and long-term (HV1-3600) ones show the similar dependence, namely increasing volume content of silicide phase (i.e., silicon content) leads to increasing heat resistance (Fig. 9). Influence of zirconium here needs also in additional investigation. Fracture toughness shows also the found dependence. Alloys having small content of silicon being more ductile are tougher too (Table 5).

1.5.2. Influence of additional alloying on mechanical properties of the cast Ti-Al-Si alloys.

Up-to-date heat resistant (high temperature) alloys are, as a rule, multi-component ones. It is due to necessity to meet the complex of physical-mechanical properties satisfying application of articles. Therefore, developing new materials a possibility of their additional alloying to improve that or another property is studied.

Mechanical tests of the cast Ti-Al-Si alloys show that the main shortcoming of studied alloys is their low low-temperature plasticity. As our opinion, it results, from one side, brittleness of α–solid solution due to dissolved silicon in it, and from other side, rough morphology of silicide phases in eutectic colonies.

There are known three the methods of improving such the structures:

1. additional alloying to change positively solubility of some elements both in matrix and in particles of the second phases as well as to increase surface interface energy that, as a rule, leads to modifying structure.
2. plastic deformation with hot pressing, extrusion, forging etc to crash eutectic colonies into isolated particles that leads to refining structure and improvement of mechanical properties.
3. using granular (powder) metallurgy leading to refining two-phase structure and, finally, improving properties.

Under this Project we applied only additional alloying of the Ti-Al-Si alloys.

Let us consider possibilities of additional alloying of the Ti-Al-Si alloys with selected elements:

Tin, as well as zirconium, does not practically influence on the temperature of the α↔β transformation, and increases high temperature properties of Ti alloys, especially in the presence of Al [14]. In α-Ti up to 18.6wt% (8.5at%) of Sn may be dissolved. Sn and Si do not form compounds. As usual, Sn additives are not more than 5 mas. %. As our previous work shows, Sn diminishes solubility of Si in Ti-Al-Si alloys that may have positive influence on plasticity.

Chromium, Manganese, Iron. They are as stabilizing and eutectic promoting elements those decreasing strongly temperature of the β↔α transformation, (670, 550 and 595°C respectively). Besides that these elements form together with titanium own brittle low temperature intermetallics which worsen the phase composition of alloys. Therefore, their additions are not exceed 1-3 wt.% [1, 14].

Vanadium and Niobium. These metals of VA group increasing concentration of electrons in Ti alloys must improve their heat resistance. **Vanadium** is known more as an element, which improves mainly Ti alloy plasticity. An addition of V more than 1 mas.% is not effective but α-Ti alloys use vanadium in amount 1-4 mas.%, α+β-alloys use 2-5 mas.% [14]. Alloying α-Ti-alloys with **niobium** is used rarely due to high melting temperature (2468°C). It, as a rule, does not exceed ~0.8 at. (1.5 wt.) %. Alloying Ti-Al alloys with high (more 19 at.%) amount of niobium is separate direction in modern materials science of titanium [19] and in this Project is not considered.

Gallium increases temperature of the β↔α transformation from 882 to 940°C resulting in improvement of heat resistance of α-Ti and its alloys. α-Ti can dissolve up to 22 at. (25 wt.) % of Ga [3]. Ga dissolves in β-Ti in amount up to 27 at. (30 wt.) %. Ga forms continuous solid solutions with Al and Ti_xAl_y compounds with similar structure type (x,y=1, 3) in the Ti-Al - based systems.

Germanium is, in some extent, as a chemical analog of silicon with lower melting temperature (973°C) and higher density (5.3 g/cm^3). It was found [20] that substituting silicon with germanium does not influence on phase equilibria in the system. The diagram of Ti-Ge phase equilibria is analogous of Ti-Si one. It is possible to explain analyzing binary systems Ti-Si and Ti-Ge [3]. Both systems form the same phases, Ti_5Si_3 and Ti_5Ge_3 those form β-Ti eutectics. The temperature of these eutectics are 1330 and 1325°C respectively. Temperatures of eutectoid transformations are the same also, 865 and 860°C. But there is the significant difference. In the Ti-Ge system, both transformations take place at higher content of the second component: eutectoid – at ~7 mas. % Ge, but eutectic – at 19 mas.% Ge. This circumstance leads to higher needs in the second components in the Ti-Ge system than in the respective Ti-Si system. Solubility of Ge in α-Ti at temperature of eutectic equilibria 897°C is 5.5 wt.(4.0 at.) %. Decreasing temperature leads to decrease solubility to ~3 wt.(2.2 at.) % at 600°C. At 1410°C eutectic β-Ti+Ti_5Ge_3 arises that is at ~16 at.% Ge. Practically only partial substitution of silicon with germanium is applied, though there are some patents for alloys Ti-Ge [21].

Table 8 gives data of tensile tests of alloys additionally alloyed with Cr, V, Sn, and Ge. Ingots weight was around 35 g. Initial iodide titanium was used. For comparison, Table 8 shows properties of the basic Ti-Al-Si-Zr alloy produced at the same conditions.

It is possible to assume those Ge additives in amount up to ~3% cannot be useful due to its increased solubility in α-solid solution resulting in an increased brittleness of its alloy. The interest is of additional alloying with germanium of higher amount (up to 16 at.%) to get eutectic compositions. However, higher, in comparison with silicon, density of germanium decreases, in some extent, and this interest. Nevertheless, germanium is used alloying titanium alloys with (Si-Ge) composition [3].

Data analysis of Table 8 allows to conclude the next:

1. Cr additives increase strength of the Ti-Al-Si-Zr alloys at temperatures up to 600°C and decrease it strongly at upper temperatures.
2. Vanadium additives in amount up to 4% are not effective.
3. Ge additives decrease strength and plasticity in all the temperature interval studied.
4. Sn additives influence positively on strength and plasticity.

In such a way, being based on the experimental data the only may be concluded that additional alloying of four-component Ti-Al-Si-Zr alloys with the fifth element like Ge, V, Cr does not result in improving mechanical properties of alloys, and, in the first turn, their plasticity. Alloying with Sn is worthy for further study.

Table 8. Mechanical properties of the cast Ti-Al-Si-Zr alloys additionally alloyed with the fifth elements.

Properties	Tempera-ture, °C	Ti-3Al-4Si-5Zr	Ti-3Al-6Si-7Zr	Ti-3Al-4Si-5Zr-5Sn	Ti-3Al-4Si-5Zr-3Cr	Ti-3Al-4Si-5Zr-3V	Ti-3Al-4Si-5Zr-3Ge
Yield strength, σ_{02}, MPa	25	1010	968	1040	-	960	-
	300	-	770	-	960	-	-
	600	593	705	720	689	-	473
	800	285	303	280	215	-	232
Strength, σ_b, MPa	25	1055	1009	1101	996	1030	716
	300	-	777	-	1052	-	594
	600	633	705	781	776	-	473
	800	303	393	314	235	-	263
Elongation, %	25	0.3	0.3	0.6	0.0	0.2	0
	300	-	0.1	-	0.5	-	0
	600	22	0.2	0.7	1.0	-	0.2
	800	14	11.4	29	14.2	-	34

1.6. TENSILE CREEP TESTS OF SELECTED COMPOSITIONS OF THE TI-SI BASED SYSTEM.

Two cast alloys, A – alloy 9 and B – alloy 18, were tested. Their typical structures are shown in (Fig. 10).

An ability of materials to work under loading at high temperature up to 800°C was determined with tensile tests at constant stress. According to acting in Ukraine the GOST 10145-81 standard samples of 5 mm diameter in working part were used.

Tensile samples were loaded with machine for creep testing AIMA-5-2. In a course of each sample test temperature and tensile stress were kept constant. Elongation, using displacement sensor, of samples and time till failure were measured. Using data on each sample, the full creep curves as well as diagrams of long-term strength as dependencies "stress – time to failure" were built. To build the diagrams of long-term strength 4-6 samples were tested under different constant load and temperatures 600, 700 and 800°C. The diagrams were built for 100 hours base.

Creep curves of alloy A for 600°C temperature were built for stress of 98 – 375 MPa. Loading with constant stress 200 MPa did not arise failure during 400 hours even giving residual deformation around 2%. Loading with 250MPa the creep curves show clear parts of unsteady and steady creep and failure. When increasing loading stress, all the part, typical for the creep, of curve are shortened, and it is naturally time to failure is shortened also. For example, the increase of load from 275 to 375 MPa decreased time to failure from 60 to 3 hours.

Increasing testing temperature to 700°C accelerates sharply the development of the creep processes in these alloys that shortened time intervals of all the stages. If under 100 MPa the curve has all the parts corresponding to all three creep stages, but already at 150 MPa the curve slope is such that finding two the first parts are not possible. The further grows of testing temperature to 800°C resulted in decreasing stress required for failure.

Comparison of the creep curves obtained at different temperatures evidenced clearly on the sharp increase of ability of alloy A to deformation along the final (failure) stage of creep. For example, if at the stages of unsteady and steady creeps of samples tested at 800°C and 50 MPa residual deformation reached 6-8%, the rest of residual deformation in 52-54% (general deformation is around 60%) happened namely in a course of the final failure. Similar or close ratios between values of residual deformation at stage of steady creep and final failure are typical for other creep curves, obtained at 800°C.

The creep curves of alloy 17 are qualitatively similar to ones of alloy 9. At testing temperature 600°C increasing initial stress leads to transformation of creep curves, namely the length of two the first stages is sharply shortened but the stage of final failure became prevailing one. At temperature 700°C, full the curve with the good expressed part of steady creep was obtained only at 125 MPa loading. The further growth of stress leads to shortening stage of steady creep, increasing slope of creep curve and shortening time to failure. Testing this alloy at 800°C shows sharp increasing plasticity. As in the case of testing at 700°C, when growing initial stress shortens the stage of steady creep, stage of final failure contributes its significant part in general deformation of sample.

To compare these two alloys, 9 and 17, as to their fracture resistance at creep conditions, the creep curves obtained at the same initial stresses were chosen for each testing temperature. Figure 11 gives those curves for temperature 800°C and stress 100 MPa. It is seen that curve of alloy 19 has the small portion corresponding a stage of steady creep. In that time, alloy 9 has no this stage. The stage of final failure contributes main portion in general deformation. Time to failure of this alloy was 3.5 hours instead of 5 hours of alloy 17.

Analysing these curves allows to build the diagrams of long-term strength of alloys studied at temperatures 600, 700 and 800°C (Fig. 12). As follows from the diagrams mentioned, in area of high temperatures (700, 800°C) as the best is alloy 17.

Analysis of structure alloys after long-term loading shows that alloy 9 does not show any visible changes after loading at temperature 600°C with 250 MPa for 10 hours. Being loaded with 300 MPa, grains of matrix show precipitations of supersaturated solid solution, β-layers undergo to eutectoid transformation like $\beta \leftrightarrow \alpha + Ti_5Si_3$ (Fig. 13a). At 700°C and 100-200 MPa stress the decomposition of solid solution takes place also, as well as eutectoid transformation and silicide spheroidizing. Grains of α-phase are drawn in direction of loading, some remarks of corrosion under stress may be recognized too (Fig. 13b). At increasing temperature up to 800°C, corrosion is enhanced that results in worsening metallographical picture.

Alloy B being tested at temperatures 600 and 700°C with different stresses does not reveal any metallographically visible changes in structure. But when being tested at 800°C, decomposition of solid solution and eutectoid transformation may be recognized. Corrosion is not visible (Fig. 14c).

Thus, these long-term tests show that near-eutectic alloy has the highest resistance to high temperature influence that corresponds well with data on hot-hardness.

1.7. PHASE RELATION AND PROPERTIES OF THE TI-AL-SI-GA IN THE TI-RICH REGION

The eutectic Ti-Si-Ga alloys studied early [22, 23] are found to possess higher strength at middle and elevated temperatures (200–900°C) but worse ductility at room temperature than the commercial alloy VT-18. Mechanical properties of these alloys in the Ti-rich region are formed under the influence of both dispersive and solid solution strengthening. Dispersion strengthening is caused by refractory particles of Ti_2Ga and $Ti_5(Si,Ga)_3$ phases.

Solution of about 15 at.% gallium in the titanium phase results in decrease of the silicon content in it from 4.7 at.% Si at the eutectic temperature in the binary Ti-Si system to ~1 at.% Si in the ternary system that, in its turn, results in increasing temperature of the $\beta \Leftrightarrow \alpha(\alpha')$ transformation and improving both ductility and high temperature strength.

It should be noticed too that gallium is an expensive metal. Attempts must be taken to decrease the cost of the Ti-Si-Ga eutectic alloys alloying them with aluminium.

Experimental results

17 alloys have been prepared to obtain an information on phase relations in the Ti-Al-Si-Ga system. They were melted in the sections of Ti-10Si-5Ga-Al, Ti-10Si-10Ga-Al and Ti-5Si-5Ga-Al. A few alloys that contained 3 at.% Si were prepared also. Compositions and temperatures of phase transformations of the alloys through section Ti-10Si-5Ga-XAl (X=5, 10, 15,20,25,30,35 (ат.%)) are given in Table 8. Table 9 shows phase composition of the as-cast alloys. All alloys were annealed at 1350 °C during 33 hours. Table 10 shows phase composition of the annealed alloys. On the base of the experimental data elements of the Ti-Si-Ga-Al phase diagram through Ti-10Si-5Ga-Al and Ti-10Si-10Ga-Al sections were constructed. They are shown in Fig. 14 and Fig. 15. The data obtained are given in comparison with eutectic line in the Ti-Si-Al system [12].

Microstructures. In alloys that lie in the section of Ti-10Si-5Ga-Al at 5, 10 and 15 at.% aluminium contents both as-cast and annealed ones, have two-phase structure ($z + \beta^*$) (Tables 9 and 10). The annealed alloys with 20 and 25 at. % Al (Fig. 16 a, b) contain silicide grains and titanium matrix with traces of the phase transformations. Appearance of the γ-phase in that alloys according to the X-ray diffraction (XRD) data indicates that the $\beta \rightarrow \alpha \rightarrow \gamma$ transformation in solid state occurs at cooling. Morphology of the fine-dispersive eutectic in the alloys with 25 and 30 at.% Ga (Fig. 16 c, d) differs from morphology of the eutectic $\beta^* + z$. X-ray patterns of these alloys contain reflexes of the γ-phase (Table 9). Hence crystallization of these alloys complete the formation of the ternary E ($\beta^* + \gamma + z$) eutectic. Both the as-cast and annealed alloys with 35 at.% Al (Fig. 16 e, f) are two-phase ones, $z + \gamma$ (Tables 9, 10). The light microscopy structure of this alloy and X-ray data point out the existence of the eutectic reaction $L \Leftrightarrow z + \gamma$. It should be noticed that in the annealed alloys with 20 and 25 at.% Ga, and in the as-cast alloys with 20, 25 and 30 ат.% Ga, the Ti_2Ga – phase may be found. It forms from β-phase at cooling in solid state.

Titanium phase crystallizes primarily only in the Ti-10Si-5Al-5Ga alloy (Fig. 16 g). All other alloys have silicide primary phase (z) (Fig. 16 c, d, e, g, h, i, j, k). The as-cast and annealed alloys in the Ti-10Si-10Ga-Al section with 5 and 10 at.% Al are two-phase ones, ($z + \beta^*$). According to their X-ray data, the as-cast alloys with 15 and 20 at.% Al (Fig. 16 k) are three-phases ones, $z + \chi + \gamma$. After annealing the reflexes of the α-phase there were found. The presence of the χ- and α-phases can be explained with transformation of the β-phase in solid state at cooling. Fine dispersive eutectic, the morphology of which differs from morphology of the eutectic $z + \beta^*$ (Fig. 16 g, h, i, j) jointly with the XRD data (Table 9) indicate on the existence of the ternary eutectic $\beta^* + \gamma + z$ in these alloys. In correspondence with metallography and XRD of these alloys with 25 and 30 ат.% Al (Table 8, 9) they contain eutectic $z + \gamma$. Alloys with 20, 25 and 30 at. % Al were melted for annealing at 1350 °C. Hence, in these alloys β^*-, γ- and z-phases at 1350 °C are in the equilibrium with the liquid phase.

DTA data: Temperature maximum at 1500 °C in the alloy № 4 (Ti-10Si-5Ga-Al) corresponds to the quasi monovariant eutectic reaction $L_{e(max)} \Leftrightarrow \beta + Ti_5(Si, Al, Ga)_3$ on Liquidus and area of the maximum temperatures in the $\beta + Ti_5(Si,Al, Ga)_3$ region on Solidus.

XRD data: Fig. 17 a, b show the concentration dependencies of the lattice parameters (LP) of the silicide phase ($Ti_5(Si, Al, Ga)_3$) of the annealed at 1350 °C alloys in the Ti-10Si-5Ga-Al section. Curves of the LP "a" and "c" demonstrate the maximum at 5 at.% Al. Then LP is increased from 5 to 25 at.% Al passing through minimum at 10 at.% Al and is decreased from 25 at.% Al. Thus, LP is the largest in the alloys with 5 and 25 at. % Al. Therefore, the total solubility of Al + Ga in the alloys via the section Ti-10Si-5Ga-Al in silicide is highest at 5 and 25 at.% Al.

Mechanical properties of the alloy Ti-5Si-5Ga-20Al: The eutectic Ti-5Si-5Ga-20Al alloy was chosen to estimate mechanical properties of the quaternary alloys (Fig. 18). It consists of titanium primary grains and $\beta + Ti_5(Si, Al, Ga)_3$ eutectic. Temperature dependencies of its short and long-term hot hardness ($HV_{1\text{-}60}$ and $HV_{1\text{-}3600}$) of this alloy is shown in Fig. 19 and 20. As it is seen, hot hardness of the alloy № 3 (Ti-5Si-15Ga) at 25-300 °C is essentially higher than of the Ti-5Si-5Ga-20Al alloy, but at the temperatures 700 - 900 °C long-term hardness of the Ti-5Si-5Ga-20Al alloy is considerably higher than of the ternary alloys. For example, at 900 °C long-term hardness of the Ti-5Si-5Ga-20Al alloy about three times higher than hardness of the Ti-5Si-15Ga alloy.

This result may be explain with increasing of the $\beta \Leftrightarrow \alpha$ transformation temperature and temperature of solidus, i.e. temperature of the eutectic reaction $L \Leftrightarrow \beta + Ti_5(Si, Al, Ga)_3$ (Table 8). On the other hand alloying with gallium result in decrease of silicon content in the eutectic that may be favorable for the ductility.

In such a way, the only might be concluded that observed similarity in a constitution of the phase diagrams of ternary systems Ti-Si-Al and Ti-Si-Ga, and the quaternary Ti-Si-Al-Ga system in their Ti-rich corners consists in the existence of the wide two-phase β-Ti + Ti_5Si_3 region formed in a course of the three-phase $L \Leftrightarrow \beta + z$ eutectic reaction. All systems have an area of the maximal temperatures in that region. Alloying with 5 at.% Ga leads to shift of the area of the highest temperatures in the side of the little contents of aluminium and silicon, moreover the temperatures of solidus decrease. Increase of the gallium content up to 10 at.% result in still more shifts the eutectic surface to the Ti-Al-Ga side and decreases of the solidus temperatures. In the area under investigation we observed reactions with participation of the following phases: α, β, z, and γ: $L + \beta + z$, $L + \gamma + z$ and $L + \beta + z + \gamma$. We can suppose existence of the 5-phases nonvariant equilibrium $L + \alpha + \beta + z + \gamma$. It arises due to three four-phase equilibria: $L + \alpha + \beta + z$, $L + \alpha + z + \gamma$ and $L + \alpha + \beta + \gamma$. Volume from four solid phase $\alpha + \beta + z + \gamma$ and volume with liquid phase $L+ \beta + z + \gamma$ are arisen due to noticed 5-phases nonvariant equilibrium.

On the base of the preliminary data about structure and hardness of the Ti-Si-Ga-Al alloys we can recommend the area of the compositions that is promising for the further inquiry. This is area when monovariant quasi eutectic reaction between β-Ti and $Ti_5(Si, Al, Ga)_3$ realises. The recommended contents of silicon are 4-6 ат.%.

Table 8. Structure of Ti-Si-Ga-Al alloys and temperature of phase transformations.

№ alloy	Composition, at.%				Structural constituents of the as-cast alloys	Temperatures of the phase transformations, °C		
	Ti	Si	Ga	Al		T_{ss}	T_s	T_l
1	80	10	5	5	<β*> + e			
2	75	10	5	10	<z> + e_1	1030, 1245	1435	1585
3	70	10	5	15	z + e_1	1250	1470	1610
4	65	10	5	20	z + e_1	1080 1190	1500	1530
5	60	10	5	25	z + E	1150 1185	1445	1490
6	55	10	5	30	z + E		1380	
7	50	10	5	35	z + e_2	1230	1390	1405
8	75	10	10	5	<z> + e_1			
9	70	10	10	10	<z> + e_1			
10	65	10	10	15	<z> + e_1 + E			
11	60	10	10	20	z + E			
12	55	10	10	25	<z> + e_2			
13	50	10	10	30	<z> + e_2? or just e_2			
47	85	5	5	5	β* + <e_1>			
48	80	5	5	10	β* + <e_1>			
49	75	5	5	20	β* + e_1	1200	1510	
40	87	3	5	5	β*			
44	67	3	10	20	β* +<e_1>			
45	61	7	7	25	z + e			
46	65	7	18	10	z + e			

β – a phase on (β-Ti)- base, which was transformed to α(α') during cooling;
z – solid solution on the Ti_5Si_3 compound base;
γ – solid solution on the TiAl-base;
e – binary eutectic;
E – ternary eutectic;
T_{ss} – temperature of the solid state transformation.

Table 9. Lattice parameters of the as-cast Ti-Si-Al-Ga alloys.

Composition, at.%				Phase composition according to XRD	Phase	Lattice parameters, nm		c/a
Ti	Si	Ga	Al			a	c	
80	10	5	5	α + z	α	0.2920(2)	0.4655(5)	1.594
					z	0.7523(9)	0.5182(6)	0.689
75	10	5	10	z + α	α	0.2901(2)	0.4654(3)	1.604
					z	0.7513(9)	0.5167(9)	0.688
70	10	5	15	z + α	α	0.2899(6)	0.4630(9)	1.597
					z	0.7512(9)	0.5176(9)	0.689
65	10	5	20	z + χ	z	0.7495(3)	0.5180(6)	0.691
					χ	0.4541(3)	0.5558(8)	1.224
60	10	5	25	z + γ + χ	χ	0.4551(4)	0.5562(5)	1.222
					z	0.7512(9)	0.5160(9)	0.686
					γ	0.4003(3)	0.4068(7)	1.016
55	10	5	30	z + γ + χ	χ	0.4554(3)	0.5566(6)	1.222
					z	0.7489(4)	0.5167(9)	0.690
					γ	0.3984(3)	0.4067(5)	1.021
50	10	5	35	z + γ	z	0.7500(5)	0.5188(6)	0.692
					γ	0.3989(4)	0.4079(5)	1.022
65	10	10	15	z + χ + γ	z	0.7496(6)	0.5187(8)	0.692
					χ	0.4531(3)	0.5534(8)	1.221
					γ	0.4007(3)	0.4062(5)	1.014
60	10	10	20	z + χ + γ	z	0.7505(6)	0.5182(9)	0.690
					γ	0.4010(2)	0.4029(7)	1.005
					χ	0.4531(3)	0.5530(9)	1.220
55	10	10	25	z + γ	z	0.7505(8)	0.5189(9)	0.691
					γ	0.3992(3)	0.4046(4)	1.013
50	10	10	30	z + γ	z	0.7517(9)	0.5147(9)	0.685
					γ	0.3980(2)	0.4055(2)	1.019
69	7	7	25	z + χ	z	0.7503(8)	0.5185(6)	0.691
					χ	0.4531(3)	0.5562(5)	1.221
65	7	18	10	z + χ	z	0.7548(8)	0.5165(6)	0.691
					χ	0.4521(3)	0.5548(5)	1.221

Table 10. *Lattice parameters in the annealed at 1350 °C Ti-Si-Al-Ga alloys.*

Composition, at %				Phase composition according to XRD	Phase	Lattice parameters, nm		c/a
Ti	Si	Ga	Al			a	c	
80	10	5	5	$\alpha^* + <z>$	α	0.2917(2)	0.4651(4)	1.594
					z	0.7522(9)	0.5190(9)	0.690
75	10	5	10	$z + \alpha^*$	α	0.2907(2)	0.4638(5)	1.595
					z	0.7501(6)	0.5167(8)	0.689
70	10	5	15	$z + \alpha_2^*$	α_2	0.5771(3)	0.4632(4)	0.803
					z	0.7499(9)	0.5173(9)	0.690
65	10	5	20	$z + <\alpha>^* + \gamma^{**} + + \chi^*$	z	0.7521(3)	0.5199(3)	0.691
					γ	0.4003(5)	0.4076(9)	1.018
					χ	0.4545(2)	0.5536(6)	1.218
60	10	5	25	$z + <\alpha>^* + \gamma^{**} + + \chi^*$	z	0.7526(6)	0.5211(7)	0.692
					γ	0.4004(9)	0.4040(9)	1.009
					χ	0.4515(7)	0.5537(9)	1.226
55	10	5	30	$z + \gamma$	z	0.7509(7)	0.5187(8)	0.691
					γ	0.3997(4)	0.4071(4)	1.018
50	10	5	35	$z + \gamma$	z	0.7502(9)	0.5178(9)	0.690
					γ	0.3990(7)	0.4081(9)	1.022
75	10	10	5	$z + \alpha^*$	α	0.2907(3)	0.4630(4)	1.593
					z	0.7481(9)	0.5157(5)	0.689
70	10	10	10	$z + \alpha^*$	α	0.2883(2)	0.4642(3)	1.610
					z	0.7522(5)	0.5208(6)	0.692
65	10	10	15	$z + <\gamma>+ \chi^* + +<\alpha>$	α	0.2907(9)	0.4619(9)	1.589
					z	0.7528(4)	0.5214(5)	0.692
					χ	0.4529(5)	0.5542(5)	1.223
					γ	0.4010(7)	0.4079(9)	1.017

1.8. CONCLUSIONS TO CHAPTER I.

1. In the Ti-Si-Al system, alloys containing around 4-6 wt.% Si and additionally alloyed with Zr of 6-9 wt.% are the most heat resistant. Al content of 2.5~3.0 wt.% ensures the best ratio between plasticity and heat resistance. Increasing Al content leads to increasing of heat resistance and decreasing plasticity.

2. Purification of initial materials (iodide titanium instead of sponge one or scrap) leads to increasing both strength in 1.7 times and plasticity from zero to 0.3%.

3. 2% and more plasticity at room temperature was obtained with the Ti-Si-Zr alloys (with no Al), but absence of Al decreases their strength.

4. Comparison of small and big ingots showed that small ingots have homogeneous structure with small grains that results in increasing both strength and plasticity.

5. Among the studied group of the Ti-Si-Al-Zr alloys additionally alloyed with the fifth element (Sn, Cr, V, Ge, Y), the tendency of increasing plasticity is observed in them only with Sn.

6. Measuring hot-hardness and creep showed that the Ti-Si-Al system alloys studied exceed commercial heat resistant titanium alloys in the region 600-900°C.

7. Increasing heat resistance of the Ti-Si-X systems with additional Ga results from both alloying Ti_5Si_3 with Ga and arising Ti_2Ga phase when Ga content is more than 10%. Comparatively high hot-hardness of Ti-5Si-5Ga-20Al alloy is connected more with high content of Al.

CHAPTER II. STRUCTURE AND PROPERTIES OF THE TI-B-X – ALLOYS.

Among titanium alloys the commercial alloy Ti-6Al-4V (mas.%) attract special attention due to high strength characteristics that are achieved with phase transformation in solid. In equilibrium state at temperature higher than 1000°C its phase composition is β, and at lower temperature it is α+β. Sufficient strengthening can be achieved with thermal treatment. Quenching from 900-950°C results in formation of metastable α' and β-phases, which decompose in aging (450-500°C, for 2-4 h) in to dispersed mixture of stable α and β phases [24, 25].

To our mind, more strengthening may be expected due to the boron alloying up to the content, at which an eutectic crystallization is possible. In this case a boride should form dispersed eutectic with titanium phase, strengthening the alloy.

Goal of the present work is to investigate phase equilibria in the systems that bounding the Ti-Al-V-B quaternary and including the Ti-B one as boundary in temperature range of crystallization of ternary alloys and in titanium-rich fields, as follows: the system Ti-V-B at boron content up to 20 at. % and the Ti-Al-B in the range of 6Al and 0-2 B (mass %). In the course of the work to investigate structure of the as-cast alloys and to determine processes occurring at them crystallization, to construct portions of solidus and liquidus surface projections, as well as to reveal relationship of structure and high-temperature hardness (that is selected as strength characteristic) for the Ti-V-B, Ti-Al-B and Ti-Al-V-B alloys.

2.1. STATE OF INVESTIGATION ON PHASE EQUILIBRIA IN THE TI-V-B, TI-AL-B, TI-AL-V AND TI-AL-V-B SYSTEMS

The binary phase diagrams for the systems, blundering the quaternary, were taken from handbook [26], for the exception of the Ti-Al that is from [27, 28].

Crystal structures of unary and binary phases are presented in Table 11, and coordinates of invariant points of the binary systems are in Table 12.

The Ti-V-B system

The phase equilibria in the Ti-V-B system were studied in the only work [29]. Samples of the ternary alloys (Fig.21) were studied with metallography and X-ray analysis after annealing at 1400°C for 100 h. The alloys were melted in arc furnace under argon using boron of 99.3 % purity, vanadium of 99.5 % and titanium of 99.9 %.

No ternary compound is found in the system. The continuous solid solution exists between the isostructural compounds TiB and VB_2. Solubility of vanadium in TiB is 25 at. %, the compound VB dissolves up to 15 at. % Ti, and solubility of titanium in V_3B_2 is equal to 15 at. %, too. Solubility of titanium in the compound V_3B_4 is little. No other boride phase was found at this temperature in [29], including Ti_3B_4, known in that time. From the [29] data the lattice parameters of VB phase in the alloy $Ti_{15}V_{35}B_{50}$, which composition corresponds to maximal solubility of titanium in VB, are a = 311, b = 819, and c = 445 pm, i.e. they decrease in comparison with the lattice parameters of VB. Solubility of vanadium in TiB causes decrease of its lattice parameters to a = 592, b = 300, and c = 445 pm. Presented data are in good agreement with the sufficient difference of metal components, titanium (r_{Ti} = 146 pm) and vanadium (r_V = 135 pm).

Thus, data on the Ti-V-B ternary system are limited by the only reference [29]. Taking into account that the modern phase diagrams of the binary Ti-B and V-B systems have become more complex, the correction of the 1400°C phase diagram is needs in the region content of the more 50 at. % B. At less boron content (namely, in the Ti-TiB-V_3B_2-V region, in which our research was concentrated), the [29] data may be used in further investigation of the system.

The ternary Ti-V-B system is not studied entirely at temperatures close to start of melting (i.e. on solidus). There are no data on liquidus of the system and reaction, occurring at crystallization of alloys. So, new data on the Ti-V-B phase diagram will be, obtained on studying the influence of vanadium on structure and properties of the eutectic alloy $Ti_{91.4}B_{8.6}$.

The Ti-Al-B system

Assessment of [30] and [31] data indicate the Ti-Al-B ternary system was studied only in Al-corner. [32] presents the partial isothermal section Al-Al_3Ti-AlB_{12} at 1000°C. And in [33,34] the phase equilibria in the Al-AlB_2-TiB_2 region were investigated.

Thus, phase equilibria in the Ti-corner of this system are not known.

The Ti-Al-V system

In the most references of wide bibliography on the ternary Ti-Al-V system the only question is considered that deals with the alloy Ti-6Al-4V (mass %), as well as studying dependence of its microstructure from thermal history and testing mechanical properties.

Assessment of literature on phase equilibria in the Ti-Al-V system was made by F.H.Hayes [35]. Presented in [35] the solidus projection and isothermal sections at 1400, 1200, 1100, 1000, and 800°C are result of assessment of large quantity of data from different works.

The Ti-Al-V-B system

The quaternary Ti-Al-V-B system is not studied.

2.2. EXPERIMENTAL INVESTIGATION OF PHASE DIAGRAM ELEMENTS

The starting materials and preparing alloys

Iodide titanium (99.99 mass %), amorphous boron (99 mass %), vanadium (99.9 mass %), aluminium (99.99 mass %), master alloy TiB_2 (67.7 Ti; 30.0 B; 0.7 C; 0.6 Fe; 0.52 O; 0.0005 mass % N), and master alloy Ti-B (~2 B; 0.050 O; 0.0005 mass % N).

Ternary alloys of 10 g mass were prepared by arc melting with a nonconsumable tungsten electrode on a water-cooled Cu hearth under an argon atmosphere that had previously been gettered by melting Ti for 3 min.

The alloys were prepared from the metals and master alloy Ti-2B (mass %), which was melted from titanium and TiB_2. For some alloys the oxygen and nitrogen contents were determined (Table 13).

Experimental methods: light metallography, XRD, microhardness after Vickers and hot hardness, and DTA (using a string thermocouple W/W-20Re (80 mass % W and 20 mass % Re), which was calibrated against the JPTS-90 reference points).

2.2.1. Investigation of the Ti-V-B system in the Ti-TiB-V_3B_2-V region

Table 14 presented nominal compositions of alloys under studying and mass losses on melting, that accounted for both the component evaporation at overheat and mechanical losses. So long as the total losses were not more than 0.8 %, the nominal alloy compositions were adopted.

2.2.1.1. Investigation of the alloys with metallography

The all melted Ti-V-B alloys were studied with metallographic analysis. Table 15 presents structure components of the alloys and phases crystallized primary.

The microstructure of the binary $Ti_{91.4}B_{8.6}$, given in Fig. 22a, indicates that its composition is hypereutectic (in agreement with the binary phase diagram), but close to the eutectic (Ti)+(TiB) composition. Grains of the primary-crystallized phase have high microhardness, ~24 GPa and were identified by us as the titanium boride TiB. The later crystallized eutectic consist of two components, boride TiB, as needlelike thin particles, and metal (Ti), which is refining as a result of polymorphous $\beta \leftrightarrow \alpha$ transformation (that is in agreement with a phase composition from XRD - α+TiB).

Microstructure of the ternary alloys, containing about 9 at. % B and a variety of vanadium contents of 5 to 40 at. %, indicates that their compositions are close to the line corresponding to the monovariant joint eutectic crystallization of metal and boride phases (Figs. 22 b, c and 23 a).

In the alloys containing 5 at. % B the primary crystallized phase is one based on β-Ti which was transformed to (α-Ti) at cooling. So, in Fig. 23 b one can see dendrites of the phase based on titanium, among those the (Ti)+(TiB) eutectic crystallized. And micrograph of the alloy with boron content of 13 at. % exhibits characteristic grains of the phase based on TiB, which are distributed in the eutectic matrix (Ti)+(TiB).

Thus, on the liquidus of the Ti-V-B ternary system the monovariant curve corresponding to joint eutectic crystallization of boride (TiB) and metal (Ti) phases runs at the unchangeable boron content of about 9 at. %, from the composition of the binary eutectic in the Ti-B system to the composition of the alloy containing 40 at. % V. That is the vanadium addition to the eutectic binary alloy $Ti_{91.4}B_{8.6}$ almost do not have an effect on volume fraction of (TiB) in the eutectic (Ti)+(TiB) in the ternary alloys comparing with the binary ones, where it is 13 vol. %.

On the liquidus surface the e_2U_2 curve separates the fields of primary crystallization of (Ti) and (TiB) phases (Fig. 24). On the liquidus from the side of another boride system V-B the curve e_1U_2 of joint eutectic crystallization of (V) and (V_3B_2) phases begins in the point e_1. The curve passes through the alloy composition $Ti_{25}V_{60}B_{15}$ and near the alloy composition $Ti_{38}V_{49}B_{13}$, separating the fields of primary crystallization of (V, Ti) and (V_3B_2) phases.

Microstructure of the $Ti_{45}V_{38}B_{17}$ alloy indicates that the peritectic type reaction between primary boride phase and liquid takes place in crystallizing. From XRD data the alloy is three-phase β + (V_3B_2) + (TiB).

2.2.1.2. Investigation of the alloys with XRD

Phase composition and lattice parameters of the as-cast Ti-V-B alloys from XRD data are presented in Table 16.

The binary as-cast alloy $Ti_{91.4}B_{8.6}$ is α+TiB from XRD data, that is the β-phase is not quenched in cooling and is transformed to α. The vanadium additions of 5 to 15 at. % favor partial quenching β-phase, with its amount increasing (in the alloys containing 20 at. % V and 5 and 9 at. % B only β-phases reflexes were detected).

As the vanadium content in the alloys grows, the lattice parameters decrease, that is connected with the less atomic vanadium radius (134.6 pm) in comparison with titanium one (146.2 pm). The binary alloy Ti-V containing 30 at. % V, consists of β -phase with lattice parameter a = 320.8 pm. Fig. 25 shows the lattice parameters of β-phase as a function of the vanadium content for the binary Ti-V alloys after [36] data. For the pure vanadium used the lattice parameter is a =

302.9 pm, being in agreement with literature. Extrapolation of the linear concentration dependence of $a_{\square}$ as function of the vanadium content to titanium side results in a = 328.6 pm, which is in god agreement with literature a = 328.4 pm.

So long as the boron solubility in titanium and vanadium are negligibly little, there is no reason to expect them to be appreciable in the Ti-V alloys. That's why the dependence of Fig. 25 may be used for estimation of the β-phase composition, being in equilibrium with (TiB) in the ternary alloys, with the estimated compositions relating to subsolidus temperatures.

2.2.1.3. Investigation of the alloys with DTA

The results of DTA investigation are presented in Table 17. It is seen that the start temperatures of melting (solidus temperatures) of the ternary alloys are less than those of the binary. So, as the vanadium content grows, the solidus temperatures decrease from 1500°C for the binary alloy $Ti_{91.4}B_{8.6}$ to 1430°C for the alloy $Ti_{58}V_{33}B_9$. The latter is the minimal solidus temperature in the concentration range under investigation. The two-phase alloy $Ti_{51}V_{40}B_9$, containing more vanadium, has a little higher solidus temperature, 1432°C, and the temperature of the three-phase (V_3B_2)+(TiB)+ β ones is equal to 1445°C. Thus, one see that in the two-phase (TiB)+ β region there exist the minimum in solidus surface. This minimum in the ternary system reflects the minimum in the solidus and liquidus of the β solid solution in the Ti-V system The solidus temperature obtained for the Ti-V-B alloys were used for construction of the solidus and liquidus surfaces in the region Ti-TiB-V_3B_2-V.

2.2.1.4. The investigation of alloys by microdurometric analysis

The microdurometric data on the as-cast alloys of the Ti-V, Ti-B, V-B binary systems and Ti-V-B ternary system are summarized in the Table 18.

The boride phases V_3B_2 and TiB have sufficiently higher microhardness ~30 and ~24 GPa, respectively, than the metallic phase based on titanium (~2 GPa). The composition of alloy $Ti_{91.4}B_{8.6}$ is close to the binary eutectic (Ti)+TiB, and microhardness of eutectic colonies in it (3.5 GPa) is higher than that for titanium phase, due to presence of the hard ingredient (TiB) in this eutectic.

The microhardness of the (Ti)+TiB eutectic colonies sufficiently increases with additions of vanadium (up to ~5 GPa, in 1.5 times as many as in the binary system), and microhardness stays high up to the vanadium content of ~17.5 at. % (Fig. 26). At the high vanadium content (22 at. %) the microhardness decreases to initial level of ~3.5 GPa and stays on the level of ~3.25 GPa for the alloys with vanadium content of 25 to 40 at. %.

From the XRD data (Table 18) one can see that at the vanadium low content (5 at. %) the phase composition of the alloys is α+TiB, at the vanadium content of 10 to 15 at. % it is α +β+TiB, and at 20 at. % V it is β +TiB. The alloys containing α and β titanium phases together with the TiB phase have the highest microhardness.

Thus, both the boride component and metallic component have an influence on the microhardness of the eutectic colonies. The contribution of the boride phase is approximately unchanged and is not dependent on vanadium content, because the volume fraction of the (TiB) in the eutectic (TiB)+(Ti) is almost constant (Fig. 26). The contribution of the metallic phase is changed as a function of vanadium content, because the latter influences on the phase composition of the metal component of the eutectic: α, α + β or β. The curve 3 in the Fig. 26 evidently confirms above written. This curve shows the concentration dependence of microhardness of metallic phase for the alloys with the boron content of 5 at. %. The microhardness of the phase based on titanium in the composition range of 5 to 20 at. % V are maximal.

2.2.1.5. Total characterization of the Ti-V-B ternary system in the Ti-TiB-V_3B_2-V region.

Our experimental results and the literature data on phase equilibria in the ternary system at 1400 °C [29] allow to present the phase equilibria in this system at solidus temperature.

The DTA data (Table 17) indicated that the starting melting temperature of the ternary alloys in the Ti-TiB-V_3B_2-V region is close to 1400°C (higher by 30-80°C). That's why the phase equilibria on solidus are considered close to the phase equilibria at 1400°C.

The solidus surface projection of the ternary system in the Ti-TiB-V_3B_2-V region are presented in Fig. 27. The extent of the homogeneity range of the boride phases were accepted from [29]. The phases composition of alloys was determined by XRD and metallography analyses. The tie-lines in the (TiB)+(Ti,V) and (V_3B_2)+(V,Ti) two-phases regions pass through the

compositions of alloys and composition of the metallic phase. The compositions of the metallic phase were calculated from composition-lattice parameter ratio for β-phase (Fig. 25). The solidus temperatures on the tie-line and the isothermal plane are quoted from DTA data. The peculiarity of the solidus surface is existence of minimum in the ruled surface of (TiB)+(Ti) region at 1430°C and presence of the isothermal tie-lines triangles (V_3B_2)-(TiB)-(Ti,V) at 1445°C.

The liquidus surface projection (the ranges of the primary crystallization of phases) is presented in Fig. 24 according to the data of XRD and metallography analyses. The invariant three-phase equilibria of the eutectic type $Le_3 \leftrightarrow$(TiB)+(Ti,V) at 1430°C corresponds to the tie-line with minimum temperature on the solidus surface. The three-phase tie-line triangle (V_3B_2)-(TiB)-(Ti,V) on the solidus surface corresponds to the invariant four-phases equilibria of the incongruent type $Lu_2+(V_3B_2) \leftrightarrow$ (TiB)+(Ti,V) at 1445°C. The reaction scheme at crystallization of the Ti-V-B alloys is presented in Fig. 28.

2.2.2. The investigation of the Ti-Al-B system

The influence of the boron on the Ti-6Al (mass %) alloy was investigated. The XRD, DTA and metallography data for this binary alloy are in good agreement with the phase diagram of the Ti-Al binary system [27]. The composition of the investigated alloys are shown in the Table 19.

Data about phase composition of as-cast ternary alloys (Table 20) bring in evidence that all these alloys contain the phase based on the α-Ti as phase component, which formed as a result of α ←→β transformation of the titanium solid solution (Table 21). The lattice parameters of the α -phase do not change with boron contents in alloys and are equal to $a_\alpha = 293.3 \pm 0.3$ and $c_\alpha = 468.2 \pm 0.5$ pm. This show the little boron solubility in the (Ti,Al) solid solution.

From the XRD data the boride phase TiB is not observed in alloys with little boron content (to 0.1 mass %), but identified in alloys with boron contents of 0.5-2 mass %.

The microstructure of alloys with boron content of 0.1-1 mass. % (Fig. 29) exhibits the primary-crystallized β-phase, between dendrites of those the (Ti)+TiB eutectic is crystallized. The amount of the boride phase increased with increased boron content. The primary-crystallized phase was not already observed in the microstructure of alloys with boron contents of 1.5 and 2 mass % (Fig. 30), that is the compositions of these alloys are close to the monovariant curve of co-crystallization of the metals and boride phases.

The start temperatures of melting the Ti-Al-B alloys decrease from 1600°C for the $Ti_{90}Al_{10}$ (94Ti-6Al, mass %) binary alloy to 1528 ± 2°C for the all ternary alloys that bring in evidence that the compositions of these alloys are close to the tie-line TiB-$Ti_{90}Al_{10}$ (Fig. 31). The solidus temperatures decrease from the Ti-Al-B ternary system to the temperature of eutectic $L_e \leftrightarrow$ (Ti) + TiB in the Ti-B binary system that is equal to 1500°C.

The microhardness versus boron content in the alloys (Fig. 32) indicates that the microhardness increases with increasing boron content almost in twice in compare with 94Ti-6Al (mass %) metal alloy.

2.2.3. The investigation of the Ti-Al-V-B system quaternary alloys.

The influence of the boron on the structure and properties of the ternary alloy Ti-6Al-4V (mass %) was investigated. The boron content in the quaternary alloys was from 0.01 to 2.5 mass % (Table 22). From XRD data (Table 23) the basis as-cast alloy consists of only α-phase, and from metallography it has martensite structure (Fig. 33). The boron addition of 0.01-0.05 mass % visibly do not influence on phase composition and microstructure of the alloys. Separation of the boride phase was not observed at magnification up to 750. The alloys with boron content of 0.1 and 0.5 mass % show the primary β dendrites with decomposition structure and intergranular structure that is easy etched. The boride phase (TiB) together with α-phase were identified in the alloys with the boron content of 0.5 mass % to 2.5 mass %. Even and refining microstructure of these alloys indicated on the congruent joint crystallization of the boride and metal phases (Fig. 34).

The lattice parameter a_α of the quaternary alloys has tendency to increasing in dependence on the boron content. The β-Ti phase along with boride and α–phases were identified in the alloys with 1.75-2.5 mass % B, but amount of this phase is little (the intensity of the reflection is faint, that lead to large error in calculation of the lattice parameters a_β).

The temperatures of the phase transformation for the quaternary Ti-Al-V-B alloys are given in Table 24. The melting temperature of alloys versus boron content sharply decreasing from 1645°C for the Ti-6Al-4V (mass %) ternary alloy to 1515°C at the boron content of 0.1 mass %, and does not change at further increasing boron content (from 0.1 to 2.23 mass

%). The alloy with 2.5 mass % B has the minimal melting temperature 1505°C. Our data show that the quaternary alloys with boron content of 0.1 to 2.25 mass % are in the same isothermal volume on the solidus.

2.3. MECHANICAL PROPERTIES OF THE TI-B-X ALLOYS.

The measurements of Vickers hardness at the temperature interval from the room temperature up to 800°C in vacuum 10^{-3} Pa at the load 10N and exposure under the indentor about 1 min were chosen as a criterion for the estimation of mechanical properties of cast alloys.

2.3.1. The Ti-B-V system

Some data on the eutectic of titanium and boride phases are in literature. The unidirectionally solidified (Ti)+(TiB) eutectic does not exhibit the significant increase of strength characteristics as was shown at the work [37]. It is responsible for the low volume content of the reinforcing phase (according to the calculated data it is 7.7 vol. %) as the authors consider. The additions of 14 and 21 vol. % TiB to $Ti_{83}Mo_{17}$ matrix enhance the stiffness, yield stress and work hardening behavior at room temperature and lower the creep rate at 600°C according the data of the work [38].

The temperature dependence of hardness of the initial eutectic alloy $Ti_{91.4}B_{8.6}$ is shown by the curve 1 in Fig. 35. The volume content of reinforcing boride phase in this alloy corresponds 13 vol. % (as we have calculated), the hardness of the alloy in the low temperature region is amply high, that is why this alloy is of the interest for further investigations. The alloying by 5 at. % V (curve 2) causes the marked growth of the hardness of the alloy it the temperature interval from room temperature to 400°C (by 0.75-0.8 GPa in comparison with initial $Ti_{91.4}B_{8.6}$ alloy). Such growth of the hardness is explained by strengthening of metallic matrix with alloying by vanadium. The significant drop of the hardness is noted at the temperatures above 400°C and at 800°C the hardness of eutectic alloy (Ti)+(TiB) alloyed by 5 at. % V does not distinguish from initial.

The further significant (two times in comparison with initial) increase of the hardness up to 3.5-4 GPa takes place at the temperature region below 400°C with increasing of vanadium content in eutectic (Ti)+(TiB) alloy to 10 and 15 at. %. It is by 1-1.5 GPa higher than in the alloy $Ti_{86}V_5B_9$ (curves 3, 4 of Fig. 35). So long as the volume content of the reinforcing phase in the eutectic of the Ti-B and Ti-B-V alloys may be considered as close to 13 vol. %, the sharp growth of the hardness with addition of 10 and 15 at. % V, obviously, is to be connected with variation of phase composition of titanium matrix of the alloys - (α+β). The sharp drop of the hardness of the $Ti_{81}V_{10}B_9$ and $Ti_{76}V_{15}B_9$ alloys up to the values practically corresponding to the hardness of the $Ti_{91.4}B_{8.6}$ alloy is noted as the temperature rises above 400°C.

The matrix of eutectic alloy (Ti)+(TiB) is a solid solution on the β-phase base with the growth of vanadium content to 20 at. %. The hardness decreases in all temperature interval under investigation (curve 5) and practically does not differ at the corresponding temperatures from the hardness of the (Ti)+(TiB) alloy alloyed by 5 at. % V. The powder composites Ti-TiB on the β-titanium base was also shown to have the tensile strength lower than Ti-TiB composites on the (α+β) base [39].

The complex character of some curves of the temperature dependence of hardness it the region of low temperatures is explained by some aging process in heating as well as by effect of dynamic deformation aging, perhaps.

The similar influence of the alloying by vanadium has an effect on the temperature dependence of the hardness of hypoeutectic alloys containing 5 at. % B (Fig. 36). The lower values of the hardness of the alloys it the temperature interval from room temperature to 400°C cause the lower volume content of the reinforcing boride phase in this group of alloys. The maximal hardness is also noted in the alloys with 10 and 15 at. % V where the matrix is (α+β).

The increase of boron content to 13 at. % in the alloy with 20 at. % V does not results in the marked change of the hardness in comparison to the corresponding alloy of eutectic composition ($Ti_{71}V_{20}B_9$).

The influence of the alloying by vanadium on the hardness of eutectic alloys at different temperatures is shown in the Fig. 37.

Thus, the eutectic alloys of Ti-B-V system may be recommended to use at the moderately high temperatures (400-450°C). Besides the eutectic alloys (Ti)+(TiB) alloyed by 10 and 15 at. % V with two-phase matrix (α+β) have the high strength characteristics at this temperature interval. The presence of β-phase in the alloy matrix will promote of plastic characteristics and manufacturability of these alloys, perhaps. Unfortunately, the alloying by vanadium does not lead to increase of hardness and therefore strength characteristics it the temperature region of 600-800°C. That is why the eutectic

alloys of the ternary Ti-B-V system should not to be recommended as the basis for the development of high-temperature alloys on the base of titanium with boride reinforcing.

2.3.2. The Ti-B-Al system

The hardness of titanium ($\alpha+\beta$)-alloy Ti-6Al (mass %) is found to be on the level of the hardness of the eutectic $Ti_{91.4}B_{8.6}$ alloy in the temperature region from room temperature to 400°C (curve 1, Fig. 38). However, in difference from the latter one, the Ti-6Al alloy is softened at high temperatures slower and at 800°C its hardness twice higher than that of the binary (Ti)+(TiB) and the ternary (Ti,V)+(TiB) eutectic alloys. It is explained with the high-temperature strength of α-phase.

The alloying of basic Ti-6Al alloy by microadditions (0.01-0.02 mass %) B does not influence on hardness (curves 2, 3, Fig. 38). The negligible growth of hardness is observes at the alloying by 0.05-0.1 mass % B (curves 4, 5) what, obviously, is connected with modifying influence of boron as well as with appearance of the precipitations of boride phase (at 0.1 mass % B), although the boride phase is not detected by the method of X-ray phase analysis, yet.

The hardness of alloy increases significantly (by 0.5-0.75 GPa) with appearance of the boron phase fixed by X-ray phase analysis at the alloying by 0.5 mass % B (curve 6 of Fig. 38). The hardness of alloy increases in accordance to growth of volume content of reinforcing boride phase with the further increase in the boron content (curves 7, 8, 9). The eutectic alloy (at 2.0 mass % B) has the maximal values of the hardness up to the temperatures 600-700°C. The hardness of alloys with small additions of boron and the hardness of alloys containing the reinforcing boride phase practically does not differ at high temperatures (600-700°C).

It is necessary to notice that although the hardness of eutectic alloys Ti-B-Al system is lower than the hardness of eutectic Ti-B-V alloys in low temperature region, their advantages at the high-temperature (up to 700°C) are evident. The high-temperature strength of eutectic alloys on the Ti-Al base with boride reinforcing is caused by the high-temperature strength of α-phase, of a matrix of these alloys.

2.3.3. The Ti-Al-V-B system

The investigation of the influence of the alloying by boron on the temperature dependence of the popular ($\alpha+\beta$) titanium alloy 6-4 (Fig. 39) has revealed the same patterns that were found while studying of the ternary Ti-B-V and Ti-B-Al systems. So, the alloying by small additions (0.01-0.1 mass %) does not lead to noticeable change of the hardness of the alloy in all temperature interval under investigation. The hardness of the alloys increases with the growth of volume content of reinforcing boride phase with the increase of boron content. The maximal hardness is registered in the alloys closely spaced to eutectic composition. The high hardness of the four-component eutectic alloys Ti-Al-V-B preserves to 500°C (for comparison the high hardness of the ternary eutectic alloys of Ti-B-V system preserves to 400°C and of the Ti-B-Al system does up to 600°C)

2.3.4. The comparative estimation of long-term hardness of the alloys

The estimation of creep behavior of the alloys under investigation was carried out by the method of long-term hardness in the vacuum 10^{-3} Pa at the load 10N and exposure under the indentor during 60 min at the temperatures 400, 500, and 600°C (Table 25).

The minimal long-term hardness in high temperature region (500-600°C) is registered in the eutectic Ti-V-B alloys as the Table 25 shows. The long-term hardness of the eutectic alloys of Ti-B-Al system and the quaternary Ti-B-Al-V system at 500 and 600°C is practically the same and significantly exceeds (2-2.5 times) the hardness of eutectic alloys not containing aluminium.

The differences in hardness of the alloys of these systems at the temperatures from room to 400°C are not so high but the reverse dependence is observed - the higher long-term hardness is registered in the eutectic alloys of Ti-V-B and Ti-Al-V-B systems and the lower - in eutectic alloy not containing vanadium.

It is necessary to mark, that long-term hardness of eutectic alloys significantly exceeds (1.5-2 times) the long-term hardness of corresponding basic alloys at all temperatures under investigation.

Thus, eutectic alloys on the base of Ti-B-Al system are of the great interest as basis alloys for the studying of influence of alloying and heat treatment for development of high-temperature strength easily producible materials.

2.4. CONCLUSION TO CHAPTER II.

1. On the base of results obtained, taking into account literature data on the Ti-V-B phase diagram, for the first time the solidus and liquidus projections were constructed in the Ti-TiB-V_3B_2-V region, as well as the reactions occurring at crystallization of the alloys in this region.

   The vanadium additions (from 0 to 40 at. %) to the eutectic alloy $Ti_{92}B_8$ almost do not influence on the volume fraction of boride phase in the eutectic (Ti) + (TiB) by comparison with the binary alloy. Melting points of the ternary alloys are lower then those for the V-B, Ti-V and Ti-B alloys. The lowest melting point of ternary alloy is 1430°C that corresponds to the invariant three-phase reaction L_{e_3}.

   Determination of hot hardness, which is selected as strength characteristic, bring in evidence the vanadium additions to the eutectic alloy $Ti_{92}B_8$ result in rise of hardness in the range to 400°C. Maximal strengthening is noted in the Ti-V-B alloys containing 10 and 15 at. % V, that is in the alloys with matrix consisting of □+□ titanium phases. The similar results were obtained on determining microhardness of eutectic components in the Ti-V-B alloys.

2. As a result of investigation of the alloys Ti-6Al-(0-2)B (mass %), the ternary phase diagram was constructed in the Ti-TiB-$Ti_{90}Al_{10}$ region at melting temperatures. The ternary Ti-Al-B alloys of this region have higher start temperatures of melting (1528±2°C) than that for the eutectic $Ti_{92}B_8$ alloy (1500°C). The aluminium addition do not influence sufficiently on the volume fraction of boride in eutectic (Ti) + (TiB).

   Hardness of the Ti-B-Al alloys is twice as high as those for the Ti-V-B alloys at temperatures of 500 to 800°C.

3. As a result of investigation of the quaternary Ti-Al-V-B alloys it was established that the eutectic (Ti) + (TiB) structure component is observed at the boron contents of 1-2.5 mass %. The latter alloy have the same start temperature of melting, that brings in evidence them to belong to the only isothermal volume on the solidus of the quaternary system.

   The hot hardness of the Ti-Al-V-B alloys is close to that of the Ti-V-B at the all temperature under studying, but the temperature of softening of the quaternary alloys exceed that of the Ti-V-B alloys by 100°C. The quaternary alloys compare unfavorably with the Ti-Al-B alloys at the temperatures higher than 600°C.

4. Investigation of hot hardness showed that the eutectic alloys of Ti-V-B and Ti-Al-B systems have an advantage at temperature to 400°C. At the temperature of 500 to 600°C the long-term hardness of the eutectic Ti-Al-B and Ti-Al-V-B alloys exceeds the same for the Ti-V-B alloys by 2-2.5 times.

GENERAL CONCLUSIONS

1. In situ eutectic composites realized with the Ti-Si-X and the Ti-B-X systems exceed well-known commercial heat resistant titanium alloys from the point of view their heat resistance in temperature region above 600°C. Taking into account well-known casting properties of eutectic alloys, manufacturing articles with near-shape casting methods is very attractive.

2. Comparison of alloys of both systems shows that alloys with silicide strengthening are more promising to obtain the highest heat resistance. The hot-hardness curves of the best Ti-Si-X alloys are shifted in comparison with the best Ti-B-X ones for at least 100-150°C in direction of high temperatures. It seems to result from the different content of strengthening phases in the systems.

3. Additives of V and Al do not notably influence on volume part of borides in eutectic Ti-B-X alloys.

4. In the Ti-Si-X system being at up-to-date level of studying, the optimal content of silicon is around 4-6 wt.%. Alloys with Al content of 2.5-3 wt.% ensure best ratio between plasticity and heat resistance. Alloys with Zr content of 6-9 wt.% ensure the highest heat resistance. These figures follow from the data on the complex of mechanical properties. Among other alloying elements studied as the most promising are Sn and Ga.

5. In the Ti-B-X system, the highest heat resistance was obtained with alloys alloyed with Al. In future, it is necessary to check alloying with elements, which lead to higher resistant α-matrix.

6. The main disadvantage of the *in situ* studied is their low temperature plasticity. Nevertheless it was found that changing conditions of solidification, increasing purity of initial components lead to increasing plasticity. The highest plasticity (more than 2% at room temperature) was obtained with the Ti-Si-Zr alloys, i.e. with no Al. It means that we have to search the compromise between heat resistance and plasticity and new approaches to structural refinement with new alloying elements and modifiers.

REFERENCES

1. Solonina O.R., Glazunov S.P. Heat resistant titanium alloys. Moscow, Metallurgiya, 1976, 447 p., in Russian.
2. Anciferov V.N., Ustinov V.S., Olesov Yu.H. Sintered alloys based on titanium. Moscow, Metallurgy, 1984,165 p., in Russian.
3. Molchanova E.K. Atlas of diagrams of titanium alloys state. Moscow, Mashinostroenie, 1980, 701 p., in Russian.
4. Fromm E., Hebhardt E. Gases and carbon in metals. Moscow, Metallurgy, 1980, 634 p., in Russian.
5. Titanium 92 Science and Technology. Edited by Froes F.H. and Caplan I. 1993, p.16-22.
6. Povarova K.B., Tostobrov YuO., Proskurin V.V. et al. Reaction sintering of mechanically activated alloys based on TiAl. The first International Conf. of the CIS countries. Moscow, VILS, 1994, p. 365-371, in Russian.
7. Saito T., Furuda T. and Yamaguchi T. Development of the low cost titanium matrix composite. Titanium'95, Science and Technology. Edited by F.Froes and I.Storer.1995. Vol.2.
8. Furrer D., Hoffman R., Fuchs G. TiAl-based ingot conversion via forging. Titanium'95, Science and Technology. The Eighth World Conference on Titanium. v.1., 1-924 p.
9. Moiseev V.N. Structural titanium alloys and perspectives of their development. The First International Conf. of the CIS countries. Moscow, VILS, 1994, p. 567-579, in Russian.
10. U.S. Patent. No. 4,915,904. Process for stabilization of Titanium Silicide particles within titanium aluminide containing metal matrix composites. Chris Leontio et al.- Apr.10, 1990.
11. Wu T., Beaven P. and Wagner R. The $Ti_3(Al,Si)+Ti_5(Si,Al)_3$ eutectic reaction in the Ti-Al-Si System. Scripta Metallurgica, Vol.24., 1990, p.207-212.
12. Bulanova M., Tretyachenco L., Golovkova M. Phase Equilibrium in the Ti-rich Corner of the Ti-Si-Al System. Z. Metallkunde, 88(1997), 3, p. 257-265.
13. Zakharov M.V., Zakharov A.M. Heat resistant alloys. Moscow, Metallurgia, 1972, 384 p., in Russian.
14. Titanium alloys in mashinebuilding. Ed. Kapyrin G.I., Leningrad, Mashinostroenie, 1977, 245 p., in Russian.
15. Mazur V.I., Kapustnikova S.V., Ryabukhina R.Ya. Influence of chemical composition on microstructure, phase composition and mechanical properties of titanium alloys for heat loaded parts of engines. Dvigatelestroenie, 1989, N2, p.32-33, in Russian.
16. Sang N., Vang K. Technology of high-speed solidification in systems of titanium alloys. J.Mat.Sci., **21**(1986), p.2224-2238.
17. Trefilov V.I., Moiseev V.F. Dispersive particles in refractory metals. Kyiv, Naukova Dumka, 1978, 240 p., in Russian.
18. Samsonov G.V., Dvorina L.A., Rud' B.M. Silicides. Moscow, Metallurgiya, 1979, 272 p., in Russian.
19. Titanium'99. Abstracts. The 9th World Conference on Titanium. 7-11 June, 1999, S-Peterburg, Russia.
20. Bulanova M.V., Tret'yachenko L.A., Golovkova M., Soroka A. Microstructure and properties of Ti-reach Ti-Si-Ge-Al alloys. Z.Metalkunde, **89**(1998), N9, p.1-10.
21. Barber et al. Method of producting titanium alloys. Titanium Ltd., c22c14/00. g02430056 publication 87.10.28UCM, N7/88, **23**(2).
22. Antonova, N. V., Ban'kovsky, O. I., Firstov, S. A., Tretyachenko, L. A., Velikanova, T. Ya., "Long-term hardness of the Ti-Si-Ga alloys in the Ti-rich coner", J. Poroshkovay metallurgiy, Kiev, $N_0$3/4, 1998, pp. 62-66, in Russian.
23. Antonova N., Ban'kovsky O., Firstov S., Tretyachenko L., Velikanova T. "Structure and mechanical properties of the Ti-Ga-Si alloys in the Ti-rich coner", J. Materials Science, 34(1999), 3413-3416.
24. Zakharov A.M. Commerial Alloys of Nonferrous Metalls. Moscow: Metallurgiya, 1980.
25. Titanium Alloys. Metallography of Titanium Alloys (Eds. S.G. Glazunov and B.A. Kolachev). - Moscow: Metallurgiya, 1980.
26. Massalski T.V., Subramanian P.R., Okomoto H., Kasprzak L. (Eds.) Binary Alloy Phase Diagrams. 2nd ed., 1 vol. - Ohio: ASM International Materials Park.-1990.
27. Kattner U.R., Lin J.-C., Chang Y.A., Metall. Trans. A, 23 (8), 2081-2090 (1992).
28. Okamoto H., J. Phase Equilibria, 14 (1), 120-121 (1993).
29. Kuz'ma Yu.B., Paitash T.P., and Baidala S.I., Visnyk L'vivskoho Universytetu, Ser. Khimiya, issue 11, pp. 18-20 (1969).
30. Hayes F.H., Lukas H.L., Effenberg G and Petzows G., Z. Metallkd., **80** (5), 361-365 (1989).
31. Villars P., Prince A., and Okamoto H. Handbook of Ternary Alloy Phase Diagrams. ASM, **3** (1995).
32. Stolz U.K., Sommer F and Predel B. Aluminium, **71** (3), 350-355 (1995).
33. Zupanic F., Spaic S., and Krizman A., Mat. Sci. Technol., vol. 14, 601-607 (1998).
34. Zupanic F., Spaic S., and Krizman A., Mat. Sci. Technol., vol. 14, 1203-1212 (1998).
35. Hayes F.H. Aluminium-Titanium-Vanadium, Ternary Alloys A Comprehensive Compendium of Evaluated Constitutional Data and Phase Diagrams. Ed. G. Petzow and G. Effenberg. vol. 8 (1993).
36. Ming L.C., Manghnani M.H., Katahara K.W., Acta met., No 3, 479-485 (1981).
37. F.W.Grossman and A.S.Yue: Metal. Trans., vol. 2, june, 1545-1555 (1971).
38. J.A.Philliber, F.C.Dary, F.W.Zok and C.G.Levi, Titanium 95: Science and Technology, 2714-2721 (1995).
39. T.Saito, Takamiya and T.Furuta, Titanium'95, Science and Technology, 2859-2866 (1995).

Table 11.

CRYSTAL STRUCTURE AND LATTICE PARAMETERS OF PHASES IN THE SYSTEMS TI-V, TI-B, AND V-B [26, 40].

Phase	Prototype	Pearson symbol, space group	Lattice parameters, pm		
			a	*b*	*c*
(βTi, V) 0-100 % V	W	*cI2*, $Im\bar{3}m$	330.65-302.40	–	–
(αTi)	Mg	*hP2*, $P6_3/mmc$	295.06	–	468.35
TiB_2	AlB_2	*hP3*,	303	–	322
		P6/mmm	303.8	–	323.9
			303.1	–	322.9
TiB	FeB	*oP8*, *Pnma*	612 (1)	306 (1)	456 (1)
Ti_3B_4	Ta_3B_4	*oI14*, *Immm*	325.9	1373	304.2
V_3B_2	U_3Si_2	*tP10, P4/mbm*	572.8	–	302.6
VB	CrB	*oC8, Cmcm*	305.8	804.3	296.6
V_3B_4	Ta_3B_4	*oI14, Immm*	305.8	1322	298.1
V_5B_6	-	*oC*, Cmmm*	305.8	2125	297.4
VB_2	AlB_2	*hP3, P6/mmm*	299.8* 299.4**	-	305.6* 304.8**
V_2B_3	CrB (V_2B_3)	*oC8, Cmcm*	306.1	840	298.4

Notes: * - From V-side,

** - From B-side.

Table 12.

INVARIANT POINTS OF THE TI-V, TI-B, AND V-B PHASE DIAGRAMS [26]

Invariant equilibrium	Content of second component, at. %	Temperature, °C	Equilibrium type
System Ti-V			
	Vanadium content		
$(\beta Ti) \Leftrightarrow (V) + (\alpha Ti)$	18 ~80 2.7	675	Monotectoid
$(\beta Ti,V) \Leftrightarrow (\beta Ti) + (V)$	~50	850	Critical point
$L \Leftrightarrow (\beta Ti,V)$	32	1605	Point of congruent melting
$L \Leftrightarrow (\beta Ti)$	0	1670	Melting point
$L \Leftrightarrow (V)$	100	1910	Melting point
$(\beta Ti) \Leftrightarrow (\alpha Ti)$	0	882	Allotropic transformation
System Ti-B			
	Boron content		
$L \Leftrightarrow (\beta Ti) + TiB$	7±1 < 1 ~50	1540± 10	Eutectic
$L + TiB_2 \Leftrightarrow Ti_3B_4$	42±1 ~65.5 ~58.1	2200± 25	Peritectic
$L + Ti_3B_4 \Leftrightarrow TiB$	~39 58.1 50	2180	Peritectic
$L \Leftrightarrow TiB_2$	66.7	3225 ±25	Point of congruent melting
$L \Leftrightarrow (\beta B) + TiB_2$	~98 ~100 ~66.7	2080± 20	Eutectic
$(\beta Ti) + TiB \Leftrightarrow (\alpha Ti)$	~0.1 49 ~0.2	884± 2	Peritectoid
$L \Leftrightarrow (\beta Ti)$	0	1670	Melting point
$(\beta Ti) \Leftrightarrow (\alpha Ti)$	0	882	Allotropic transformation
$L \Leftrightarrow (\beta B)$	100	2092	Melting point
System V-B			
	Boron content		
$L \Leftrightarrow V + V_3B_2$	15 0 40	1735	Eutectic
$L + VB \Leftrightarrow V_3B_2$	25 50 40	1925	Peritectic
$VB + V_3B_4 \Leftrightarrow V_5B_6$	49 57 50	2551	Peritectic
$L + V_2B_3 \Leftrightarrow V_3B_4$	50 57 54.5	1727	Peritectic
$L + VB_2 \Leftrightarrow V_2B_3$	56 60 57	2640	Peritectic
$L + VB_2 \Leftrightarrow V_2B_3$	57 67 60	2653	Peritectic
$L \Leftrightarrow VB_2$	67	2750	Point of congruent melting
$L \Leftrightarrow VB_2 + B$	98 67 100	2068	Eutectic

Table 13.

Content of oxygen and nitrogen in alloys from chemical analysis data.

Alloy composition, mass %				Oxygen content, mass %	Nitrogen content, mass %
Ti	V	Al	B		
92.1	5.7	–	2.2	0.06	<0.005
75.25	22.6	–	2.15	0.075	<0.005
89.5	6	4	0.5	0.20	<0.005
88.25	6	4	1.75	0.05	<0.005

Table 14.

Composition of the studied Ti-V-B alloys
by initial mixture and mass losses on melting.

Alloy number	Alloy composition						Mixture mass, г	Ingot mass, g	$(\Delta p/p)\cdot 100$, %
	at. %			mass %					
	Ti	V	B	Ti	V	B			
1	70	30	-	67.7	32.3	-	10	9.9999	0.001
2	91.4	-	8.6	97.92	-	2.08	40	39.8406	0.4
3	-	85	15	-	96.39	3.61	2.5	2.4863	0.5
4	86	5	9	92.1	5.7	2.2	10	9.9995	0.005
5	81	10	9	86.5	11.3	2.2	10	9.9918	0.08
6	76	15	9	82.1	15.9	2.0	10	9.9944	0.06
7	71	20	9	75.25	22.6	2.15	10	9.9920	0.08
8	90	5	5	93.3	5.5	1.2	10	9.9998	0.002
9	85	10	5	87.8	11	1.2	10	9.9998	0.002
10	80	15	5	83.3	15.6	1.1	10	9.9998	0.004
11	75	20	5	77.0	21.84	1.16	10	9.9830	0.17
12	67	20	13	73.45	23.33	3.22	10	9.9556	0.4
13	25	60	15	27.11	69.22	3.67	5	4.9573	0.8
14	38	45	17	42.36	53.36	4.28	5	4.9990	0.002
15	64	27	9	67.6	30.3	2.1	10	9.98905	0.11
16	58	33	9	60.6	37.3	2.1	10	9.99400	0.06
17	51	40	9	53.4	44.5	2.1	10	9.99015	0.1
18	50	41	9	52.3	45.6	2.1	10	9.99530	0.05
19	38	49	13	40.8	56.0	3.2	10	9.96920	0.3
20	35	45	20	40.0	54.8	5.2	10	9.92225	0.8

Table 15.

Structure components and phase composition of the Ti-V-B alloys.

Alloy composition, at. %			Primary crystallized phase	Structure component	Phase composion from XRD
Ti	V	B			
91.4	0.0	8.6	TiB	TiB; e*(TiB + β**)	α + TiB
70	30	0.0	β	β	β
0.0	85	15	-	e (V + V_3B_2)	(V) + V_3B_2
90	5	5	β**	β**; e (TiB + β**)	α + (TiB)
85	10	5	β**	β**; e (TiB + β**)	α + β + (TiB)
80	15	5	β**	β**; e (TiB + β**)	α + β + (TiB)
75	20	5	β	β; e (TiB + β)	β + (TiB)
86	5	9	-	e (TiB + β)	α + (TiB)
81	10	9	-	e (TiB + β)	α + β + (TiB)
76	15	9	-	e (TiB + β)	-
71	20	9	-	e (TiB + β)	β + (TiB)
64	27	9	-	e (TiB + β)	β + (TiB)
58	33	9	-	e (TiB + β)	β + (TiB)
51	40	9	-	e (TiB + β)	β + (TiB)
50	41	9	-	e (TiB + β)	β + (TiB)
67	20	13	(TiB)	TiB; e (TiB + β)	β + (TiB)
38	49	13	(V_3B_2)	V_3B_2; e (V_3B_2 + β)	β + (V_3B_2) + (TiB)
25	60	15	-	e (V_3B_2 + β)	β + $(V_3B)_2$
38	45	17	-	e (V_3B_2 + TiB)	β + (V_3B_2) + (TiB)
35	45	20	(V_3B_2)	V_3B_2; e (V_3B_2 + TiB)	β + (V_3B_2) + (TiB)

* e - eutectic (in bracket its structure components are presented).

** β-phase is not conserved on cooling, being transformed to α completely or partially.

Table 16.

Phase composition and lattice parameters of the as-cast Ti-V-B alloys.

Alloy composition, at. %			Phase composition from XRD and metallographic data	Lattice parameters, pm		
Ti	V	B		*a*	*b*	*c*
91.4	–	8.6	α	294.6 ± 0.3	–	469.3 ± 0.2
			(TiB)	608.7 ± 1.0	310.7 ± 1.0	457.1 ± 1.0
70	30	0.0	β	320.8 ± 0.4	–	–
–	85	15	(V)	302.8 ± 0.9	–	–
			(V_3B_2)	577.0 ± 0.3	–	305.1 ± 0.2
80	15	5	β	323.4 ± 0.2	–	–
			α	–	–	–
			(TiB)	–	–	–
75	20	5	β	323.3 ± 0.2	–	–
			(TiB)	612 ± 4	302 ± 3	457 ± 3
86	5	9	α	294.2 ± 0.3	–	466.5 ± 0.5
			(TiB)	612 ± 3	304.5 ± 1.3	461 ± 4
71	20	9	β	323.0 ± 0.1	–	–
			(TiB)	–	–	–
64	27	9	β	321.2 ± 0.1	–	–
			(TiB)	606.6 ± 1.6	300.3 ± 1.4	454.4 ± 0.9
58	33	9	β	319.6 ± 0.1	–	–
			(TiB)	600.3 ± 1.5	300.4 ± 0.5	449.7 ± 1.5
50	41	9	β	317.5 ± 0.1	–	–
			(TiB)	610.9 ± 1.6	297.1 ± 1.7	448 ± 5
51	40	9	β	317.6 ± 0.1	–	–
			(TiB)	600.7 ± 1.7	299.1 ± 0.6	449.8 ± 1.3
67	20	13	β	321.4 ± 0.7	–	–
			(TiB)	617 ± 3	303 ± 4	453 ± 7
25	60	15	β	309.6 ± 0.1	–	–
			(V_3B_2)	–	–	–
38	45	17	β	314.3 ± 0.4	–	–
			(TiB)	603 ± 1	305 ± 2	456 ± 4
			(V_3B_2)	–	–	–
35	45	20	β	314.2 ± 0.1	–	–
			(TiB)	–	–	–
			(V_3B_2)	–	–	–

Table 17.

Temperature of phase transformations in the as-cast Ti-V-B alloys from DTA data.

Alloy composition, at. %			Phase composition from XRD and metallographic data	Tamperature of $\alpha \Leftrightarrow \beta$ (°C) heating/ cooling	Start temperature of melting, °C	Maximal temperature of heating, °C	Sample state after test
Ti	V	B					
91.4	0.0	8.6	α + TiB	880 / 710	1495	1660	melted
70	30	0.0	β	–	1580	1670	melted
0.0	85	15	(V) + V_3B_2	–	1700	1805	melted
75	20	5	β + (TiB)	–	1430	1565	melted
86	5	9	α + (TiB)	740 / –	1480	1625	melted
71	20	9	β + (TiB)	–	1440	1560	melted
64	27	9	β + (TiB)	–	1445	1555	melted
58	33	9	β + (TiB)	–	1430	1515	melted
51	40	9	β + (TiB)	–	1432	1550	melted
67	20	13	β + (TiB)	–	1440	1560	melted
25	60	15	β + (TiB)	–	1470	1740	melted

Table 18.

Phase microhardness of the Ti-V-B alloys.

Alloy composition, at. %			Phase composition from XRD data	Structure component	Microhardness, GPa
Ti	V	B			
91.4	0.0	8.6	α + (TiB)	(Ti)	2.15 ± 0.05
				TiB	24.5 ± 0.4
				e*(Ti+TiB)	3.56 ± 0.10
50	0.0	50	α + (TiB) + TiB_2	TiB	22.9 ± 0.6
70	30	0.0	β	(Ti,V)	2.28 ± 0.17
0.0	85	15	(V) + (V_3B_2)	e(V+V_3B_2)	4.5 ± 0.3
90	5	5	α + (TiB)	(Ti)	3.14 ± 0.07
				e(Ti+TiB)	3.86 ± 0.10
85	10	5	α + β + (TiB)	(Ti)	3.20 ± 0.07
				e(Ti+TiB)	5.36 ± 0.11
80	15	5	α + β + (TiB)	(Ti)	3.60 ± 0.10
				e(Ti+TiB)	5.36 ± 0.12
75	20	5	β + (TiB)	e(Ti+TiB)	3.00 ± 0.07
86	5	9	α + (TiB)	e(Ti+TiB)	3.86 ± 0.10
				(TiB)	(16 ± 1)**
81	10	9	α+β+(TiB)	e(Ti+TiB)	4.52 ± 0.20
76	15	9	–	e(Ti+TiB)	5.03 ± 0.18
71	20	9	β + (TiB)	(Ti,V)	3.97 ± 0.07
				(TiB)	(17.8 ± 1.2)**
64	27	9	β + (TiB)	e(Ti+TiB)	3.39 ± 0.10
58	33	9	β + (TiB)	e(Ti+TiB)	3.30 ± 0.13
				(TiB)	22.2 ± 0.8
51	40	9	β + (TiB)	e(Ti+TiB)	3.57 ± 0.15
50	41	9	β + (TiB)	e(Ti+TiB)	3.22 ± 0.07
67	20	13	β + (TiB)	e(Ti+TiB)	3.1 ± 0.2
				(TiB)	22.9 ± 1.9
25	60	15	β + (V_3B_2)	e(Ti+V_3B_2)	4.39 ± 0.18
38	45	17	β + (V_3B_2) + (TiB)	e(V_3B_2+TiB)	3.97 ± 0.20
				(TiB)	26 ± 2
38	49	13	β + (V_3B_2) + (TiB)	(V_3B_2)	30 ± 3
				e(Ti+V_3B_2)	3.86 ± 0.08
35	45	20	β + (V_3B_2) + (TiB)	(V_3B_2)	30 ± 3
				e(TiB+V_3B_2)	3.97 ± 0.10

*e – eutectic (in brackets its structure components are presented)

** Tentatively estimated value.

Table 19.

Composition of the studied Ti-Al-B alloys by initial mixture and mass losses.

Alloys number	Alloy composition, at. %			Alloy composition, mass %			Mixture mass, g	Ingot mass, g	$\frac{\Delta p}{p} \cdot 100\%$
	Ti	Al	B	Ti	Al	B			
1	89.82	10.18	–	94.0	6	–	10	9.9976	0.02
2	89.79	10.17	0.04	93.99	6	0.01	10	9.9983	0.02
3	89.75	10.17	0.08	93.98	6	0.02	10	9.9983	0.02
4	89.63	10.16	0.21	93.95	6	0.05	10	9.9982	0.02
5	89.44	10.14	0.42	93.9	6	0.1	10	9.9978	0.02
6	87.91	10.01	2.08	93.5	6	0.5	10	9.9983	0.02
7	86.05	9.85	4.10	93.0	6	1.0	10	9.9991	0.01
8	84.25	9.70	6.05	92.5	6	1.5	10	9.9927	0.07
9	82.51	9.55	7.94	92.0	6	2.0	5	4.9973	0.05

Table 20.

Phase composition and lattice parameters of the as-cast Ti-Al-B alloys.

Alloy composition, at.%			Phase composition from XRD and metallographic data	Lattice parameters of α-phase, pm		
Ti	Al	B		*a*	*c*	*c/a*
89.82	10.18	–	α	293.4 ± 0.1	468.2 ± 0.5	1.596 ± 0.002
89.63	10.16	0.21	α	293.6 ± 0.1	468.8 ± 0.6	1.596 ± 0.002
89.44	10.14	0.42	α	293.2 ± 0.1	467.7 ± 0.4	1.595 ± 0.002
87.91	10.01	2.08	α+(TiB)	293.4 ± 0.1	468.0 ± 0.6	1.595 ± 0.002
86.05	9.85	4.10	α+(TiB)	293.5 ± 0.2	468.0 ± 0.3	1.595 ± 0.002
84.85	9.70	6.05	α+(TiB)	293.4 ± 0.1	468.1 ± 0.3	1.595 ± 0.001
82.51	9.55	7.94	α+(TiB)*	292.9 ± 0.1	468.6 ± 0.1	1.5998 ± 0.0007

* $a = 612 \pm 4$; $b = 306.3 \pm 1$; $c = 458.5 \pm 3$; $c/a = 0.749 \pm 0.006$

Table 21.

Temperature of phase transformation in the as-cast Ti-Al-B alloys from DTA data.

Alloy composition, mass %			Phase composition from XRD and metallographic data	Tamperature of α⇔β (°C) heating/ cooling	Start temperature of melting, °C
Ti	Al	B			
94	6	–	α	1005 / -	1660
93.95	6	0.05	α	– / -	–
93.9	6	0.1	α	985 / 950	1530
93.5	6	0.5	α + (TiB)	985 / 935	1530
93	6	1	α + (TiB)	980 / 995	1525
92.5	6	1.5	α + (TiB)	985 / -	1530
92	6	2	α + (TiB)	985 /1035	1525

Table 23.

Phase composition and lattice parameters of the as-cast Ti-Al-V-B alloys.

Alloy composition at. %				Phase composition from XRD and metallographic data	Lattice parameters, pm					
					α-phase		TiB			
Ti	Al	V	B		*a*	*c*	*a*	*b*	*c*	*c/a*
86.2	10.2	3.6	–	α	292.4 ± 0.1	466.3 ± 0.6	–	–	–	–
86.15	10.20	3.60	0.04	α			–	–	–	–
86.03	10.17	3.59	0.21	α	293.0 ± 0.1	466.8 ± 0.6	–	–	–	–
84.35	10.02	3.54	2.09	α + (TiB)	292.8 ± 0.1	466.7 ± 0.2	–	–	–	–
82.55	9.86	3.49	4.10	α + (TiB)	293.2 ± 0.1	467.1 ± 0.3	–	–	–	–
80.78	9.72	3.43	6.06	α + (TiB)	292. 6 ± 0.1	466.9 ± 0.1	–	–	–	–
79.95	9.63	3.40	7.02	α + β* + (TiB)	292.7 ± 0.1	467.0 ± 0.3	612 ± 2	305.9 ± 0.5	456 ± 1	0.745 ± 0.003
79.88	9.67	3.41	7.04	α + β* + (TiB)	293.4 ± 0.2	468.2 ± 0.7	611 ± 2	305.8 ± 0.8	457 ± 3	0.748 ± 0.005
78.26	9.50	3.35	8.89	α + β* + (TiB)	293.4 ± 0.3	468 ± 2	612 ± 3	306 ± 2	457 ± 3	0.746 ± 0.006
77.45	9.42	3.33	9.80	α + β* + (TiB)	293.6 ± 0.2	467.6 ± 0.1	610 ± 2	306.1 ± 0.6	457 ± 1	0.748 ± 0.003

*A little quantity of phase.

Table 22.

Alloy composition by initial mixture and mass losses on melting.

Alloys number	Alloy composition, at. %				Alloy composition, mass %				Mixture mass, g	Ingot mass, g	$\frac{\Delta p}{p} \cdot 100\%$
	Ti	Al	V	B	Ti	Al	V	B			
1	86.2	10.2	3.6	–	90	6	4	–	20	19.9924	0.04
2	86.16	10.20	3.60	0.04	89.99	6	4	0.01			
3	86.14	10.18	3.60	0.08	89.98	6	4	0.02	10	9.9898	0.102
4	86.03	10.17	3.59	0.21	89.95	6	4	0.05	10	9.9956	0.04
5	85.84	10.15	3.59	0.42	89.90	6	4	0.1	10	9.9999	0.001
6	84.35	10.02	3.54	2.09	89.50	6	4	0.5	10	9.9958	0.04
7	82.55	9.86	3.49	4.10	89.00	6	4	1.0	10	9.9906	0.09
8	80.80	9.70	3.43	6.06	88.50	6	4	1.5	10	9.9943	0.06
9	79.95	9.63	3.40	7.02	88.25	6	4	1.75	10	9.9633	0.37
10	79.88	9.67	3.41	7.04	88	6	4	2	10	9.9735	0.3
11	78.26	9.50	3.35	8.89	87.75	6	4	2.25	10	9.9817	0.2
12	77.45	9.43	3.33	9.80	87.50	6	4	2.5	10	9.9231	0.8

Table 24.

Temperature of phase transformation in the as-cast Ti-Al-V-B alloys from DTA data.

Alloy composition, mass %				Phase composition from XRD and metallographic data	Temperature of α⇔β (°C) heating / cooling	Start temperature of melting, °C
Ti	Al	V	B			
90	6	4	–	α	855 / 705	1645
89.99	6	4	0.01	α	860 / 755	1625
89.95	6	4	0.05	α	880 / 750	1600
89.9	6	4	0.1	α + (TiB)	875 / 780	1515
89.5	6	4	0.5	α + (TiB)	875 / 830	1515
89	6	4	1	α + (TiB)	890 / -	1515
88.5	6	4	1.5	α + (TiB)	895 / 720	1515
88.25	6	4	1.75	α + (TiB)	900 / -	1515
88	6	4	2	α + (TiB)	– / 885	1515
87.75	6	4	2.25	α + (TiB)	900 / -	1515
87.5	6	4	2.5	α + (TiB)	– / 910	1505

Table 25.

The long-term hardeness of the alloys.

Alloy	HV, GPa		
	400°C	500°C	600°C
$Ti_{81}V_{10}B_9$	2.78	0.84	0.28
$Ti_{76}V_{15}B_9$	3.83	0.90	0.31
$Ti_{71}V_{20}B_9$	2.74	0.72	0.39
Ti-6Al (mass %)	1.08	0.99	-
Ti-6Al-2B (mass %)	2.41	2.1	0.94
Ti-6Al-4V (mass %)	1.92	1.24	0.69
Ti-6Al-4V-2B (mass %)	2.72	1.95	0.94

List of Figures:

Figure 14. Liquidus surface projection of the Ti-Si-Al-Ga alloys along section 5 at.% Ga (---) and euetctic curve in the Ti-Al-Si system (-..-) according to [27].

Figure 15. Liquidus surface projection of the Ti-Si-Al-Ga alloys along section 10 at.%.
1. e_1 – eutectic β + z; 2. e_2 – eutectic β + γ; 3. E – eutectic β + γ + z.

Figure 16-1. Structure of different alloys of the Ti-Si-Al-Ga system. Light microscopy, x200.
Description see in the text.

Figure 16-2. Structure of different alloys of the Ti-Si-Al-Ga system, continued. Light microscopy, x200.
Description see in the text.

Figure 17. Lattice parameters of the phase $Ti_5(Si,Al,Ga)_3$ *a* (a) and *c* (b) of the Ti-Si-Al-Ga alloys annealed at 1350°C.

Figure 18. Structure of the eutectic Ti-5Si-5Ga-20Al alloy. Scanning microcsopy, x1000.

Figure 19. Short-term hardness of the Ti-Ga alloys.

Figure 20. Long-term hardness of the Ti-Ga alloys.

Figure 21. Isothermal section of the Ti-V-B system at 1400°C [29].

Figure 22. Microstructures of the as-cast Ti-V-B alloys with the boron content of 9 ат.%,
a) $Ti_{91.4}B_{8.6}$ – grains of TiB, eutectic TiB+(Ti), ×200;
b) $Ti_{86}V_5B_9$ – eutectic (TiB)+(Ti), ×200;
c) $Ti_{76}V_{15}B_9$ – eutectic (TiB)+(Ti), ×200;
d) $Ti_{64}V_{27}B_9$ - eutectic (TiB)+(Ti), ×200;
e) the same, ×750;
f) $Ti_{51}V_{40}B_9$ - eutectic (TiB)+(Ti), ×200.

Figure 23. Microstructures of the as-cast Ti-V-B alloys with the vanadium content of 20 ат.%, ×200:
a) $Ti_{71}V_{20}B_9$ – eutectic (TiB)+(Ti);
b) $Ti_{75}V_{20}B_5$ – grains of metal β-phase (βTi), eutectic (TiB)+(Ti);
c) $Ti_{67}V_{20}B_{13}$ – grains of boride phase (TiB), eutectic (TiB)+(Ti)

Figure 24. Solidus surface projection of the Ti-V-B system.

Figure 25. Lattice parameters of β-phase *vs.* the Ti-V binary alloy composition:
1 – the present data, 2 – lattice parameters of the Ti-V-B ternary alloys, 3 – [36].

Figure 26. Microhardness of the eutectic (Ti)+(TiB) component (curves 1 and 2)and metal phase (Ti,V) (curve 3) *vs.* the vanadium content in the Ti-V-B alloys:
1 – the alloys with boron content of 9 at. %; 2 and 3 – the alloys with boron content of 5 at. %.

Figure 27. Solidus surface projection of the Ti-B-V system in the Ti-TiB-VB-V region.

Figure 28. Reaction scheme at crystallization of the Ti-V-B alloys.

Figure 29. Microstructures of the as-cast Ti-Al-B alloys containing from 0 to 1 mass % B:
a) Ti-6Al (mass %), ×100;
b) the same, ×750;
c) Ti-6Al-0.5B (mass %), ×200;
d) the same, ×750;
e) Ti-6Al-1B (mass %), ×200;
f) the same, ×750.

Figure 30. Microstructures of the as-cast Ti-Al-B alloys containing from 1.5 to 2 mass % B:
a) Ti-6Al-1.5B (mass %), ×200;
b) the same, ×750;
c) Ti-6Al-2B (mass %), ×200;
d) the same, ×750.

Figure 33. Microstructures of the as-cast Ti-6Al-4V-B alloys containing from 0 to 1 mass % B:
a) Ti-6Al-4V (mass %), ×200;
b) Ti-6Al-4V-0.01B, ×200;
c) Ti-6Al-4V-0.02B, ×200;
d) Ti-6Al-4V-0.05B, ×200;
e) the same, ×750;
f) Ti-6Al-4V-0.1B, ×200;
g) Ti-6Al-4V-0.5B, ×200;
h) Ti-6Al-4V-1B, ×200.

Figure 34. Microstructures of the as-cast Ti-6Al-4V-B alloys containing from 1.5 to 2 mass % B:
a) Ti-6Al-4V-1.5B (mass %), ×200;
b) Ti-6Al-4V-1.75B (mass %), ×200;
c) Ti-6Al-4V-2B (mass %), ×200;
d) the same, ×750;
e) e) Ti-6Al-4V-2.25B (mass %), ×200;
f) Ti-6Al-4V-2.5B (mass %), ×200.

Figure 35. The temperature dependence of hardness for eutectic alloys $Ti_{91.4}B_{8.6}$ – 1, $Ti_{86}V_5B_9$ – 2, $Ti_{81}V_{10}B_9$ – 3, $Ti_{76}V_{15}B_9$ – 4, and $Ti_{71}V_{20}B_9$ – 5.

Figure 36. The temperature dependence of hardness for hypoeutectic alloys $Ti_{90}V_5B_5$ – 1, $Ti_{85}V_{10}B_5$ – 2, $Ti_{80}V_{15}B_5$ – 3, and $Ti_{75}V_{20}B_5$ – 4.

Figure 37. The hardness dependence for the Ti-B-V alloys on the vanadium content at the temperatures: 400°C (1 – eutectic alloy, 2 – hypoeutectic alloy); 600°C (3 – eutectic alloy, 4 – hypoeutectic alloy); 700°C (5 – eutectic alloy, 6 – hypoeutectic alloy); 800°C (7 – eutectic alloy, 8 – hypoeutectic alloy).

Figure 38. The temperature dependence of hardness for the Ti-B-Al alloys:
1 – Ti6Al (mass %), 2 – Ti6Al0.01B, 3 – Ti6Al0.02B, 4 – Ti6Al0.05B,
5 – Ti6Al0.1B, 6 – Ti6Al0.5B, 7 – Ti6Al1.0B, 8 – Ti6Al1.5B,
9 – Ti6Al2.0B.

Figure 39. The temperature dependence of hardness for the Ti-Al-V-B alloys:
1 – Ti6Al4V (mass %), 2 – Ti6Al4V0.01B, 3 – Ti6Al4V0.02B,
4 – Ti6Al4V0.05B, 5 – Ti6Al4V0.1B, 6 – Ti6Al4V0.5B,
7 – Ti6Al4V1.0B, 8 – Ti6Al4V1.5B, 9 – Ti6Al4V1.75B.

Figure 1. Projections of liquidus and solidus surfaces in the Ti-tich corner of the Ti-Si-Al-system.

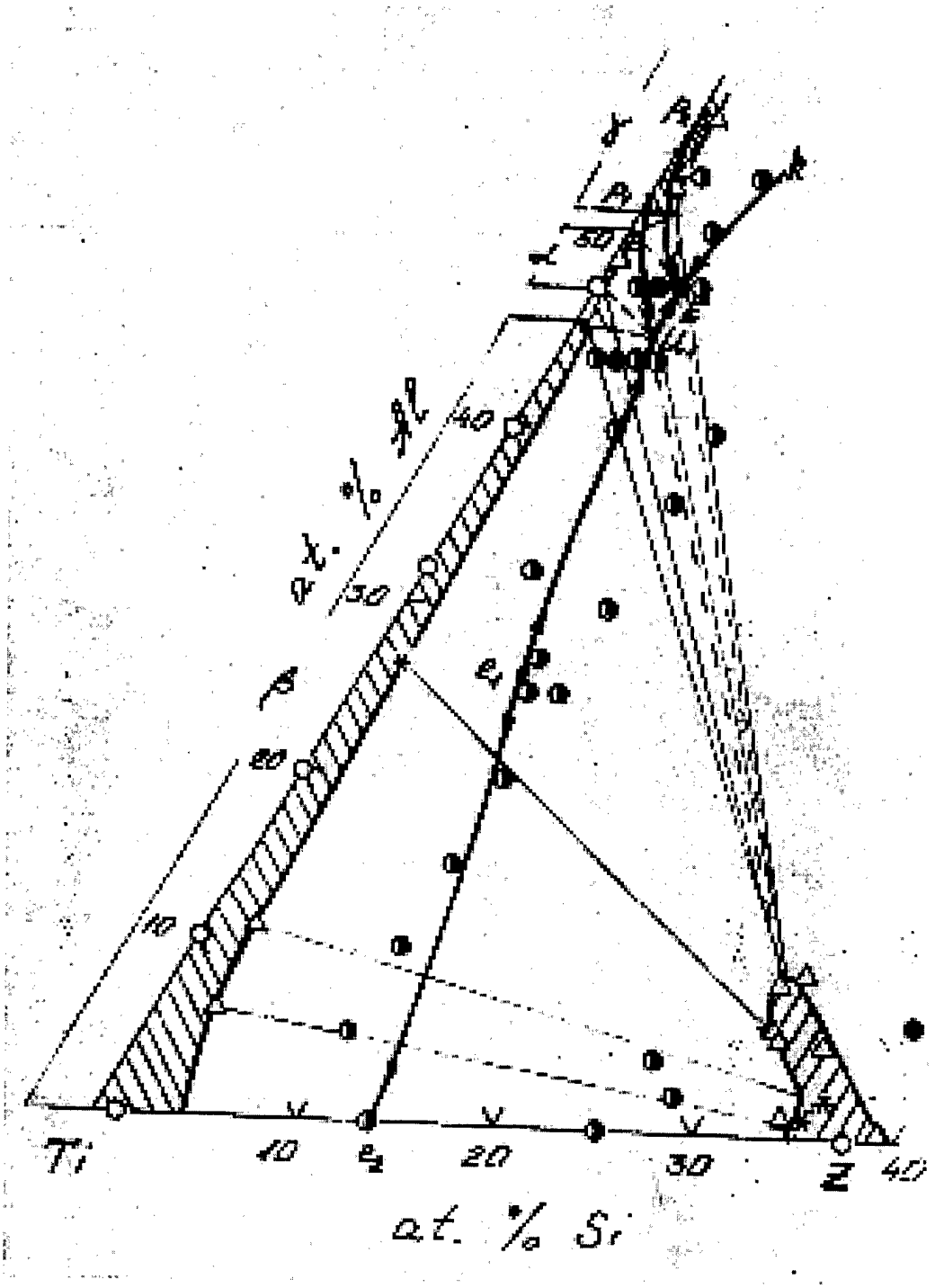

Figure 2. Polytermal section of the T-Si-Al system along the 10 at.% Si isoconcentrate.

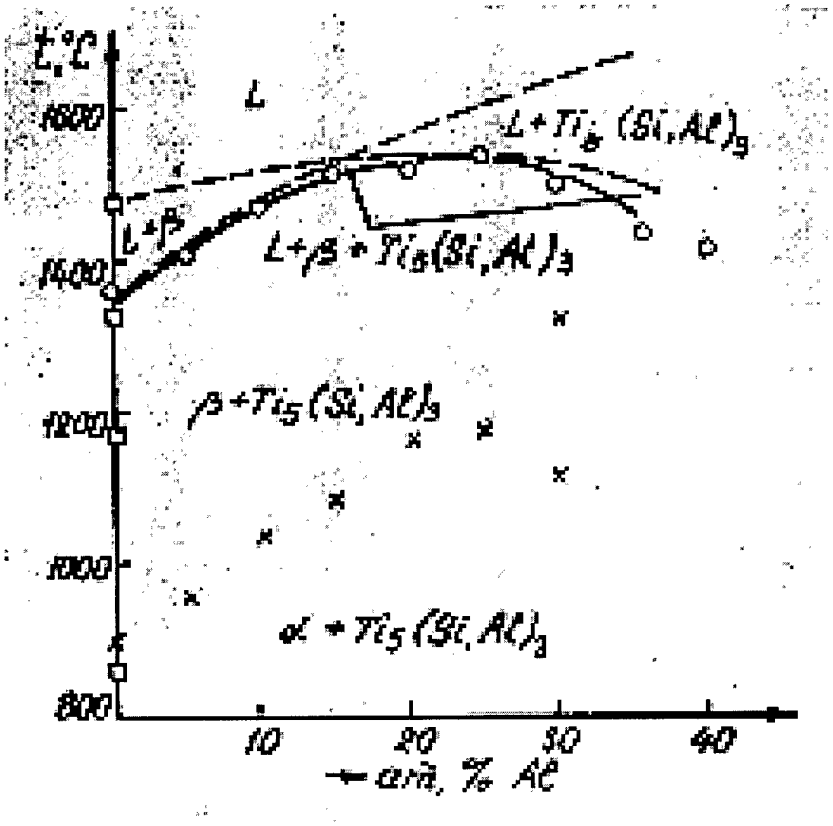

Figure 3. Structure of the cast alloys of the Ti-Si-Al system (light microscopy):
a – Ti - 2Si - 5.4Al - 6.2Zr (alloy 7), x200; b – Ti – 4.7Si - 4.4Al - 9.4Zr (alloy 12), x600;
c – Ti – 9.5Si – 3.5Al (alloy 6), x200; d – heat treated alloy 7, x320.

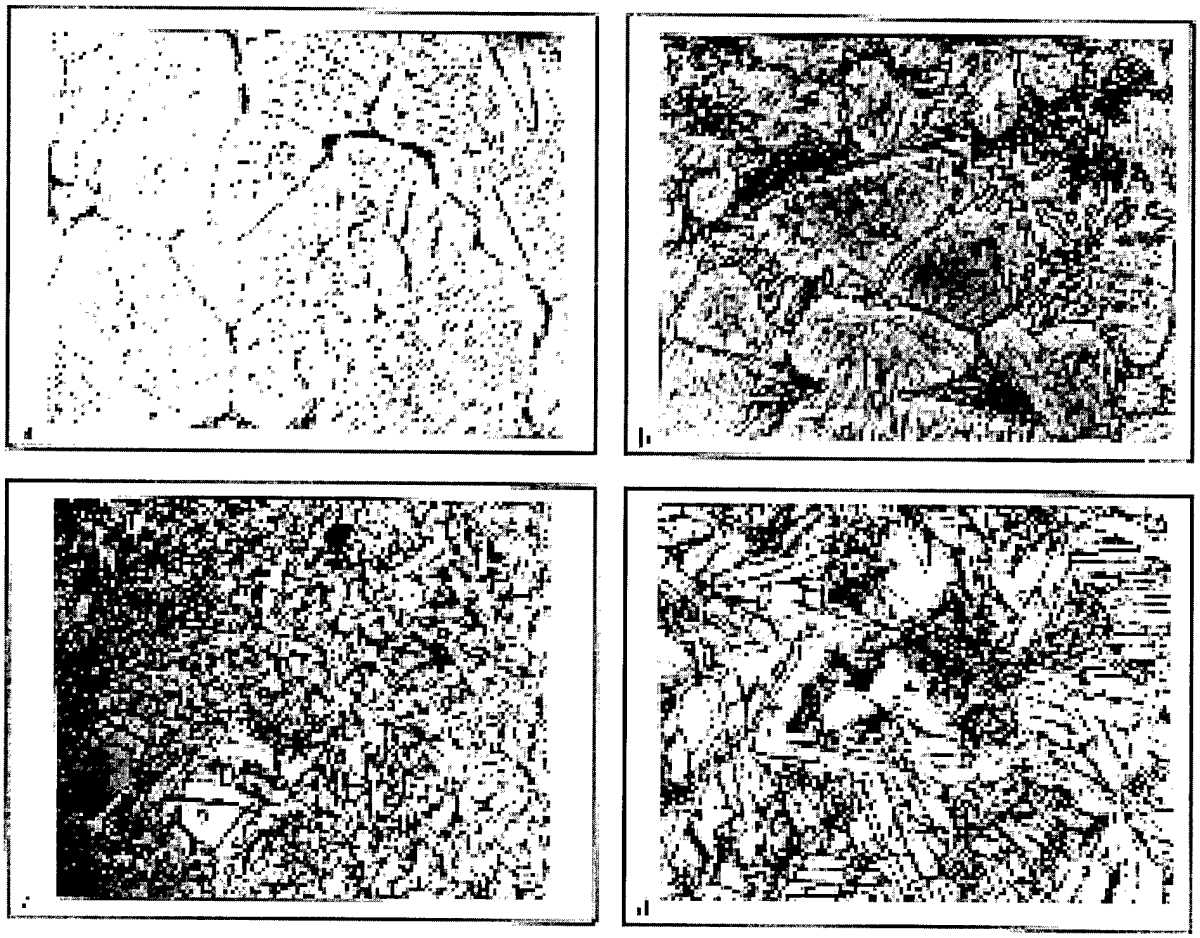

Figure 4. Long-term hardness of the cast Ti-Si-Al system in dependence of the silicon content.
Smoth curves contour the data corresponding to alloys containing small (up to 4 wt.% Zr) and large .

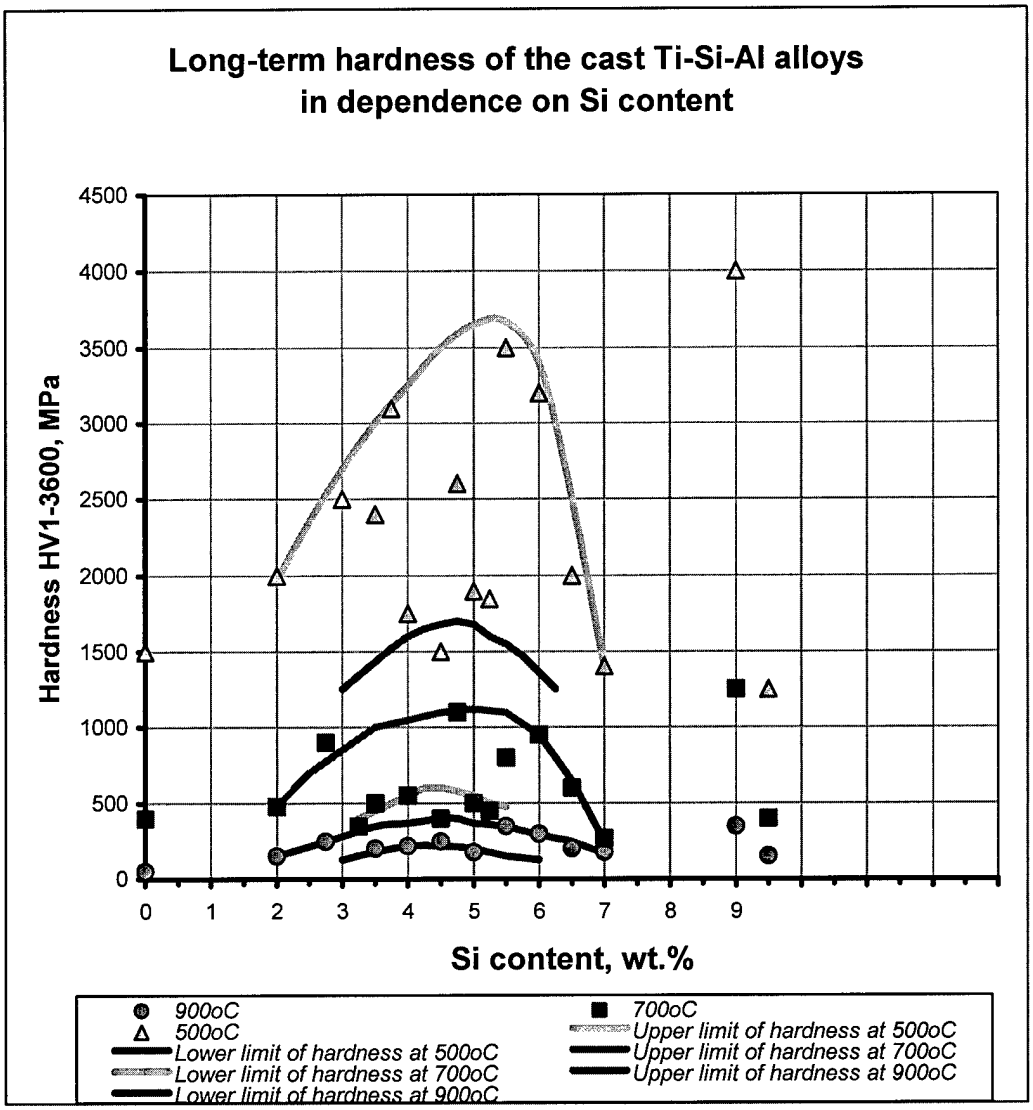

Figure 5.	Long-term hardness of cast Ti-Si-Al -alloys in dependence on zirconium content. Compositions of alloys are given in Table 1.

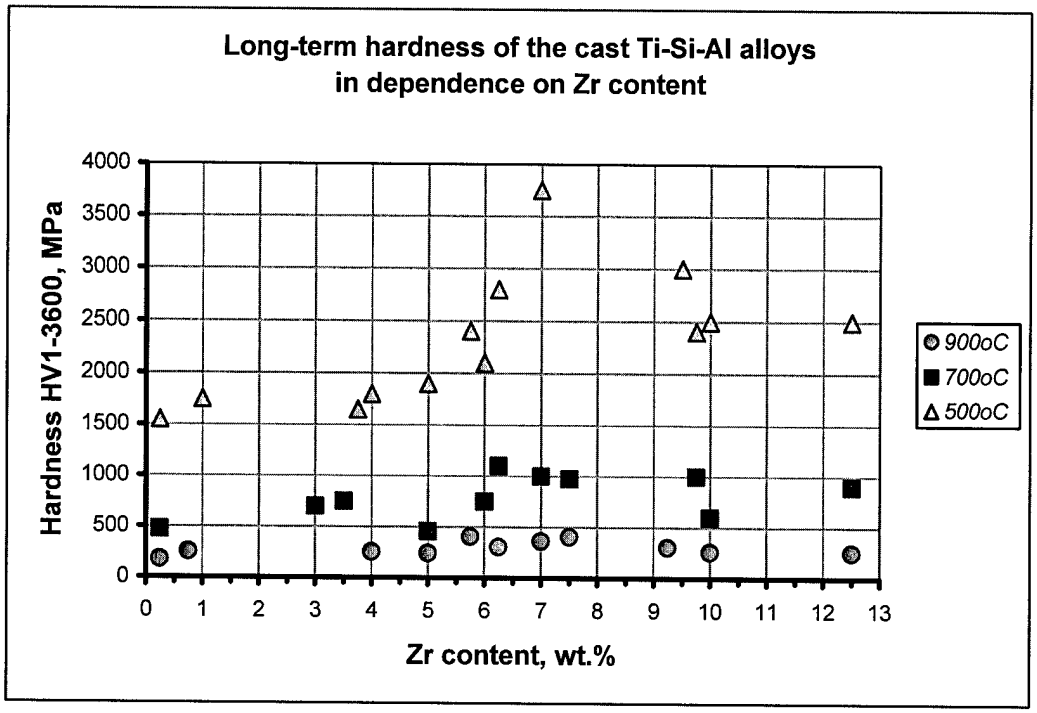

Figure 6. Structure of the cast Ti-Si-Al alloys.
Compositions of alloys, wt%:
a – alloy 7: Ti-2Si-5.4Al-5.3Zr, x200; b – alloy 14: Ti-5Si-5Al-5Zr, x200; c – alloy 6: Ti-7.5Si-3Al, x200;
d – alloy 7 heated 900°C for 1 hour and quenched in water, x200;
e – alloy 14 heated 1000°C for 1 hour and quenched in water and annealed 800°C for 10 hours, x250

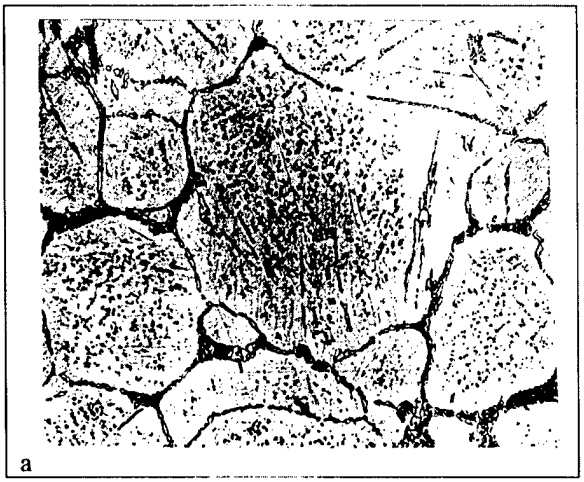

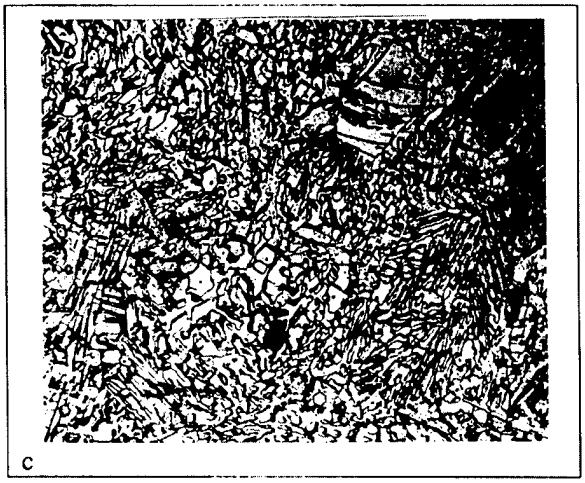

Figure 7. Fracture surface of the alloy 14 - Ti – 5.5Si – 5.1Al – 7.2Zr (scanning electron microscopy):
d) 20°C, x1500,
e) 800°C, x1500,
f) 20°C, x1500.

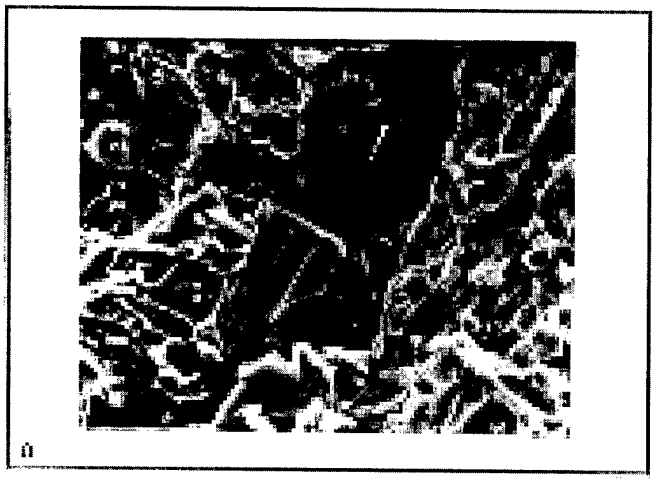

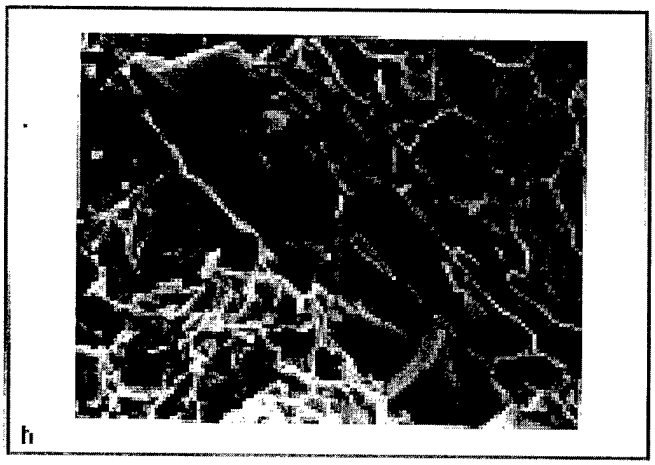

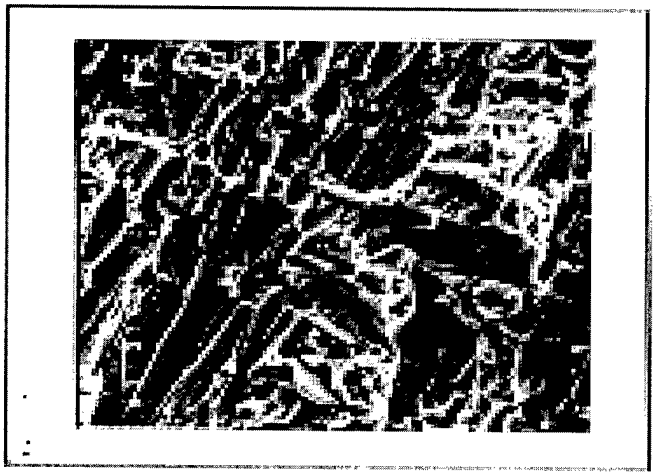

Figure 8. Temperature dependencies of bent strength and plasticity (bending deflection) of three the Ti-Al-Si-Zr alloys under bending. Content of elements is in mas. %.

- ● alloy 7, Ti – 2Si – 5.4Al – 5.3Zr - volume of phase f ≈ 10%;
- ▩ alloy 3, Ti – 5.3Si – 5Al - volume of phase f ≈ 26%;
- ▲ alloy 17, Ti – 6.2Si – 5.4Al – 6Zr - volume of phase f ≈ 31%.

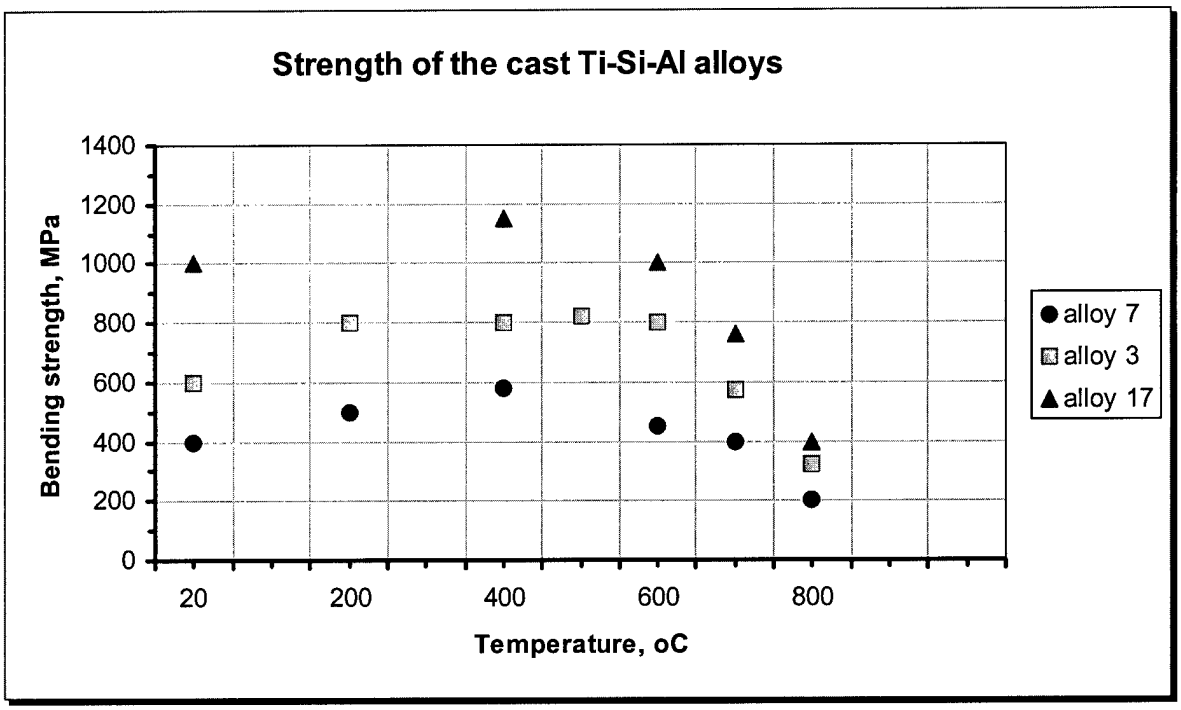

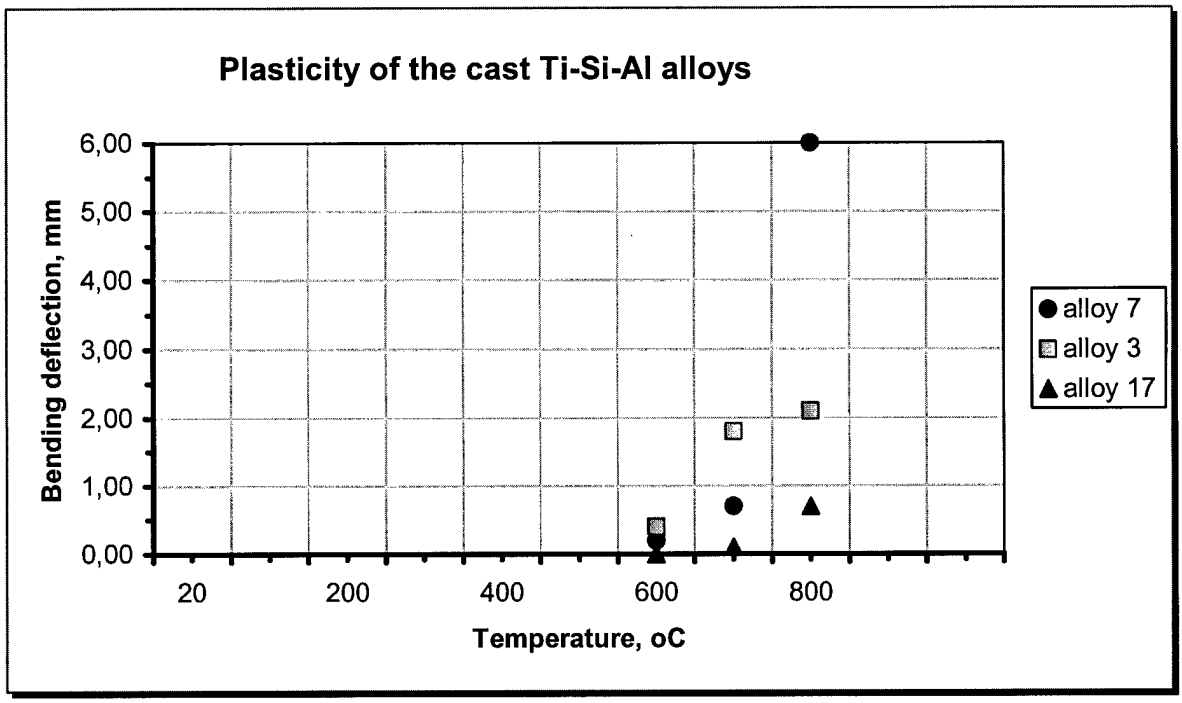

Figure 9. Short-term, 1 min (a) and long-term, 60 min (b) hardness of the cast Ti-Al-Si alloys additionally alloyed with zirconium. Content of elements is in mas. %.

– alloy 7, Ti – 2Si – 5.4Al – 5.3Zr - volume of phase f ≈ 10%;
– alloy 10, Ti – 3.5Si – 5.4Al – 5.3Zr - volume of phase f ≈ 17%;
– alloy 17, Ti – 6.2Si – 5.4Al – 6Zr - volume of phase f ≈ 31%;
– alloy 12, Ti-4.7Si-4.4Al-9.4Zr - volume of phase f ≈ 23%.

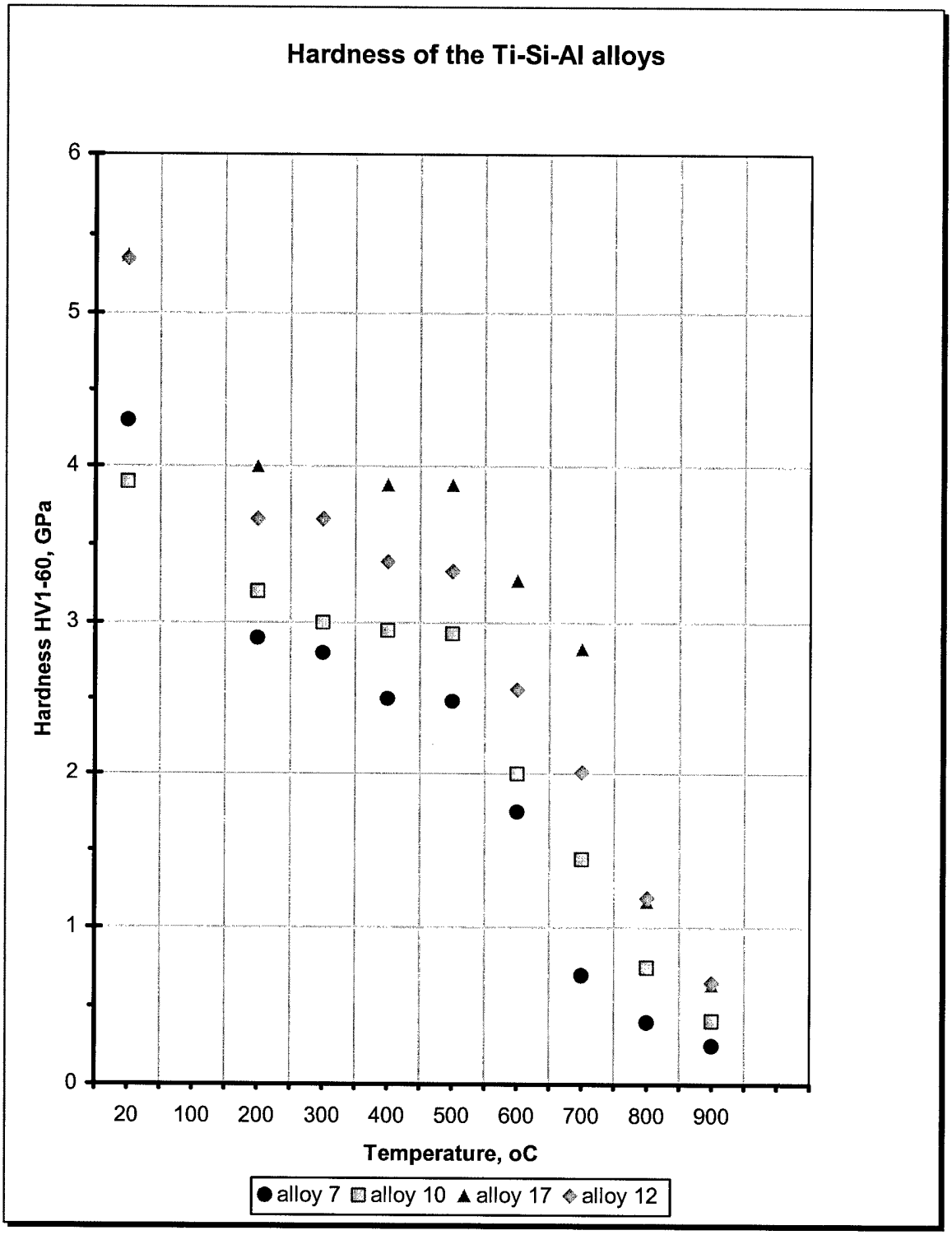

a

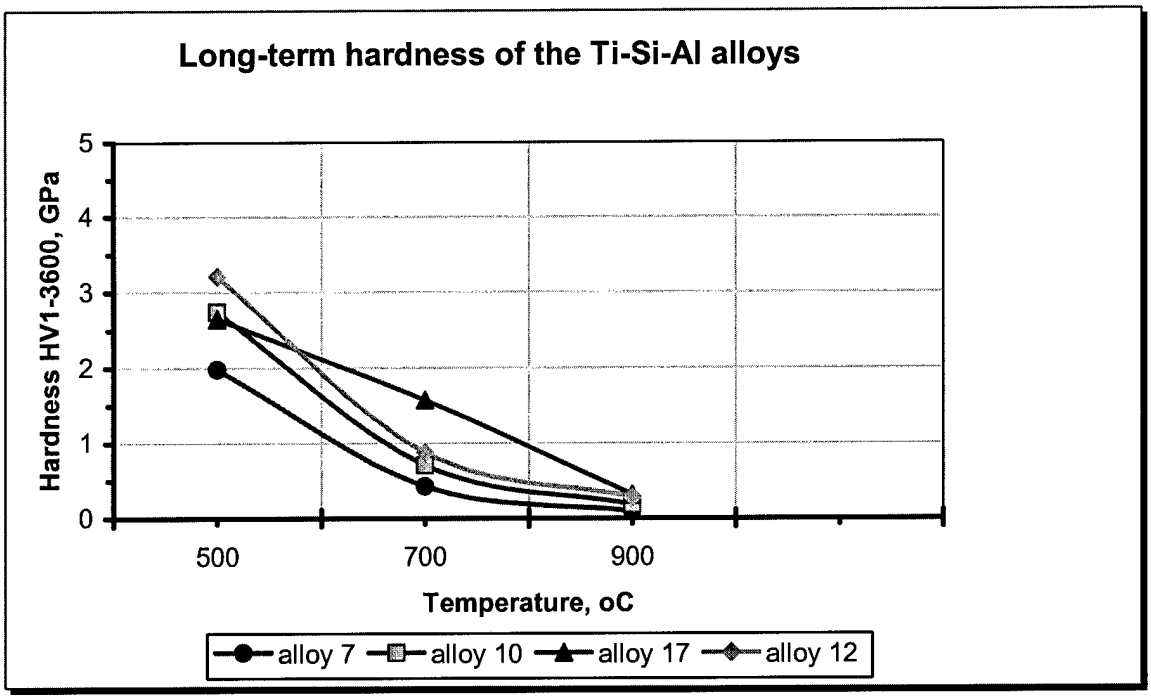
Long-term hardness of the Ti-Si-Al alloys
Hardness HV1-3600, GPa
5
4
3
2
1
0
500
700
900
Temperature, oC
alloy 7
alloy 10
alloy 17
alloy 12

b

Figure 10. Microstructure of alloys subjected to long-term testing. Light microscopy, x200.
a – (A) – alloy 17, Ti-6Al-3.5Si-9.6Zr;
b – (B) – alloy 9, Ti-5.6Al-6.6Si-5.4Zr.

Figure 11. Creep curves for testing alloys A and B at 800°C under 100 MPa.
Compositions of alloys:
A, alloy 9 – Ti-6Al-3.5Si-9.6Zr; B, alloy 17 – Ti-6.2Si-5.4Al-6Zr.

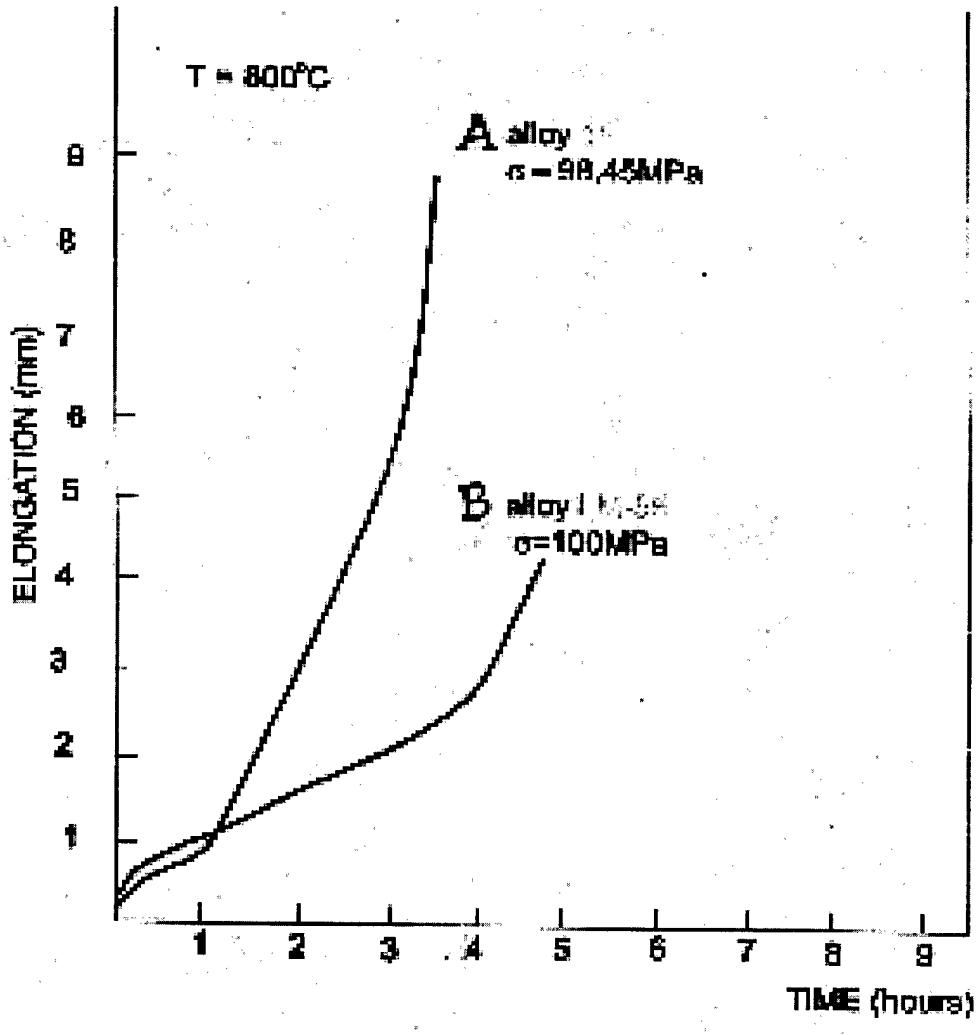

Figure 12.	Creep-rupture strength diagramm of testing materials under 600, 700 and 800°C. Compositions of alloys: A, alloy 9 – Ti-6Al-3.5Si-9.6Zr; B, alloy 17 – Ti-6.2Si-5.4Al-6Zr.

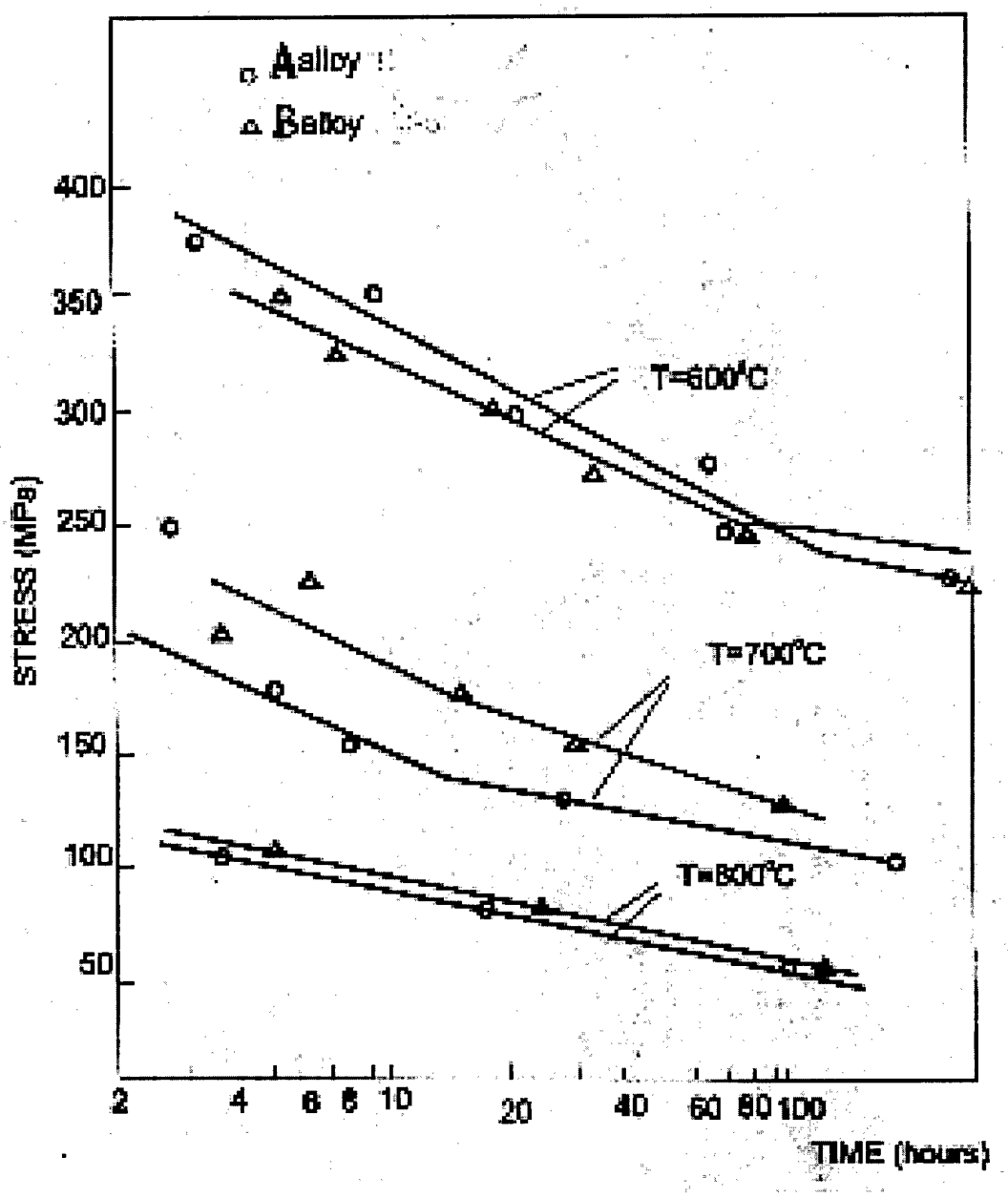

Figure 13. Structure (light microscopy, x200) of alloys 9 – A (a,b) and 17 – B (c,d) after creep testing:
a – T = 600°C; σ = 299 MPa; time to failure = 20 hours.
b – T = 700°C; σ = 177 MPa; time to failure = 5 hours.
c – T = 800°C; σ = 100 MPa; time to failure = 5 hours.
d – T = 800°C; σ = 100 MPa; time to failure = 24 hours.

Compositions of alloys: alloy 9 – A – Ti-6Al-3.5Si-9.6Zr; alloy 17 – B – Ti-6.2Si-5.4Al-6Zr.

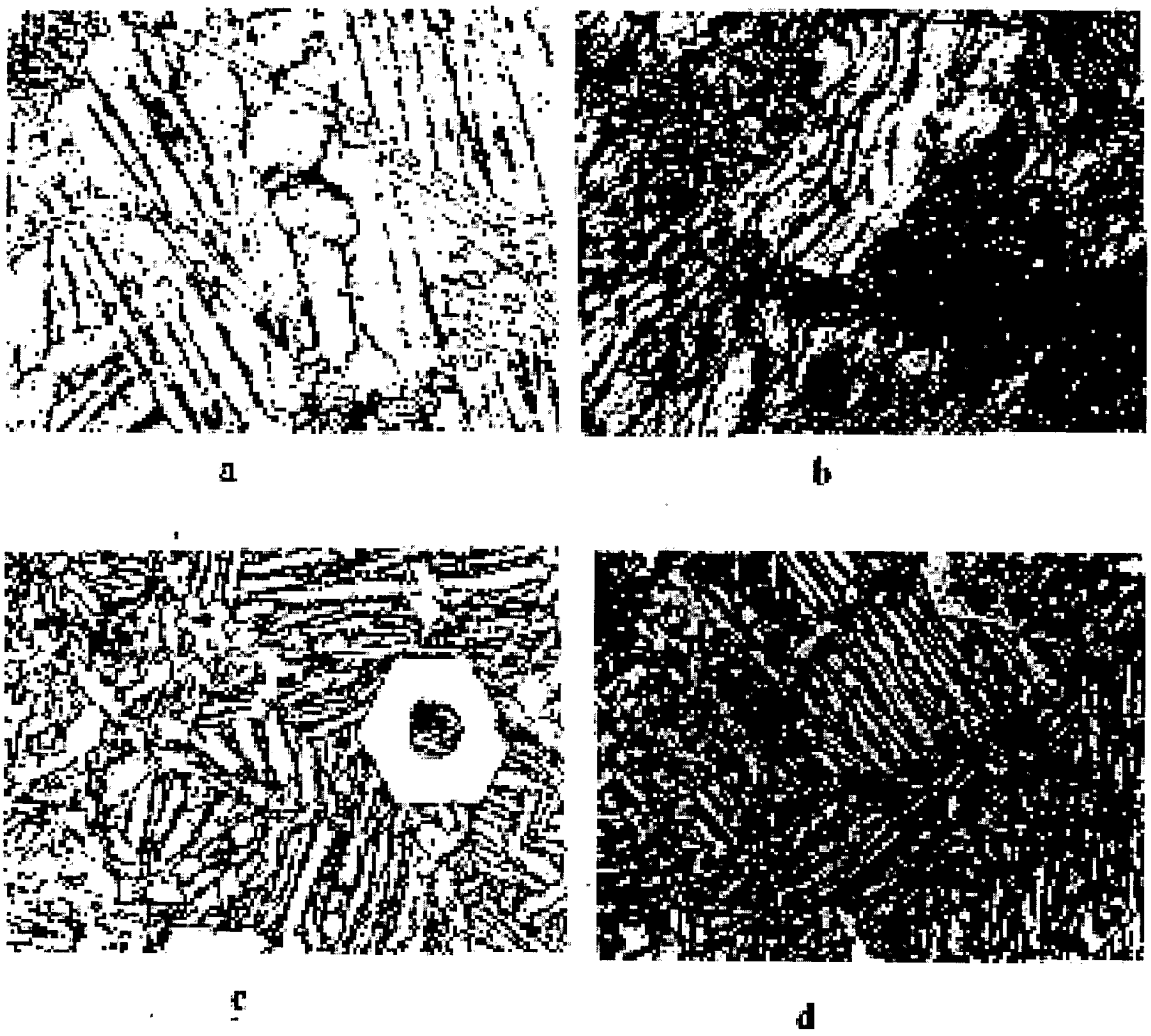

Figure 14.	Liquidus surface projection of the Ti-Si-Al-Ga alloys along section 5 at.% Ga (---) and euetctic curve in the Ti-Al-Si system (-...-) according to [27].

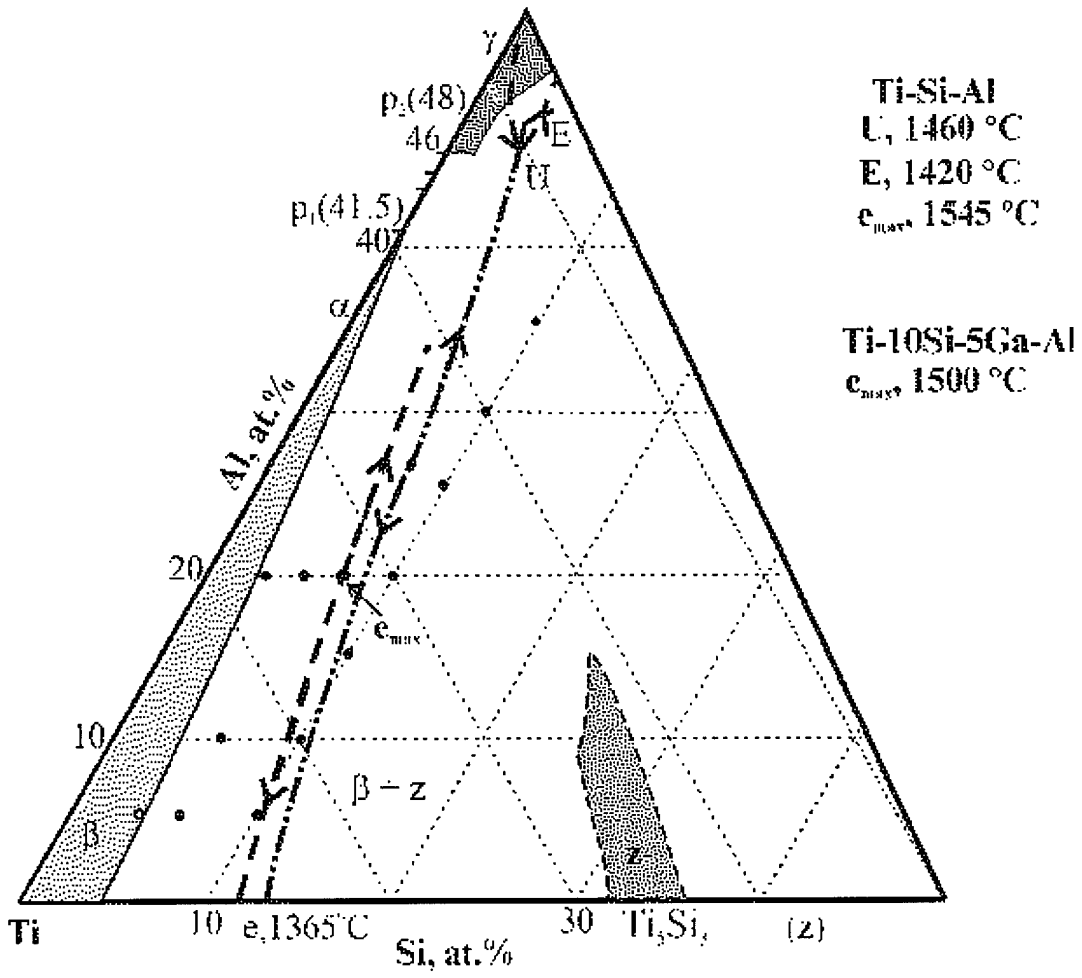

Figure 15. Liquidus surface projection of the Ti-Si-Al-Ga alloys along section 10 at.%.
1. e_1 – eutectic β + z; 2. e_2 – eutectic β + γ; 3. E – eutectic β + γ + z.

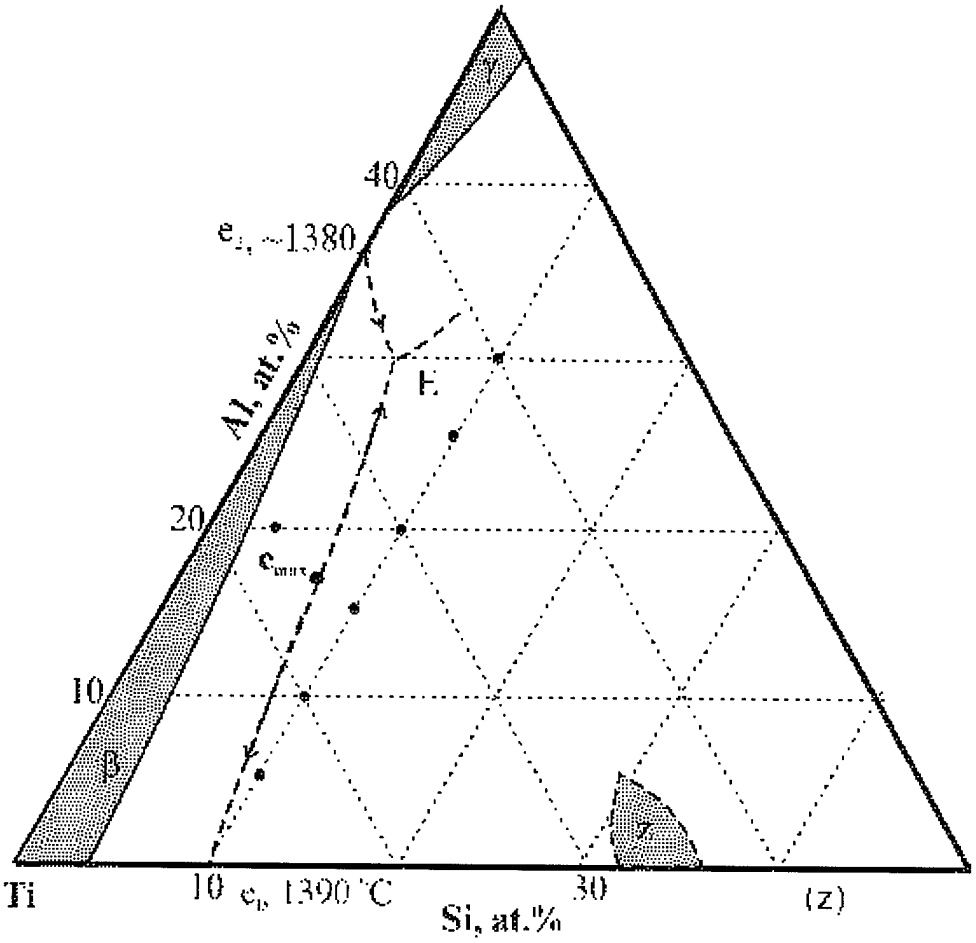

Figure 16-1. Structure of different alloys of the Ti-Si-Al-Ga system. Light microscopy, x200. Description see in the text.

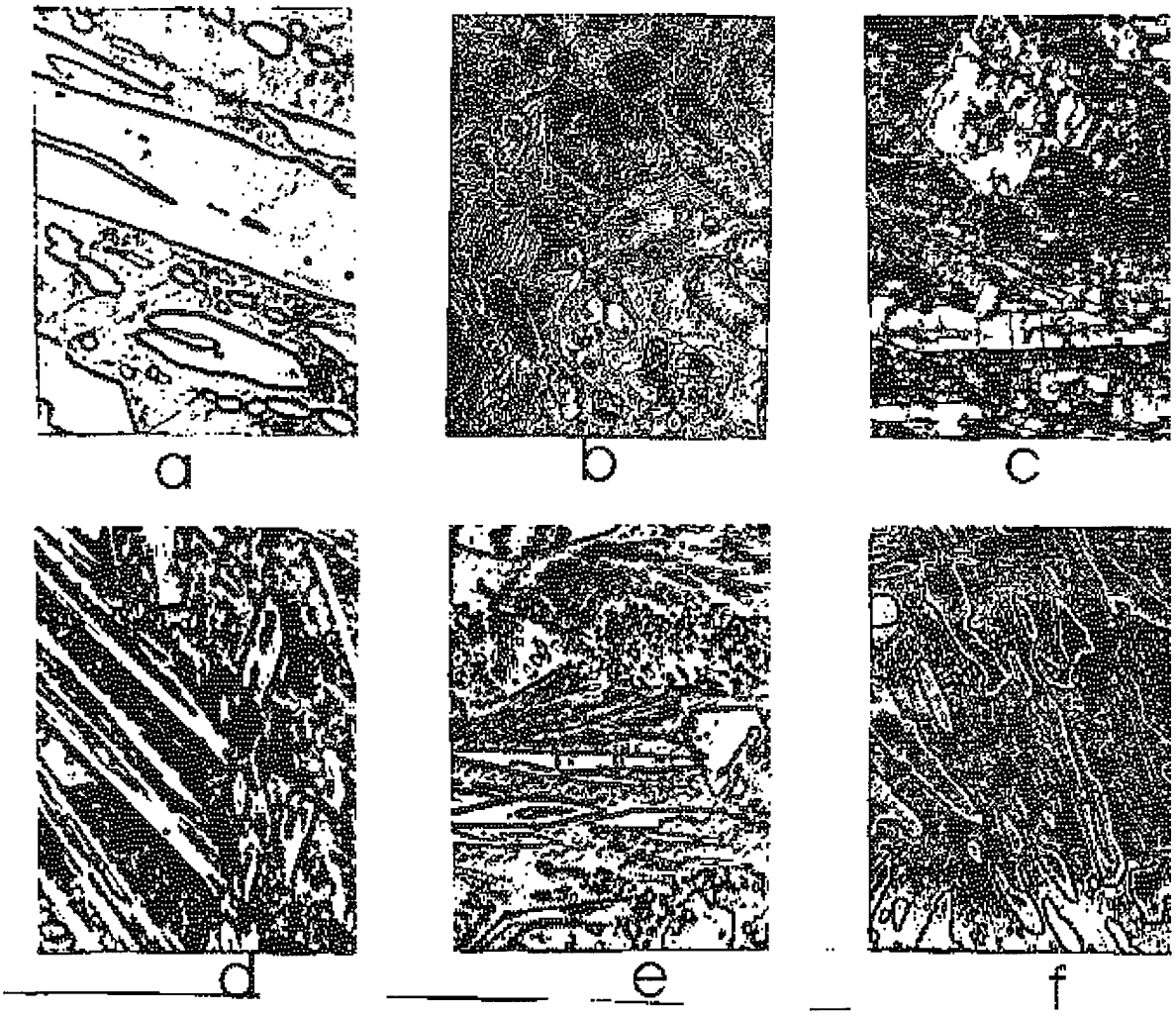

Figure 16-2. Structure of different alloys of the Ti-Si-Al-Ga system, continued. Light microscopy, x200. Description see in the text.

g

h

i

j

k

Figure 17. Lattice parameters of the phase $Ti_5(Si,Al,Ga)_3$ *a* (a) and *c* (b) of the Ti-Si-Al-Ga alloys annealed at 1350°C.

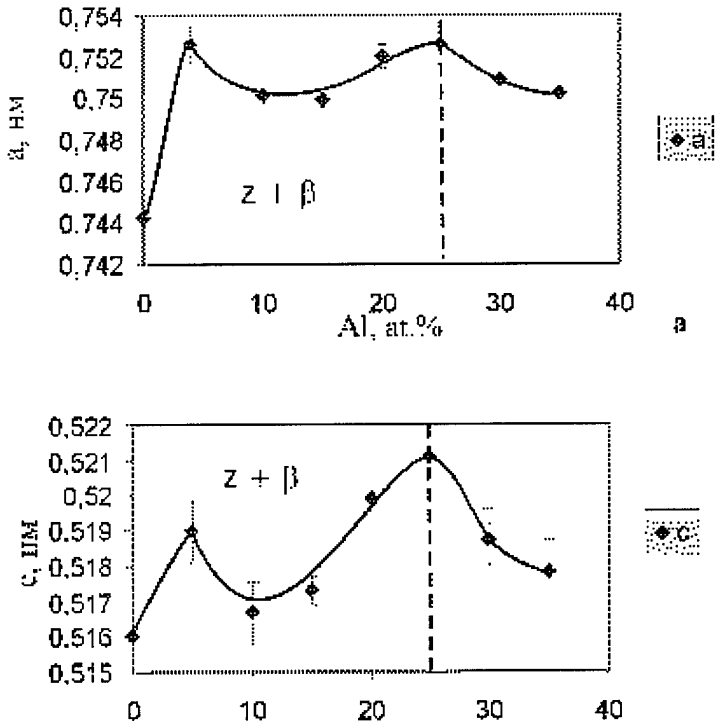

Al, at.%

Figure 18. Structure of the eutectic Ti-5Si-5Ga-20Al alloy. Scanning microcsopy, x1000.

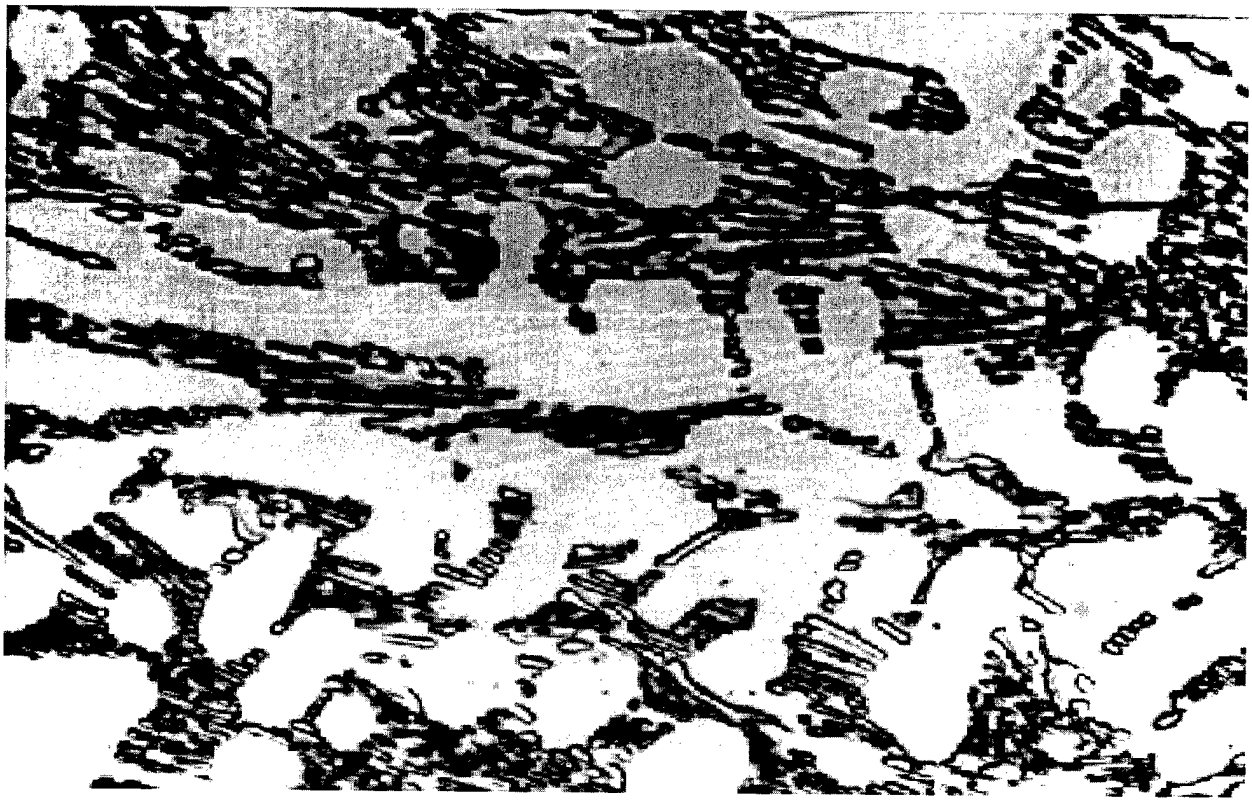

Figure 19. Short-term hardness of the Ti-Ga alloys.

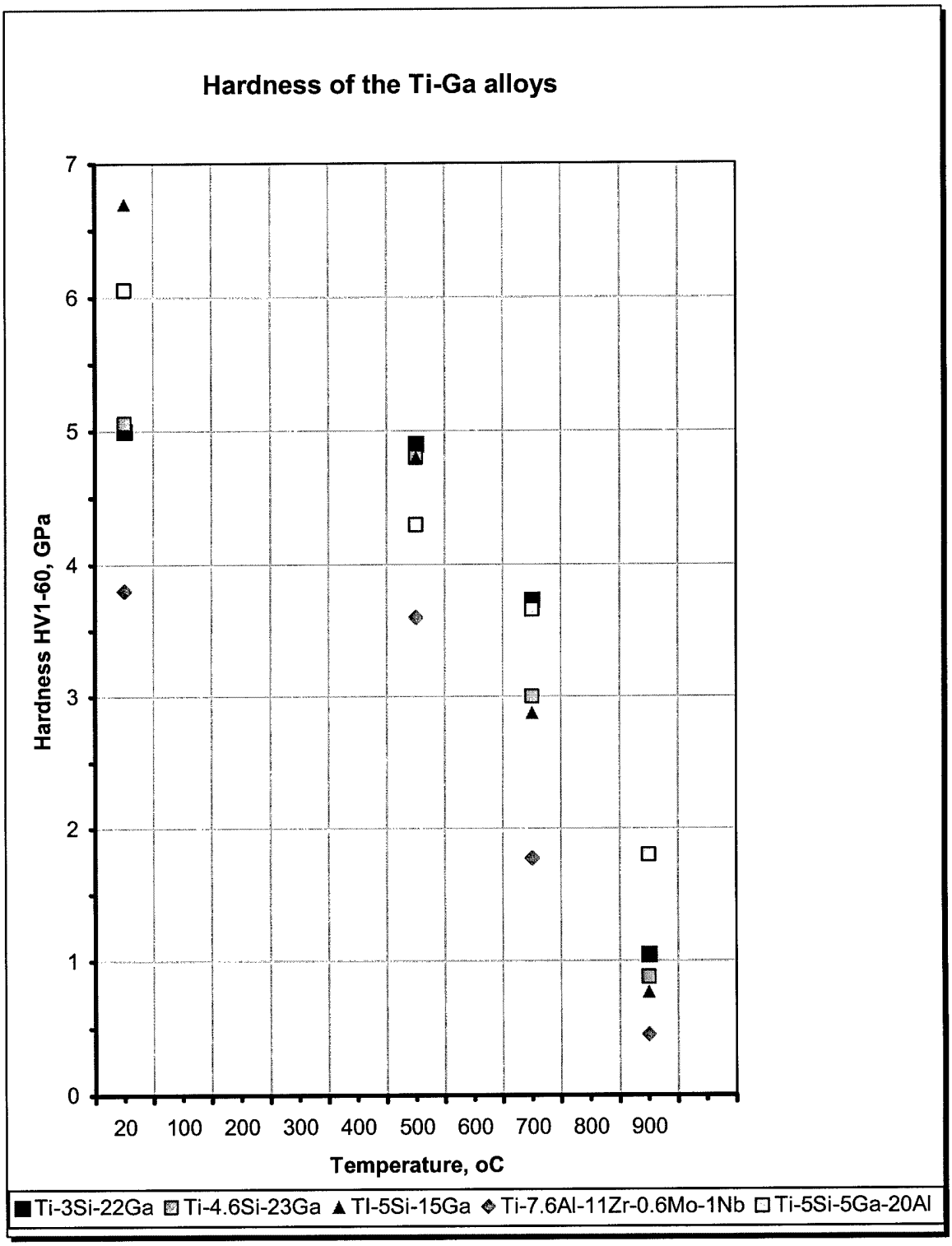

Figure 20. Long-term hardness of the Ti-Ga alloys.

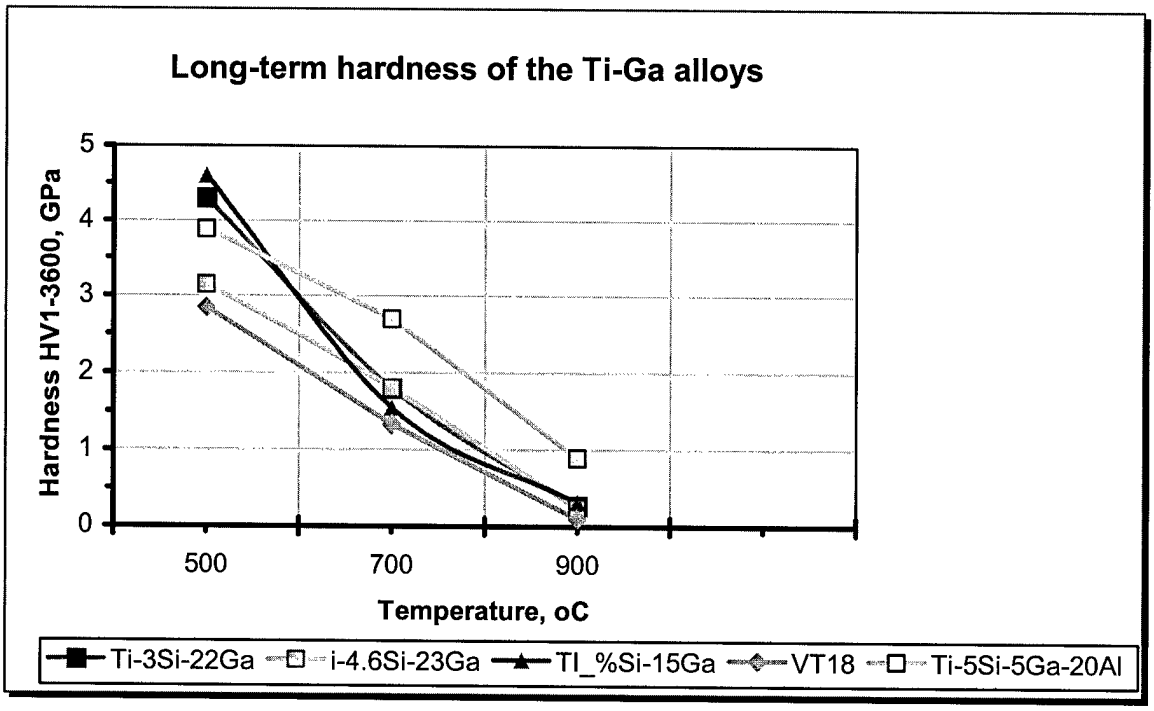

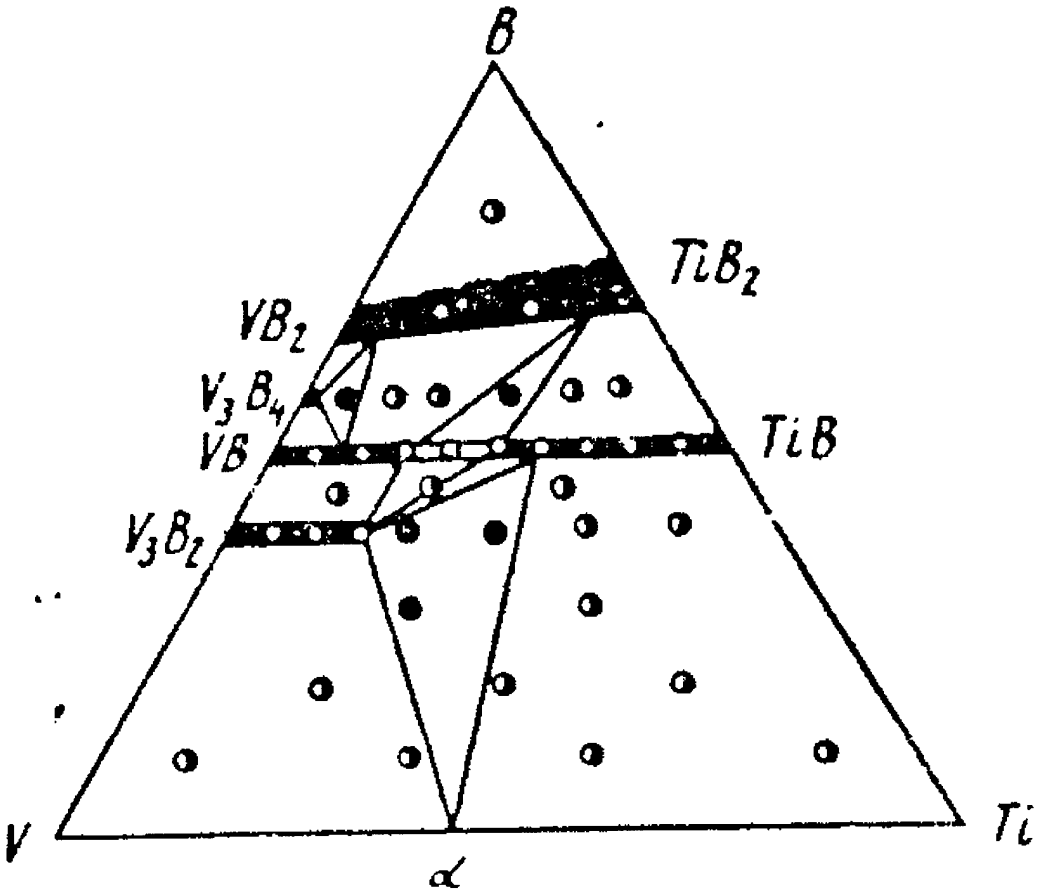

Fig. 21. Isothermal section of the Ti-V-B system at 1400°C [29].

Figure 22 Microstructures of the sintered Ti-V-B alloys with the boron content of 9 at %:
a) $Ti_{91}B_{9}$ – grains of TiB, eutectic TiB+(Ti). ×200;
b) $Ti_{80}V_{11}B_{9}$ – eutectic (TiB)+(Ti). ×200;
c) $Ti_{71}V_{20}B_{9}$ – eutectic (TiB)+(Ti). ×200;
d) $Ti_{60}V_{31}B_{9}$ - eutectic (TiB)+(Ti). ×200; e) the same, ×500;
f) $Ti_{51}V_{40}B_{9}$ - eutectic (TiB)+(Ti). ×200

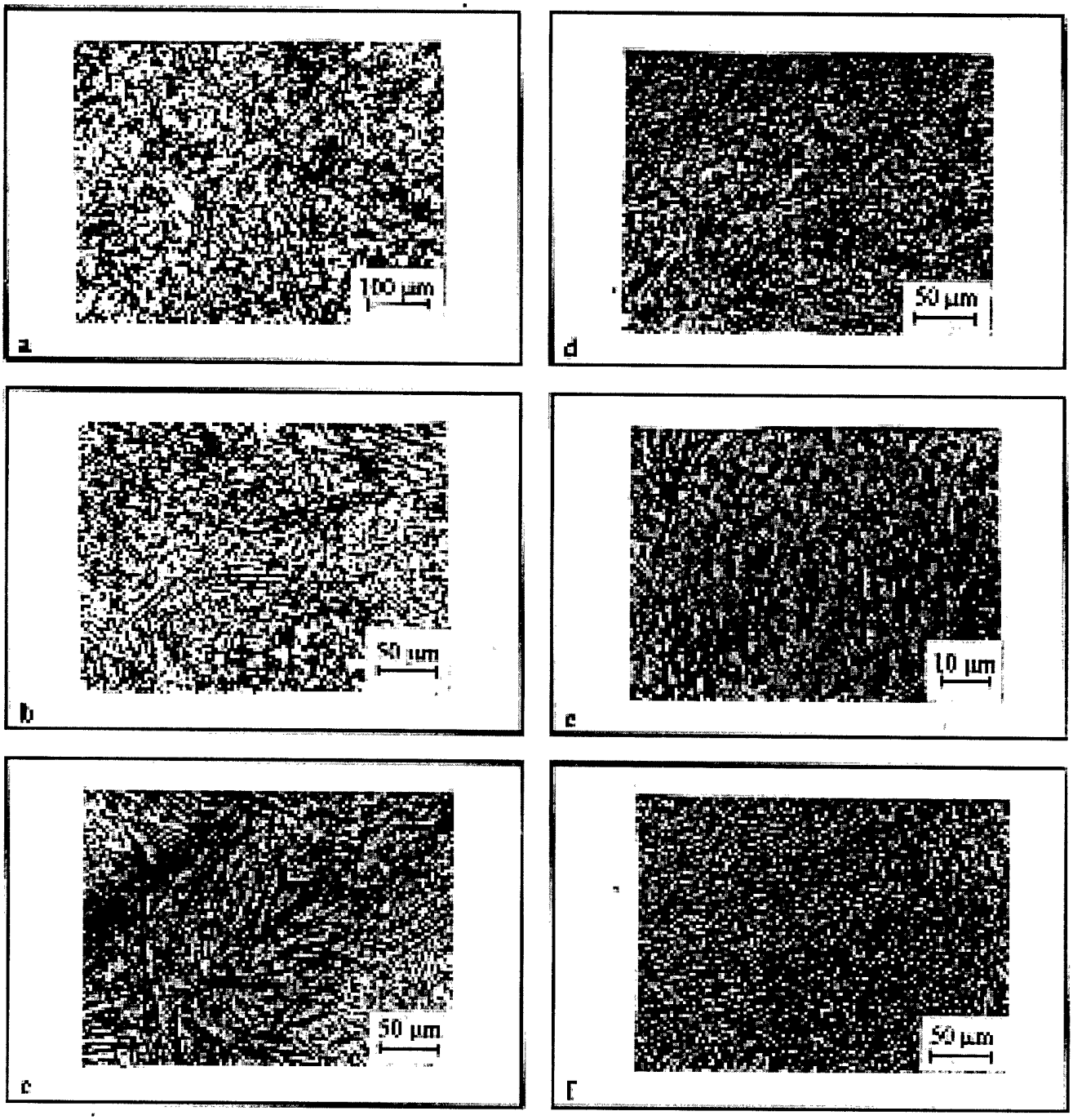

Figure 23 Microstructures of the as-cast Ti-V-B alloys with the vanadium content of 20 at %, ×200.
a) $Ti_{77}V_{20}B_3$ – eutectic (Ti)+(Ti);
b) $Ti_{74}V_{20}B_6$ – grains of metal β-phase (βTi), eutectic (Ti)+(Ti);
c) $Ti_{57}V_{20}B_{23}$ – grains of boride phase (TiB), eutectic (TiB)+(Ti).

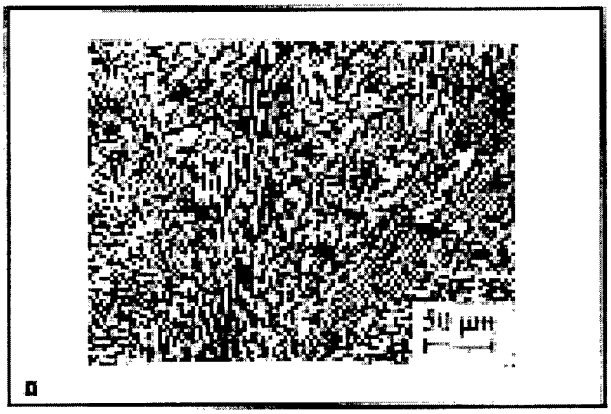

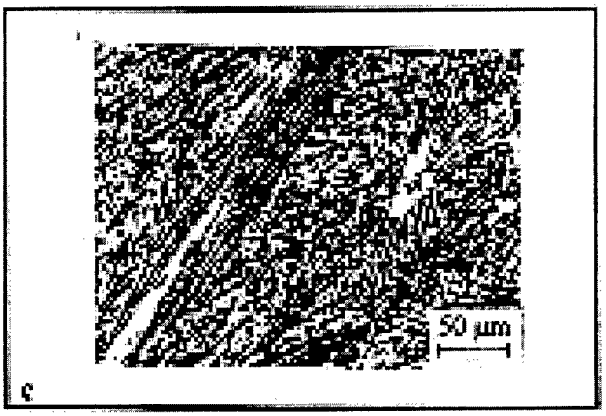

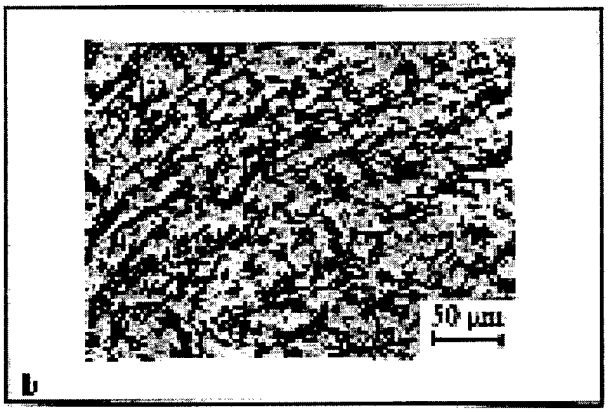

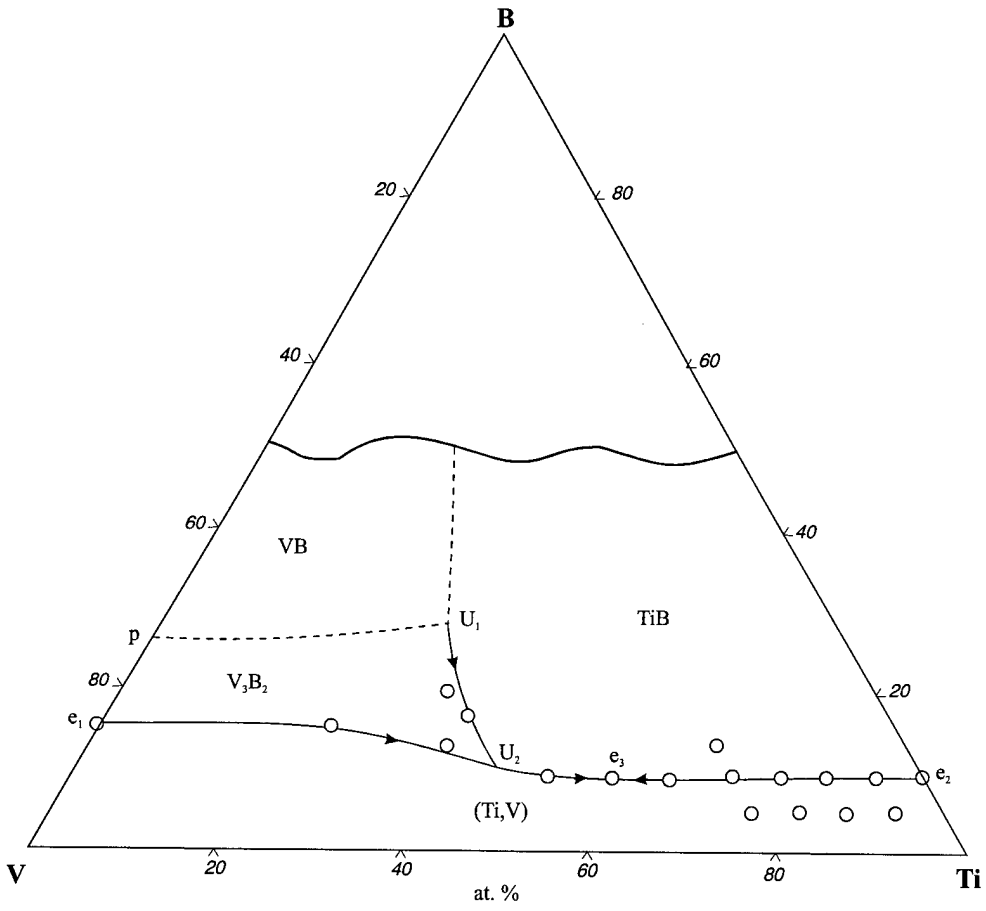

Fig. 24. Solidus surface projection of the Ti-V-B system.

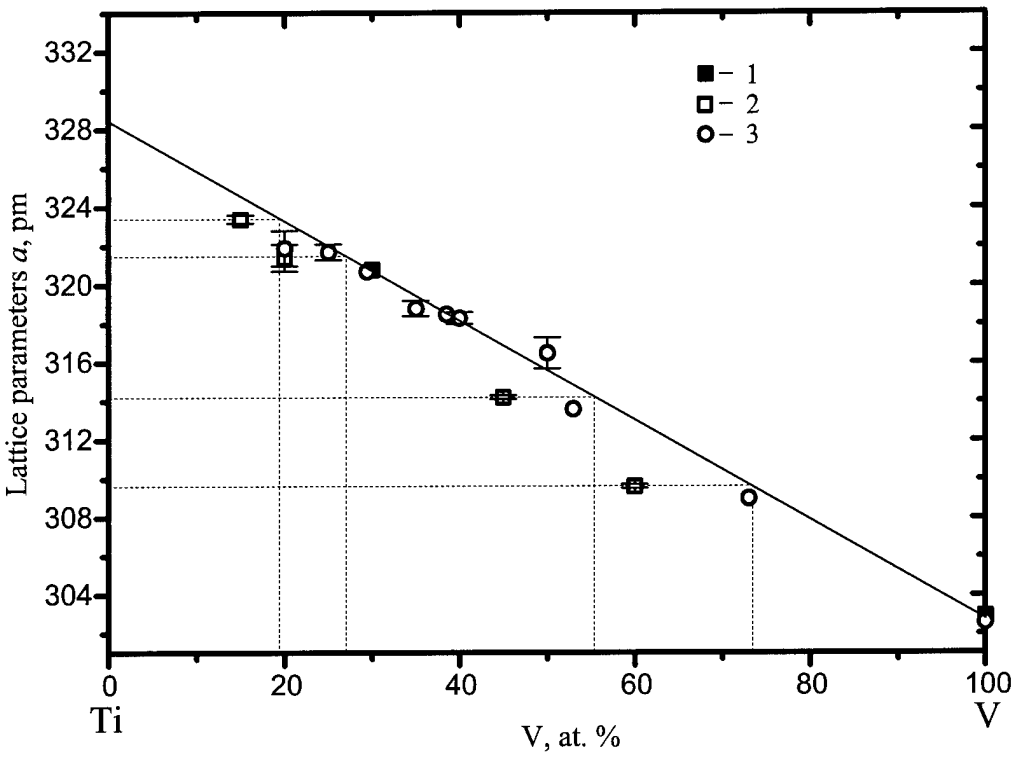

Fig. 25. Lattice parameters of β-phase *vs.* the Ti-V binary alloy composition: 1 – the present data, 2 – lattice parameters of the Ti-V-B ternary alloys, 3 – [36].

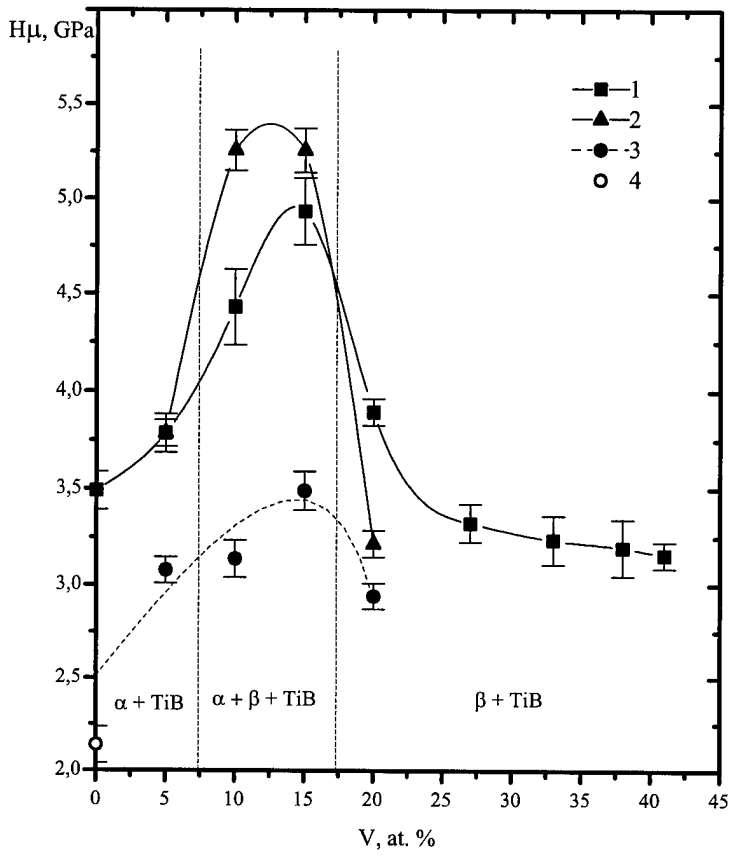

Fig. 26. Microhardness of the eutectic (Ti)+(TiB) component (curves 1 and 2)and metal phase (Ti,V) (curve 3) *vs.* the vanadium content in the Ti-V-B alloys: 1 – the alloys with boron content of 9 at. %; 2 and 3 – the alloys with boron content of 5 at. %.

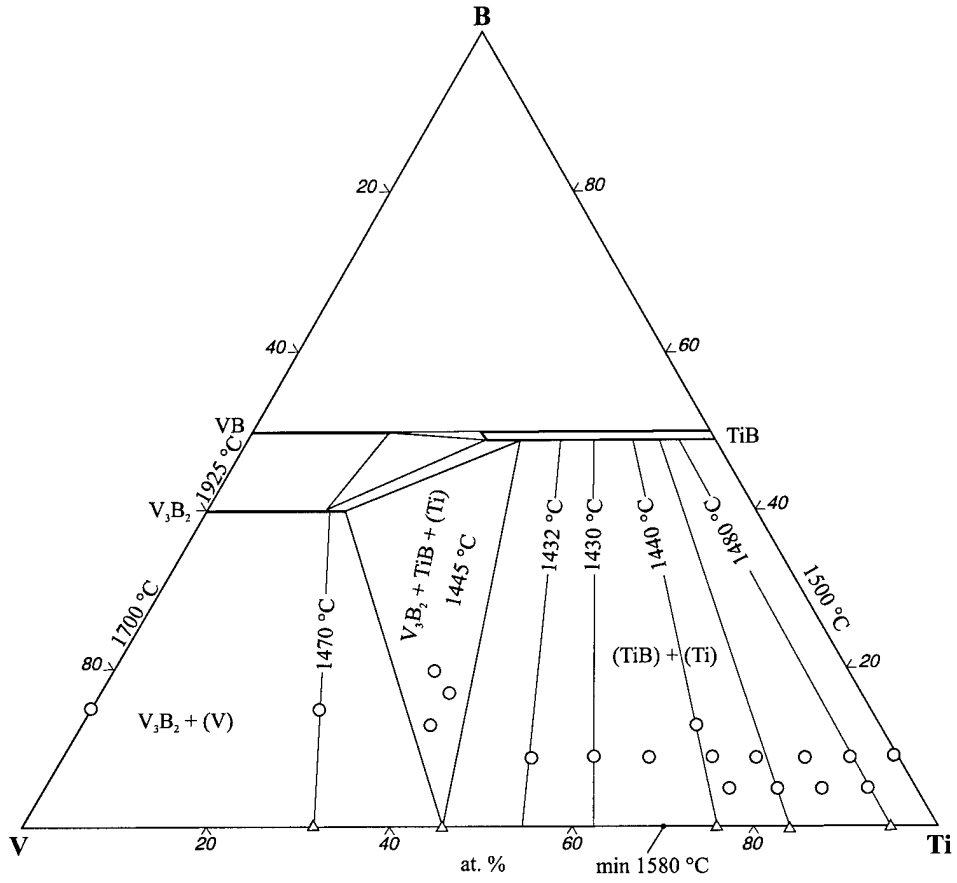

Fig. 27. Solidus surface projection of the Ti-B-V system in the Ti-TiB-VB-V region.

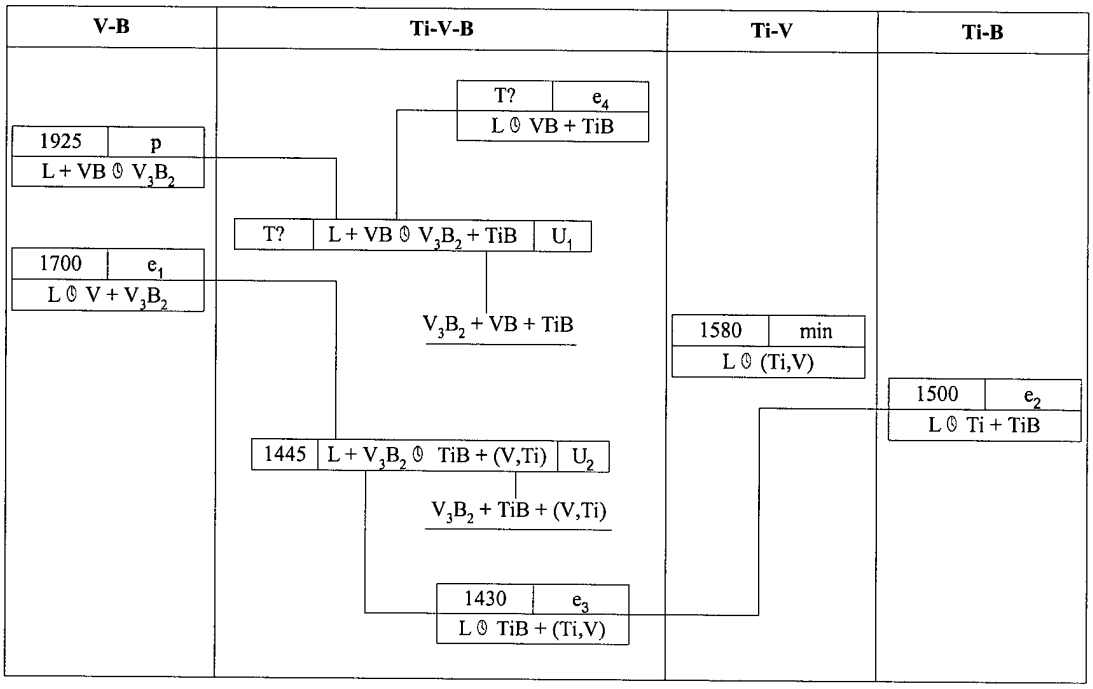

Fig. 28. Reaction scheme at crystallization of the Ti-V-B alloys.

Figure 29 Microstructures of the as-cast Ti-Al-B alloys containing from 0 to 1 mass % B:
a) Ti-6Al (mass %), ×100; b) the same, ×750,
c) Ti-6Al-0.5B (mass %), ×200, d) the same, ×750,
e) Ti-6Al-1B (mass %), ×200, f) the same, ×750

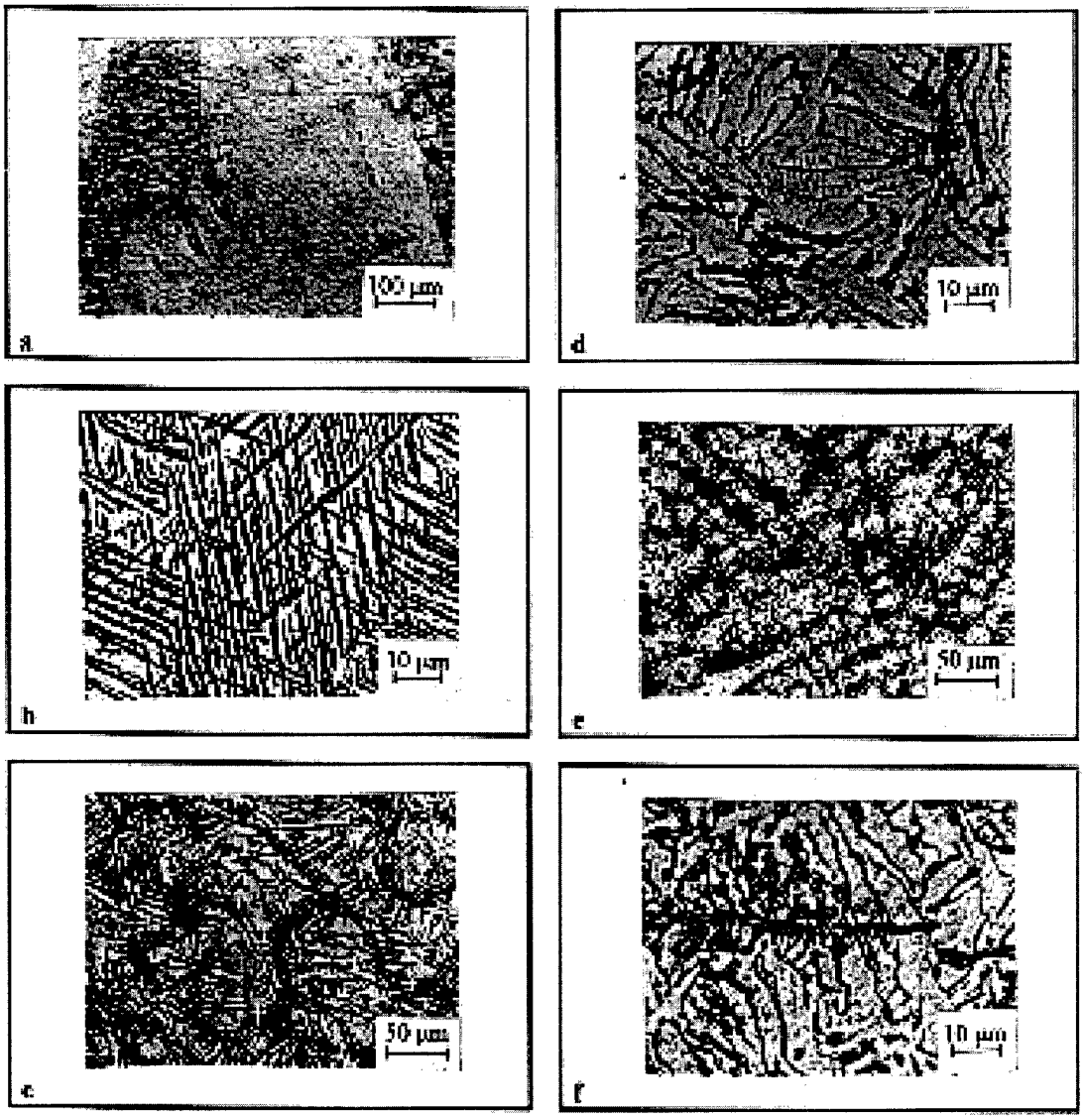

Figure 30. Microstructures of the as-cast Ti-Al-B alloys containing from 1.5 to 2 mass % B:
a) Ti-6Al-1.5B (mass %, ×200; b) the same, ×750;
c) Ti-6Al-2B (mass %), ×200; d) the same, ×750.

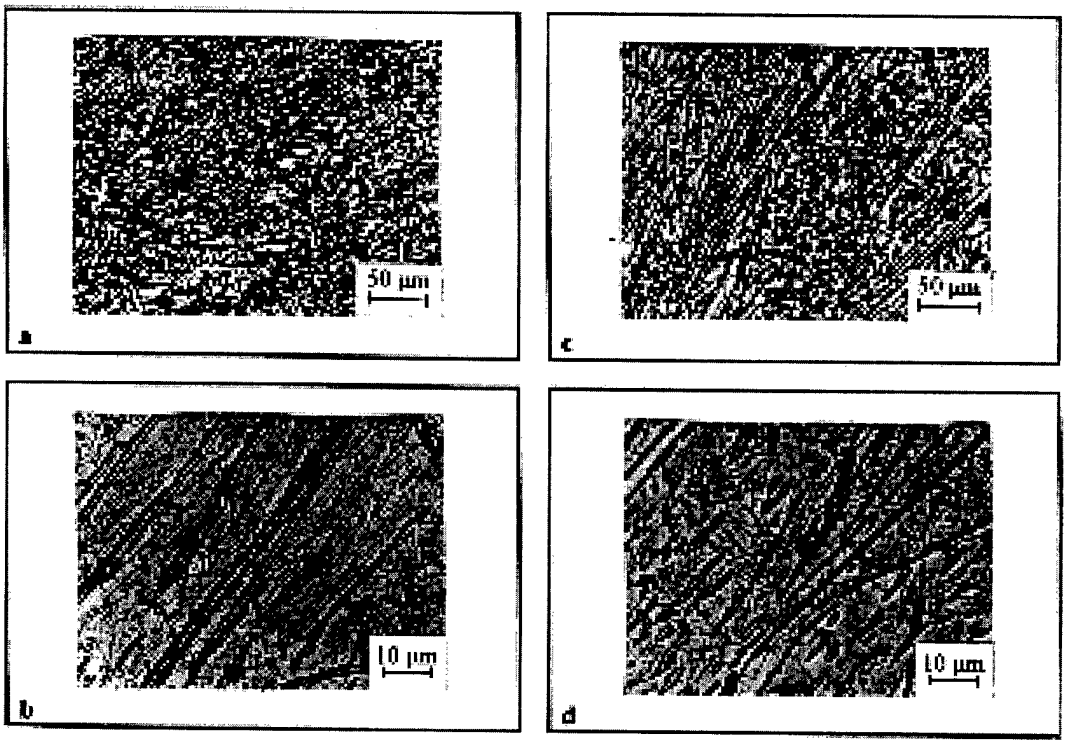

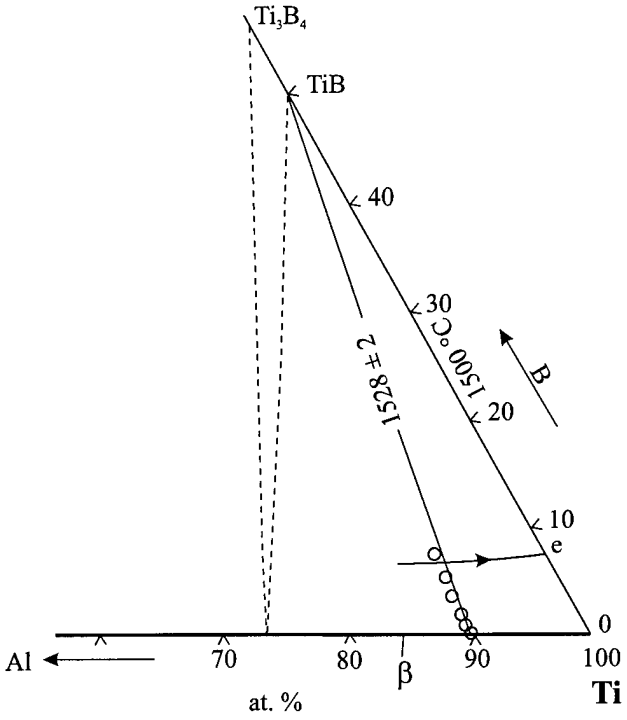

Fig. 31. The Ti-Al-B phase diagram in the range of melting alloys of the Ti-TiB-$Ti_{74}Al_{26}$ region.

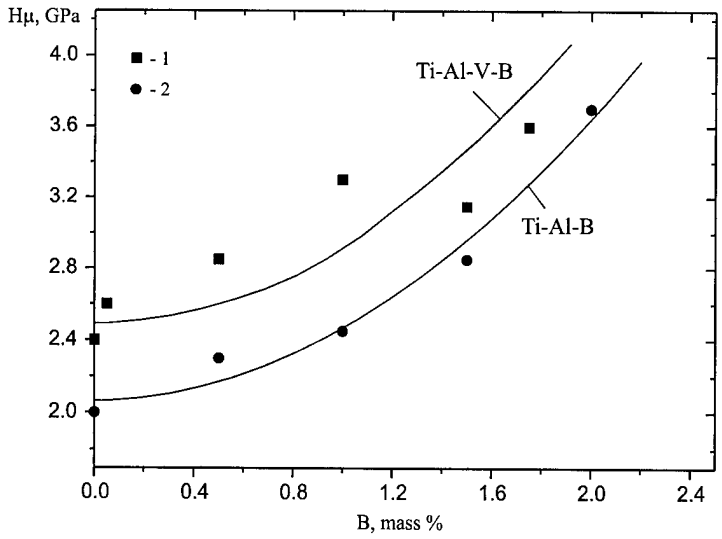

Fig. 32. Microhardness of the Ti-Al-V-B (1) and Ti-Al-B (2) alloys (for metal and eutectic structure components) *vs.* the boron content in the alloys.

Figure 13 Microstructure of the as-cast Ti-6Al-4V-B alloys containing from 0 to 1 mass % B:
a) Ti-6Al-4V (mass %), ×200; b) Ti-6Al-4V-0.01B, ×200; c) Ti-6Al-4V-0.03B, ×200;
d) Ti-6Al-4V-0.05B, ×200; e) the same, ×500;
f) Ti-6Al-4V-0.1B, ×200; g) Ti-6Al-4V-0.5B, ×200; h) Ti-6Al-4V-1B, ×200.

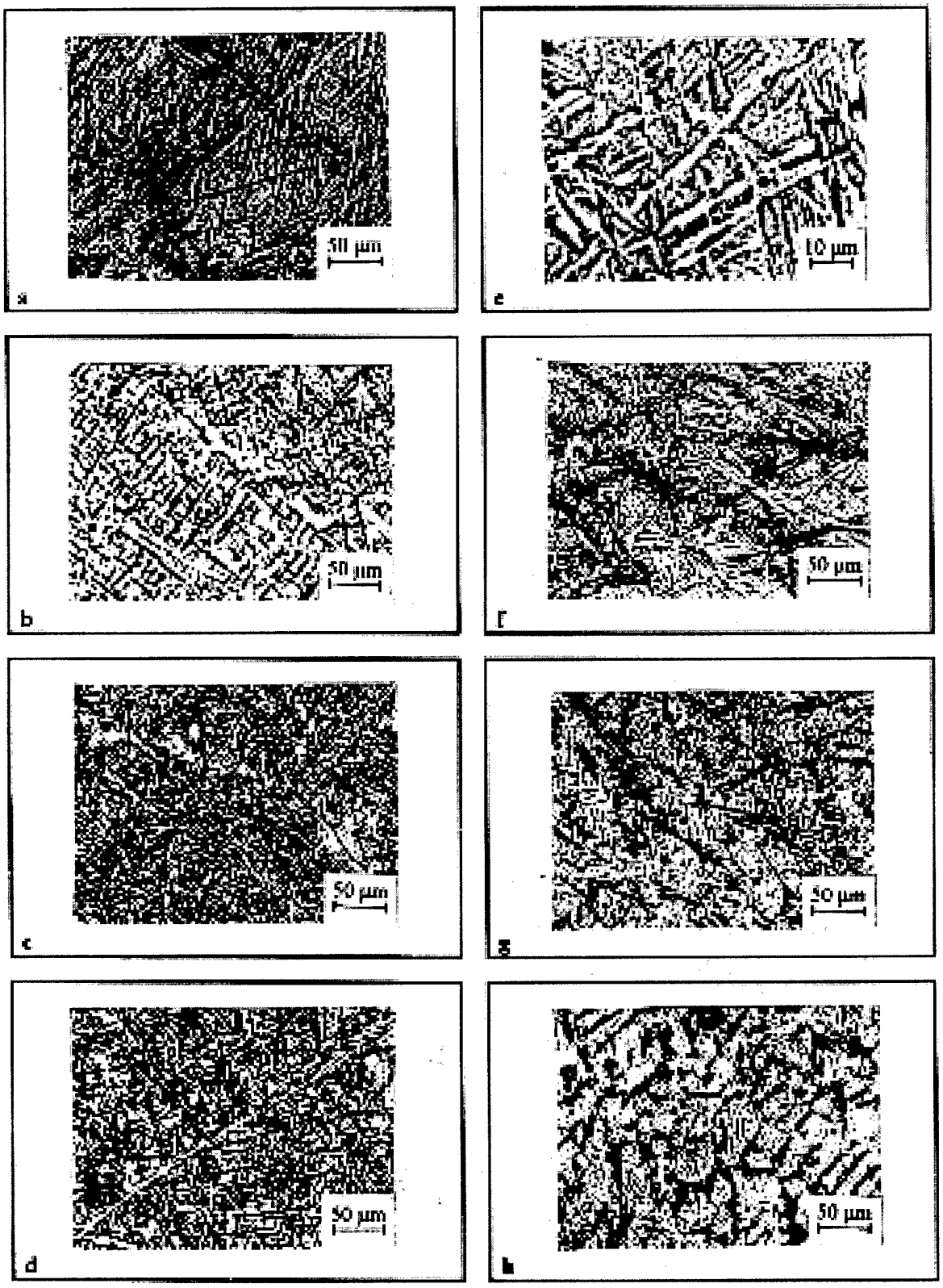

Figure 34. Microstructures of the as-cast Ti-6Al-4V-xB alloys containing from 1.5 to 2 mass % B:
a) Ti-6Al-4V-1.5B (mass %), ×200;
b) Ti-6Al-4V-1.75B (mass %), ×200;
c) Ti-6Al-4V-2B (mass %), ×200; d) the same, ×750;
e) Ti-6Al-4V-2.25B (mass %), ×200;
f) Ti-6Al-4V-2.5B (mass %), ×200

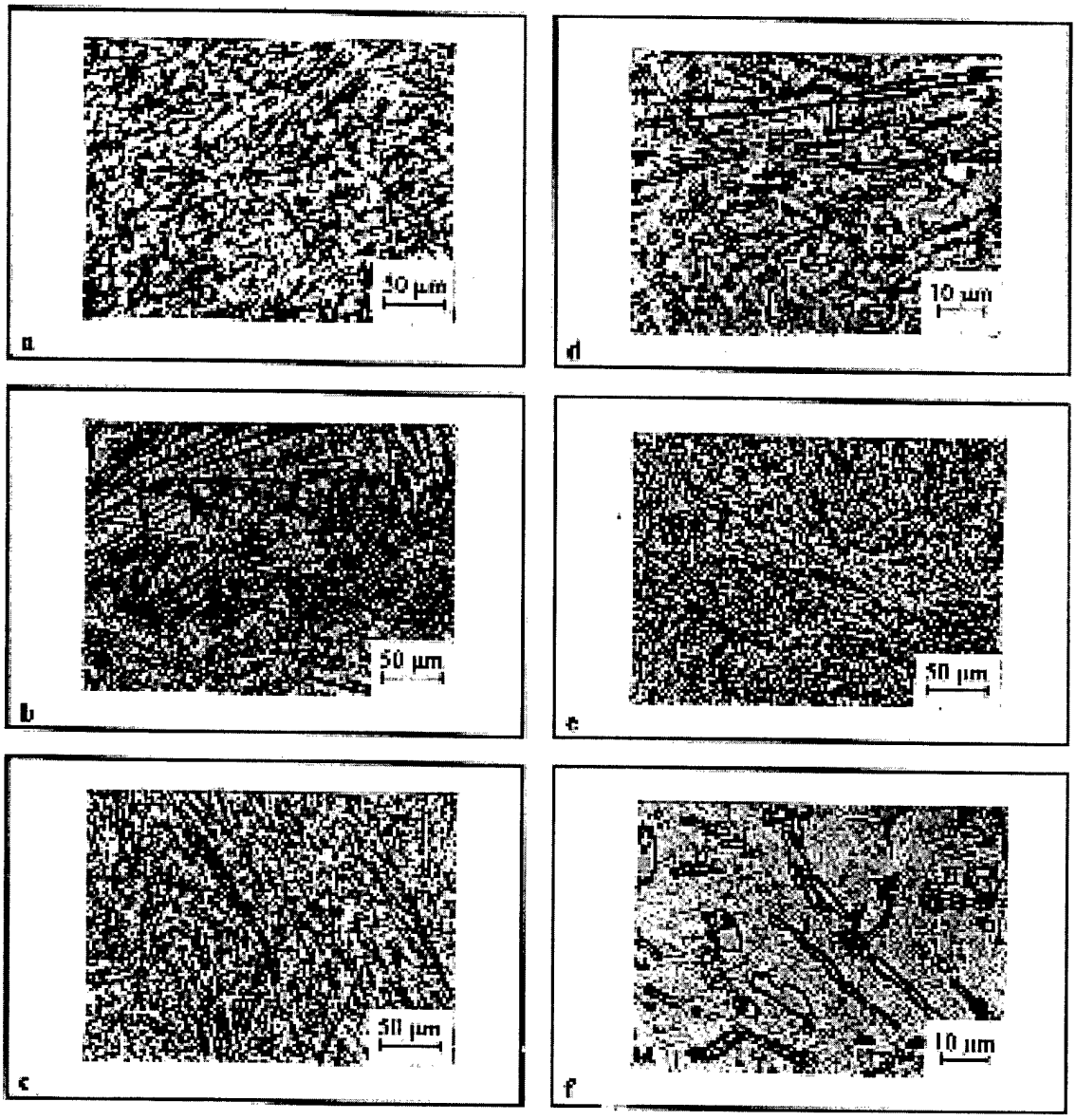

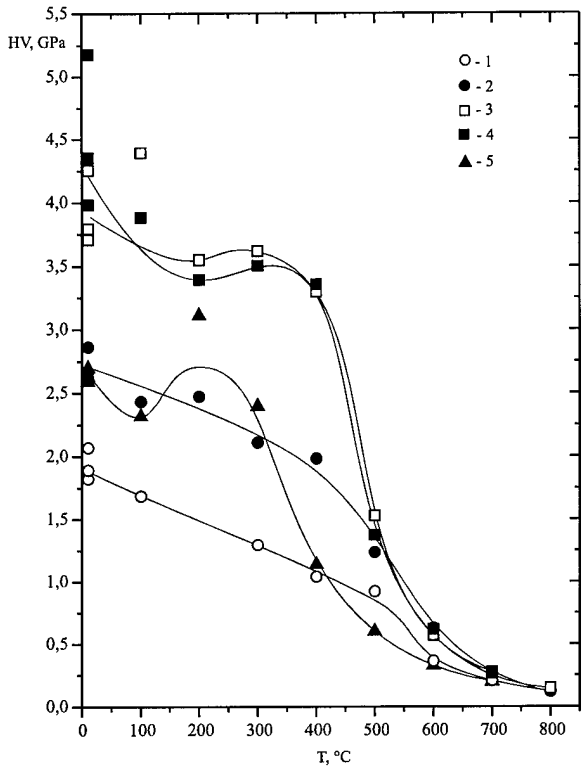

Fig. 35. The temperature dependence of hardness for eutectic alloys $Ti_{91.4}B_{8.6}$ – 1, $Ti_{86}V_5B_9$ – 2, $Ti_{81}V_{10}B_9$ – 3, $Ti_{76}V_{15}B_9$ – 4, and $Ti_{71}V_{20}B_9$ – 5.

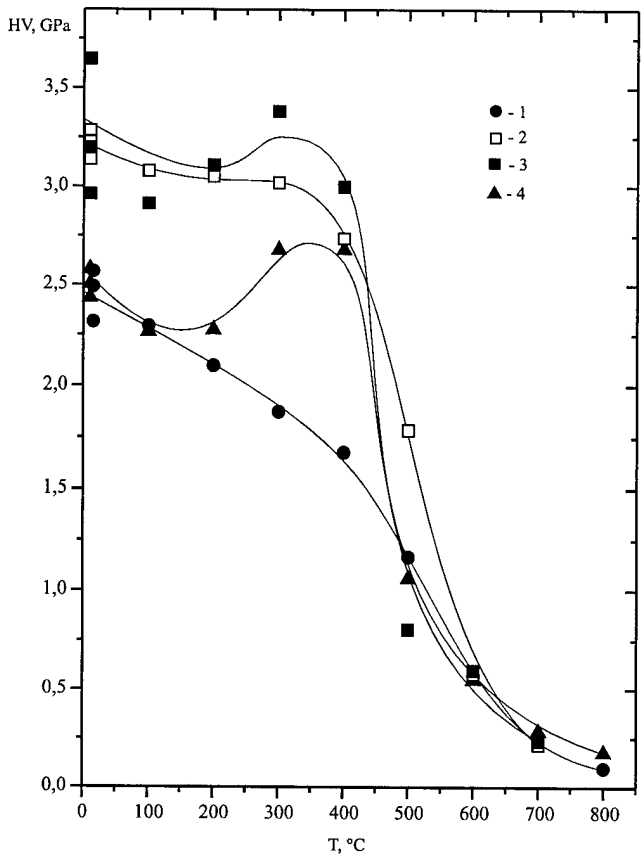

Fig. 36. The temperature dependence of hardness for hypoeutectic alloys $Ti_{90}V_5B_5$ – 1, $Ti_{85}V_{10}B_5$ – 2, $Ti_{80}V_{15}B_5$ – 3, and $Ti_{75}V_{20}B_5$ – 4.

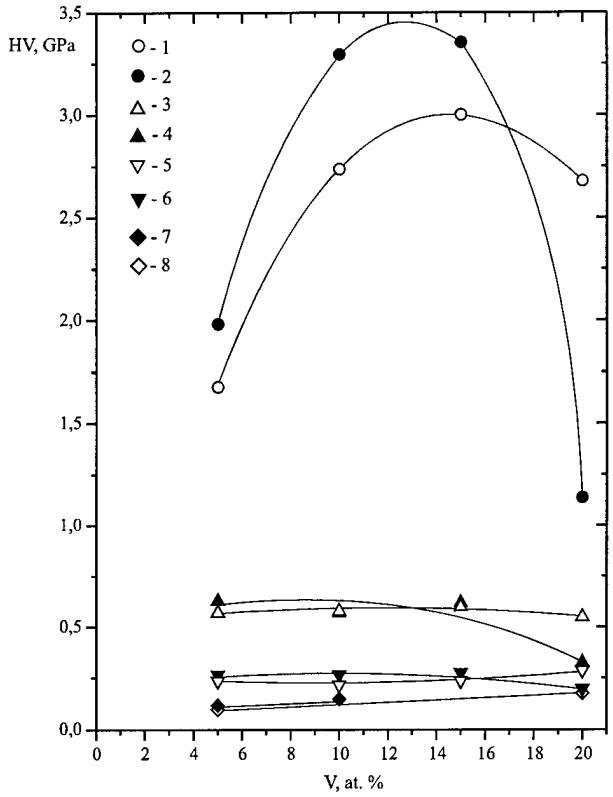

Fig. 37. The hardness dependence for the Ti-B-V alloys on the vanadium content at the temperatures: 400°C (1 – eutectic alloy, 2 – hypoeutectic alloy); 600°C (3 – eutectic alloy, 4 – hypoeutectic alloy); 700°C (5 – eutectic alloy, 6 – hypoeutectic alloy); 800°C (7 – eutectic alloy, 8 – hypoeutectic alloy).

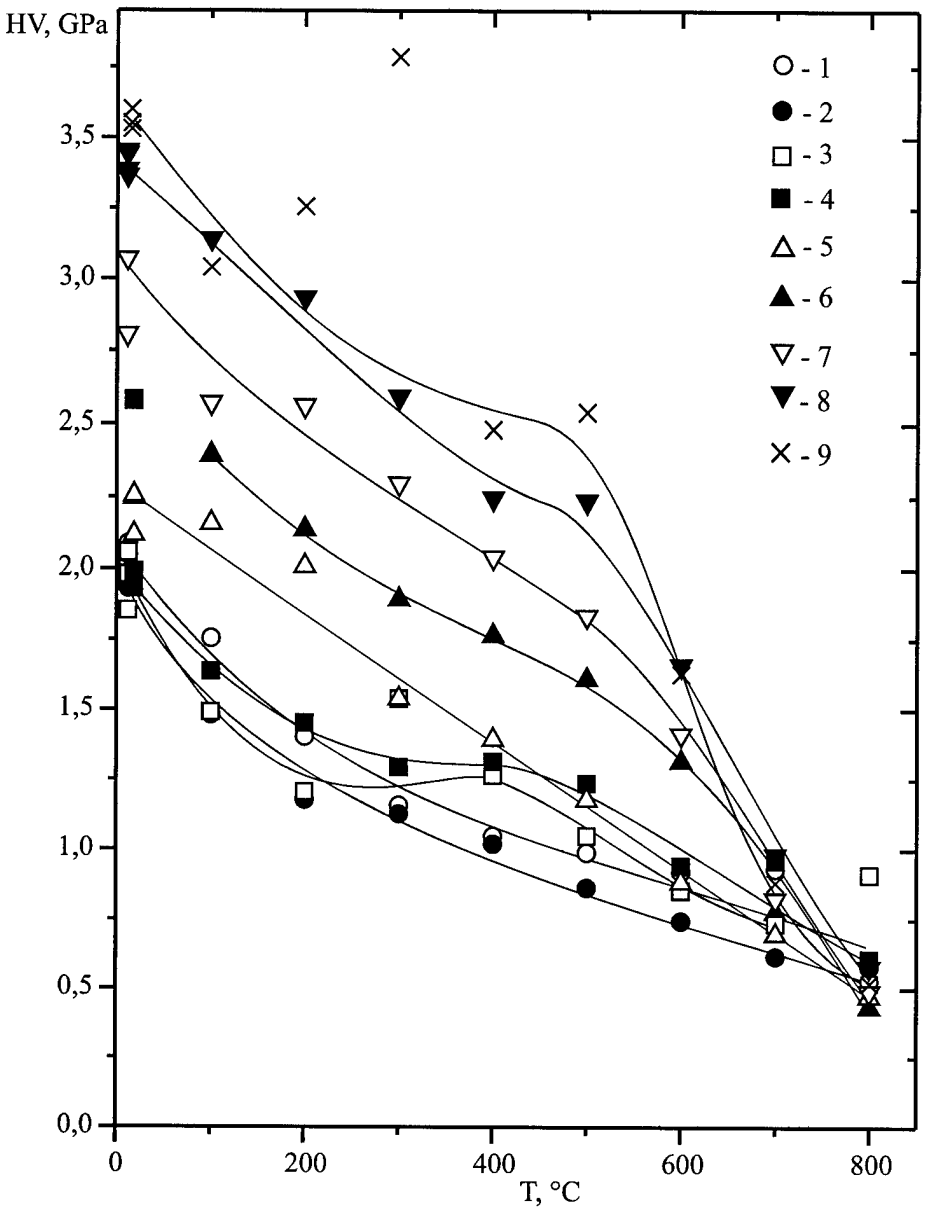

Fig. 38. The temperature dependence of hardness for the Ti-B-Al alloys:
1 – Ti6Al (mass %), 2 – Ti6Al0.01B, 3 – Ti6Al0.02B, 4 – Ti6Al0.05B,
5 – Ti6Al0.1B, 6 – Ti6Al0.5B, 7 – Ti6Al1.0B, 8 – Ti6Al1.5B,
9 – Ti6Al2.0B.

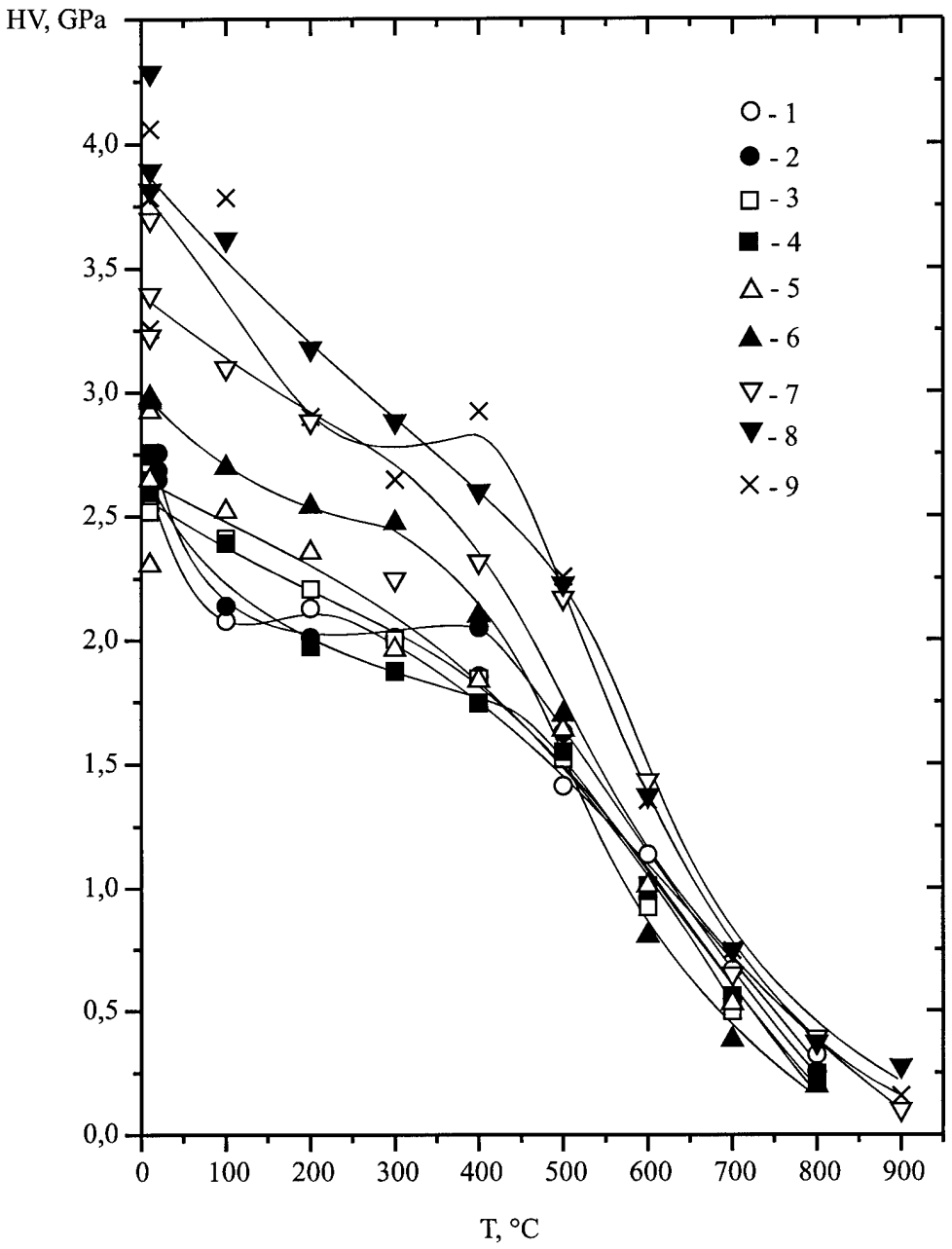

Fig. 39. The temperature dependence of hardness for the Ti-Al-V-B alloys:
1 – Ti6Al4V (mass %), 2 – Ti6Al4V0.01B, 3 – Ti6Al4V0.02B,
4 – Ti6Al4V0.05B, 5 – Ti6Al4V0.1B, 6 – Ti6Al4V0.5B,
7 – Ti6Al4V1.0B, 8 – Ti6Al4V1.5B, 9 – Ti6Al4V1.75B.